Institute of Applied Mechanics
Faculty of Mechanical Engineering and Informatics
University of Miskolc

**Abderrazek Messaoudi**

# STABILITY AND VIBRATION OF LOADED STRUCTURAL MEMBERS

PhD thesis

**István Sályi Doctoral School of Mechanical Engineering Sciences**

Topic Field of Basic Engineering Sciences
Topic Group of Mechanics of Solids

Head of Doctoral School:
**Dr. Gabriella Bognár**
DSc, Full Professor

Head of the Topic Field:
**Dr. István Páczelt**
DSc, Professor Emeritus

Head of the Topic Group:
**Dr. György Szeidl**
DSc, Professor Emeritus

Scientific Supervisor:
**Dr. László Péter Kiss**
Associate Professor

Miskolc
2024

## Declaration

The author hereby certifies that this thesis contains no material that has been previously published or written by another person. Furthermore, no portion of this thesis has been submitted, in the same or a different form, to any other university for the award of a PhD degree.

The author affirms that the research and findings presented in this thesis are entirely his own work. Proper acknowledgements and credit are given within the text whenever references are made to the work of other scholars. Additionally, all sources of information and data have been accurately cited to maintain academic integrity.

Miskolc, 12 December 2024

Abderrazek Messaoudi

## Recommendation of the supervisor

Mr. Messaoudi finished his Mechanical Engineering BSc studies in 2019 at the National Engineering School of Monastir, Tunisia. Then, he enrolled to the University of Miskolc for the master level. After successfully completing it, he began his PhD studies at the István Sályi Doctoral School of Mechanical Engineering Sciences in September 2021. Since then, he succeeded in solving some selected issues on mechanics, concerning straight and curved beams. The major findings are gathered in this PhD thesis. It is my pleasure to recommend it to the Reader.

Mr. Messaoudi has dedicated his past three and a half years to the theoretical investigation of beam problems within linear elasticity. Chapter 2 of the thesis is about the stability of compressed straight non-homogeneous beams with three supports. The intermediate support is a spring at an arbitrary position, which restrains transverse movement. He managed to construct the Green function in closed-form for multiple end-support arrangements and evaluate the results. In Chapter 3, the Green function definition is generalized to four-point boundary value problems. The properties are clarified and the way to construct it is also discussed. The demonstration of the technique is illustrated in beams having four supports. The free vibrations are solved after finding the related Green functions. Chapter 4 is about coupled three-point boundary value problems. Compared to the previously mentioned three-point boundary value problems, although the differential operator is of the same order in the two sub-intervals, but are now different. For this reason, the Green function definition is extended. Application is given for the free, loaded vibrations and also for the stability of stepped beams. It is common in these previous chapters that numerical results were obtained by a boundary element technique.

I would like to express our deepest gratitude to Prof. György Szeidl for his kind and unselfish assistance in these topics.

Chapter 5 is dedicated to the static stability of curved beams with geometrical imperfections. Possible initial displacements cause initial strain, which effect is incorporated into a geometrically nonlinear beam model. Analytical solutions and parametric studies are given for multiple symmetric and anti-symmetric shape errors regarding the lowest buckling loads and in-plane behaviour.

Beyond doubt, the presented investigations prove the qualities of Mr. Messaoudi as a researcher. His work rate and everyday approach to the research work was exemplary. Difficulties never discouraged him, instead, helped him become more and more creative. He has a total of 23 publications listed in the Hungarian Scientific Bibliography. The number of Scopus listed articles is 4. I am absolutely convinced there is a fruitful carrier ahead and I sincerely wish him a bright future.

Miskolc, December 2024

L. P. Kiss

# Contents

CHAPTER 1

# Introduction

## 1.1. Stability problems of straight beams

The stability of beams is a critical aspect of structural engineering, influencing the safety and durability of buildings, bridges, and various mechanical systems. Beams, as fundamental structural elements, must withstand diverse loading conditions without experiencing failure due to instability. Since Euler's pioneering work, significant advancements have been made in understanding buckling. Numerous sources discuss the stability of shells, columns, arches, and other structures [**1**, **2**, **3**]. Comprehensive solutions to various engineering issues, along with practical applications, are detailed in books such as those by Wang and Jerath [**3**, **4**]. Focusing specifically on the buckling of columns, book [**5**] provides an in-depth exploration of the theory of elastic stability for continuously axially loaded columns. Additional significant findings are discussed in subsequent works [**6**, **7**], which include the effects of compressive forces exerted by ball-socket joints. Paper [**8**] also investigates the static and dynamic stability of columns under self-weight through experimental, analytical, and numerical approaches. Study [**9**] addresses the impact of geometric and load imperfections on column buckling. Research [**10**] evaluates the influence of end-restraints, modelled as linear rotational and translational springs, and proposes the introduction of a new standard due to the significant discrepancies found with existing ones. In [**11**], variational iterative method is applied for columns with variable cross-sections. Singh [**12**] focuses on functionally graded (FG) non-uniform columns. These are replaced equivalently with columns of constant material and geometric properties. Study [**13**] examines the buckling behaviour of geometrically imperfect columns, utilizing 3D printing so ideal geometries are perturbed with their eigenshape for the experimental investigations. Article [**14**] also relies on additive manufacturing to produce high-precision columns for buckling behavioral testing. Study [**15**] explores optimization strategies against buckling in the presence of initial imperfections.

Regarding the concept of the Green function, its first appearance dates back to Green's 1828 publication [**16**], which included the Green theorem, presented the Green function with application to electrostatic problems determined by partial differential equations. Bocher extended the Green function definition for two-point boundary value problems (BVPs) governed by ordinary differential equations in [**17**]. Book [**18**] systematically covers the Green function concept. Early works [**19**, **20**] provide definitions and properties of the Green function for two-point boundary value problems governed by ordinary linear differential equations, including a collection of the Green functions in closed form for multiple conditions. As for degenerated ordinary differential equation systems, some new findings are reported in [**21**]. For some three-point boundary value problems governed by linear ordinary differential equations of order two, the Green functions are detailed in the paper of Zhao [**22**]. Multi-point BVPs are also prevalent in the literature – see, e.g., [**23**, **24**, **25**] which establish and solve specific four-point BVPs, including singular fourth-order $p$-Laplacian equation, nonlinear BVPs using fixed points of strict set-contractions, and applications of the Leray-Schauder theorem. Article [**26**] introduces a numerical iterative algorithm for non-linear four-point BVPs. Wolfe [**27**] explores buckling using multiple theories, including global bifurcation theory, direct variational calculus, phase plane analysis, and singular perturbation

theory. These methods are compared to show how they complement each other. The bifurcation theory, in particular, employs the Green function for a classical compressed column with two supports. Khan and Al-Hayani [**28**] utilize the Adomian decomposition method in conjunction with the Green function technique to solve the non-linear buckling equations of a column in compression. This method is proven efficient and advantageous as it eliminates the need for perturbation. Huang and Li [**29**] propose an efficient technique using Fredholm integral equations instead of differential equations to address the stability of axially graded material columns with variable cross-section.

### 1.2. Vibration problems of straight beams

The issue of beam vibrations is a key area of focus with a bunch of past scientific works. For example, study [**30**] highlights transverse vibrations of buckled beams using partial differential equations that account for nonlinear mid-plane strain. The given equations are then converted into ordinary differential equations using the Galerkin method. In [**31**], the transverse vibrations of Timoshenko beams with cracks are examined, with the model comprising two segments connected by internal springs whose stiffnesses are proportional to the shear force and bending moment at the crack. The beams are place on Winkler foundation. Free vibrations of beams on an elastic Pasternak foundation with variable material properties along their length are explored in [**32**]. The equation of motion are gained by Hamilton's principle. The effect of various parameters such as geometry, material, and foundation stiffness are assessed. The study [**33**] investigates the free vibration of composite beams with higher-order shear deformation using the isogeometric collocation method. The advantage of the technique is that it requires only a single integration point per element. Double beam systems are considered in [**34**], assuming a Winkler-type layer between them. The mentioned study incorporates both rotational inertia and shearing effects. In [**35**], the focus is on large amplitude vibrations of beams on elastic foundation. Assuming Euler-Bernoulli hypothesis, the equations of motion are derived using the Hamilton principle, and solutions are obtained by means of the homotopy perturbation method. Research work [**36**] examines the free vibrations of stepped beams with intermediate elastic connections. The vibrations of multi-stepped beams with multiple concentrated elements are addressed in [**37**] using the continuous mass transfer matrix method, yielding closed-form free vibrational frequencies for Timoshenko beams. The Lumped Mass Transfer Matrix Method is introduced in [**38**] to study the free vibrations of stepped axially functionally graded beams with point masses. This method happens to be powerful and relatively simple, proving to yield efficient solutions for this particular problem. The Adomian Decomposition Method is applied to stepped beam vibrations in [**39**], yielding the same order of complexity as for a uniform beam. The technique handles an arbitrary number of steps, making it suitable for approximating tapered members. The same method's effectiveness is demonstrated in [**40**], but for beams on a viscoelastic foundation.

Systems made of multiple beams are analyzed in [**41**] from the perspective of transverse free and forced vibrations. It is assumed that there is visco-elastic connection between the elements. Xie et al. [**42**] implemented an improved third-order shear deformable theory for beams made of functionally graded materials. The loading is a moving, concentrated one. A direct numerical integration technique was applied to analyze the dynamic response and address convergence issues. Talik et al. [**43**] present a novel method to reduce multi-point correlated random excitation terms to a single modal excitation term for beam vibrations. The equations of motion for a Timoshenko beam with concentrated mass under large, forced vibrations are demonstrated in [**44**]. The conservation of energy principle is used in the investigations, and the dynamic response is determined via the Newmark method. Article [**45**] addresses self-weight loaded columns and cables through analytical and numerical solutions

with a finite element software. In [**46**], the non-linear extended Timoshenko theory is applied to bi-material beams which undergo both mechanical and thermal loads.

Forced vibrations of beams with damping effects are investigated in [**47**], where steady-state Green functions are given using the variable separation technique. It is concluded that for beams with a height-to-length ratio above 0.1, the Euler-Bernoulli model is not accurate enough. The forced vibration of Euler-Bernoulli beams at resonance condition is studied in [**48**] using Fourier transformation to the frequency domain. Closed-form solution is obtained via the Fredholm Alternative Theorem. In [**49**], the thermo-elastic dynamic analysis of micro- and nanobeams is presented. The related coupled equations are decoupled using the Green function method, making the model suitable for determining free vibrations, forced vibration displacements, and temperature fields. The Green functions are found using the eigenfunction expansion and Laplace transform methods, solving the resulting decoupled Fredholm integral equation with the kernel function method. Dynamic response of damped Timoshenko beams to bending and torsion are investigated in [**50**]. The Green functions are given for arbitrary boundary conditions via the Laplace transform method.

### 1.3. Stability investigations on arches

The study of buckling in beams, initiated by Euler [**51**], has spurred extensive research and numerous models in the literature. Due to their initial curvature, curved beams behave differently under mechanical loads compared to straight beams, which has attracted significant interest from researchers. The use of curved beams is increasing in popularity for their beneficial mechanical behavior under compression and their aesthetic appeal in contemporary architecture. Curved beams are widely employed in the aerospace, civil, and marine engineering sectors [**52**,**53**]. Numerous studies have examined the behavior of curved beams to provide engineers with practical knowledge about their stability. Classical theories, such as those developed by Simitses and Timoshenko, predict elastic buckling loads and provide approximations for the classical buckling load for sinusoidal shallow arches under evenly distributed loads [**54**, **55**]. Since then, researchers have expanded these approaches, resulting in closed-form solutions and finite element method analyses under various assumptions, like in [**56**, **57**]. Accurate prediction of buckling loads is essential for resistance design [**58**].

The stability of a uniform half-sine shallow arch was examined under static loading in a thermal environment in [**59**]. The kinematical theory is a modified Euler-Bernoulli hypothesis, assuming large transverse displacements. The axial force is assumed to be constant along the arch axis. The effect of concentrated, uniform and asymmetrically distributed mechanical loads were examined by tracking the equilibrium paths. In paper [**60**] an analytical model is presented from the virtual work principle capable to handle the in-plane elastic stability of a shallow parabolic arches. These are supported by horizontal springs that and are subjected to uniformly distributed load. Several investigations have examined the effect of concentrated forces at the crown point of arches [**61**, **62**, **63**, **64**]. These studies aim to improve the design against collapse. Numerical studies have also shown that the position of the radial load notably affects the non-linear equilibrium and limit-point buckling load [**65**, **66**]. The in-plane elastic static stability of circular beams with cross-sectional inhomogeneity when exposed to a vertical load at the crown point, was investigated in [**67**]. The critical loads both for symmetric snap-through and antisymmetric bifurcation buckling are assessed. The effect of an arbitrary load on fixed supports is addressed in [**68**]. The in-plane stability of rotationally restrained shallow arches subjected to temperature variations and a vertical uniform load was investigated by Cai et al [**69**]. The nonlinear equilibrium and buckling equations were established using the virtual work principle. Analytical solution for the nonlinear in-plane symmetric and asymmetric bifurcation critical loads were

found. Temperature variations had a considerable impact on the critical loads for both the symmetric snap-through and asymmetric bifurcation modes.

Understanding the factors influencing arch buckling, including load type, material properties, and arch geometry, is vital. Incorporating these factors into the design process enables engineers to develop arches better equipped to resist buckling, ensuring structural safety and stability. Early investigations into the influence of geometric imperfections on the stability of shallow arches are documented in references [**70**] and [**71**]. A more recent study, outlined in reference [**72**], highlights that slightly imperfect homogeneous shallow arches with interlayer slip may exhibit multiple unconnected remote equilibrium paths. Additionally, Yan et al. [**73**] investigated the instability observed in imperfect non-uniform circular shallow arches subjected to radial pressure. They examined how the snap-through behavior is influenced by parameters such as imperfection magnitude and mode number. Chroscielewski et al [**74**] addressed the challenge of solving nonlinear BVPs for elastic structures, specifically focusing on the post-buckling behavior of shear-deformable circular arches. Their paper discusses the numerical difficulties involved in finding solutions for these structures, particularly under highly nonlinear regimes.

## 1.4. Objectives

Based on the above literature review, the following objectives and issues are identified to be solved in my thesis.

**Objective 1.** Using the core of Green function technique, my objective can be summarized by the following points:

- To tackle the stability problem of heterogeneous beams with three supports, particularly those with intermediate spring supports. The stability problems of these beams are to be given by three-point boundary value problems.
- To develop an advanced stability analysis framework for heterogeneous beams with three supports using the Green function technique.
- To clarify the properties of the Green function for the considered three-point eigenvalue problems and provide their calculations.
- To transform the eigenvalue problems established for the critical load into eigenvalue problems governed by homogeneous Fredholm integral equations.
- Solving these integral equations numerically enables the determination of critical loads, offering fresh insights into the stability of such beams.
- To investigate the impact of the middle support position on the ultimate load bearing abilities.

**Objective 2.** Within the scope of the aforementioned discussion, my Objective 2 is articulated as follows:

- To elucidate the structure of the Green function specifically tailored for a class of four-point boundary value problems, generalizing earlier results from three-point boundary value problems.
- To utilize the constructed Green function to transform four-point eigenvalue problems into homogeneous Fredholm integral equations, with the Green function serving as the kernel.
- To calculate the eigenvalues for the free vibrations of the considered beams. To develop a solution algorithm for the eigenvalue problems governed by homogeneous Fredholm integral equations by reducing these integral equations to algebraic eigenvalue problems, which are then solved numerically.

- To provide example about the applicability of the technique, involving heterogeneous beams with four supports.
- To validate the numerical results using commercial Finite Element (FE) software.

**Objective 3.** Within the frames of what has been mentioned above, my Objective 3 is related to the application of Green function technique to study the vibration and stability of stepped heterogeneous beams. In details, my goals are

- To develop and formalize the definition of Green functions tailored specifically for coupled boundary value problems. To clarify the intrinsic properties of these Green functions and devise methodologies for calculating their specific elements.
- To demonstrate the application of these Green functions to stepped heterogeneous beams with two supports. To focus on beams fixed and pinned at both endpoints, covering scenarios both with and without axial loads.
- To calculate the eigenfrequencies for both unloaded and axially loaded stepped beams.
- To transform the eigenvalue problems into homogeneous Fredholm integral equations, solve these numerically, and provide accurate eigenfrequency data.
- To assess the impact of axial tensile or compressive loads by replacing classical eigenvalue problems with Fredholm integral equations.
- To provide detailed analysis and numerical solutions to stability problems, ensuring the robustness of the Green function approach in various loading conditions.
- To validate the proposed methods and solutions by comparing them with results obtained from other established methods, such as finite element analysis.

**Objective 4.** It is my Objective 4 to incorporate geometrical imperfections into a one-dimensional arch model to tackle the in-plane static stability of fixed arches subjected to radial concentrated load. My investigations have the following aims:

- To assemble a geometrically non-linear mechanical model that accounts for initial shape error in order to assess the arch sensitivity to this kind of imperfection.
- To derive the equilibrium equations from a variational principle.
- To solve these equations analytically.
- To identify the limit points on the non-linear equilibrium path and analyze the effects of geometric parameters on the critical load. To extend the analysis to include various arch geometries to provide a comprehensive understanding of their stability behavior.

CHAPTER 2

# Stability of straight beams with three supports with a Green function technique

## 2.1. Differential equations

**2.1.1. Governing equations.** We will consider three heterogeneous beams, each with three supports. The middle one is a linear spring. These are referred to in short as FssF (fixed-spring supported-fixed), FssP (fixed-spring supported-pinned), and PssP (pinned-spring supported-pinned) beams. They are shown in Figure 2.1. The beams have uniform cross section throughout their longitudinal axis. The centerline coincides with the axis $\hat{x}$ of the coordinate system $\hat{x}, \hat{y}, \hat{z}$. Its origin is at the left end of the centerline. It is assumed that the coordinate plane $\hat{x}\hat{z}$ is a symmetry plane of the beams, while $\hat{y}$ is a major principal axis of the cross-section. The modulus of elasticity $E$ satisfies the relation $E(\hat{y}, \hat{z}) = E(-\hat{y}, \hat{z})$. Such case is called cross-sectional heterogeneity (or inhomogeneity). The length of the beam is $L$, the position of the middle support is identified by the coordinate $\hat{b}$.

Equilibrium problems of such beams – the axial force $N$ is zero – are governed by the ordinary differential equation [**75**]:

$$\frac{\mathrm{d}^4 \hat{w}}{\mathrm{d}\hat{x}^4} = \frac{\hat{f}_z}{I_{ey}} \tag{2.1.1}$$

where $\hat{w}(\hat{x})$ is the vertical displacement of the ($E$-weighted) centerline, $\hat{f}_z(\hat{x})$ is the intensity of the distributed load reduced to the centerline and $I_{ey}$ is the bending stiffness, given by

$$I_{ey} = \int_A E(\hat{y}, \hat{z}) \hat{z}^2 \, \mathrm{d}A \,. \tag{2.1.2}$$

If $E$ is constant, i.e., the beam is homogeneous then

$$I_{ey} = IE, \qquad I = \int_A \hat{z}^2 \, \mathrm{d}A \tag{2.1.3}$$

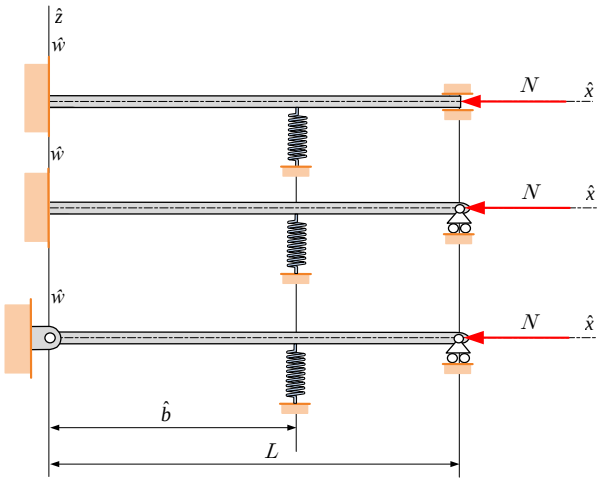


FIGURE 2.1. The considered heterogeneous beams.

in which $I$ is the moment of inertia to $\hat{y}$.

In what follows we shall use dimensionless variables defined by the following relations

$$\begin{aligned} x = \hat{x}/L, \qquad \xi = \hat{\xi}/L, \qquad w = \hat{w}/L, \\ y = \frac{\mathrm{d}\hat{w}}{\mathrm{d}\hat{x}} = \frac{\mathrm{d}w}{\mathrm{d}x}, \qquad b = \hat{b}/\hat{\ell}\,, \qquad \ell = \frac{x}{L}\Big|_{x=L} = 1\,, \end{aligned} \tag{2.1.4}$$

where $\hat{\xi}$ is also a coordinate measured on the axis $\hat{x}$ with the same origin as for $\hat{x}$. Applying dimensionless quantities to equation (2.1.1) we have

$$\frac{\mathrm{d}^4 w}{\mathrm{d}x^4} = f_z\,, \qquad f_z = \frac{L^3 \hat{f}_z}{I_{ey}} \tag{2.1.5}$$

This equation is paired with the boundary and continuity conditions of Table 21.

TABLE 21. Boundary and continuity conditions.

| Boundary conditions | | |
|---|---|---|
| Fixed-fixed beam | Fixed-pinned beam | Pinned-pinned beam |
| with an intermediate spring support | | |
| (FssF beam) | (FssP beam) | (PssP beam) |
| $w(0) = 0\,,\ w^{(1)}(0) = 0$ | $w(0) = 0\,,\ w^{(1)}(0) = 0$ | $w(0) = 0\,,\quad w^{(2)}(0) = 0$ |
| $w(\ell) = 0\,,\ w^{(1)}(\ell) = 0$ | $w(\ell) = 0\,,\ w^{(2)}(\ell) = 0$ | $w(\ell) = 0\,,\ w^{(2)}(\ell) = 0$ |
| Continuity conditions | | |
| $w(b-0) = w(b+0)\,,$ <br> $w^{(1)}(b-0) = w^{(1)}(b+0)\,,$ <br> $w^{(2)}(b-0) = w^{(2)}(b+0)\,,$ <br> $w^{(3)}(b-0) - \chi w(b) = w^{(3)}(b+0)\,.$ | | |

Here it has been taken into account that

$$\frac{d^3\hat{w}}{d\hat{x}^3}\Big|_{(\hat{b}-0)} - \hat{\chi}\hat{w}(\hat{b}) = \frac{d^3\hat{w}}{d\hat{x}^3}\Big|_{(\hat{b}+0)}; \qquad \hat{\chi} = \frac{k}{I_{ey}}\,,$$

where $k$ is the rigidity of the spring, and

$$\chi = \frac{k}{I_{ey}} L^3 = \hat{\chi} L^3.$$

We remark that the general solution of the homogeneous differential equation

$$w^{(4)} = 0\,, \qquad w^{(n)} = \begin{cases} w & \text{if } n = 0 \\ \dfrac{\mathrm{d}^n w}{\mathrm{d}x^n} & \text{if } n = 1, 2, \ldots \end{cases} \tag{2.1.6a}$$

is very simple with the $a_i$ integration constants:

$$w = \sum_{\ell=1}^{4} a_\ell w_\ell(x) = a_1 + a_2 x + a_3 x^2 + a_4 x^3\,. \tag{2.1.6b}$$

If we know the Green function $G(x, \xi)$ of the boundary value problem (2.1.5), 21 the solution for the dimensionless deflection $w$ is given by the integral

$$w(x) = \int_0^\ell G(x, \xi) f_z(\xi)\, \mathrm{d}\xi\,. \tag{2.1.7}$$

The Green functions we shall need are presented in Section 2.2.

**2.1.2. Stability issue.** Equilibrium problems of axially loaded, uniform heterogeneous beams are governed by

$$w^{(4)} \pm \mathcal{N}\, w^{(2)} = f_z, \qquad \mathcal{N} = L^2 \frac{N}{I_{ey}}, \tag{2.1.8}$$

when the axial force $N$ is constant ($N > 0$ for compression).

If the stability problem is considered the axial force is compressive and $f_z = 0$. We have, therefore, three eigenvalue problems (one for each beam shown in Table 21 ) – the eigenvalue sought is $\mathcal{N}$ – determined by the differential equation

$$w^{(4)} = -\mathcal{N}\, w^{(2)} \tag{2.1.9}$$

and the boundary and continuity conditions in Table 21. If we write $-\mathcal{N}\, w^{(2)}$ for $f_z$ in (2.1.7) we get

$$w(x) = -\mathcal{N} \int_0^\ell G(x,\xi) \frac{\mathrm{d}^2 w(\xi)}{\mathrm{d}\xi^2}\, \mathrm{d}\xi = -\mathcal{N} \left( G(x,\xi) \frac{\mathrm{d}w(\xi)}{\mathrm{d}\xi}\bigg|_{\xi=0}^{\ell} - \int_0^\ell \frac{\partial G(x,\xi)}{\partial \xi} \frac{\mathrm{d}w(\xi)}{\mathrm{d}\xi}\, \mathrm{d}\xi \right)$$

where

$$G(x,\xi) \frac{\mathrm{d}w(\xi)}{\mathrm{d}\xi}\bigg|_{\xi=0}^{\ell} = 0$$

since the Green function should satisfy the boundary conditions. Thus,

$$w(x) = \mathcal{N} \int_0^\ell \frac{\partial G(x,\xi)}{\partial \xi} \frac{\mathrm{d}w(\xi)}{\mathrm{d}\xi}\, \mathrm{d}\xi\,.$$

After derivation, is is found that

$$\frac{\mathrm{d}w}{\mathrm{d}x} = \mathcal{N} \int_0^\ell \frac{\partial^2 G(x,\xi)}{\partial x\, \partial \xi} \frac{\mathrm{d}w(\xi)}{\mathrm{d}\xi}\, \mathrm{d}\xi\,.$$

Now with the new variables:

$$\frac{\mathrm{d}w}{\mathrm{d}x} = y, \qquad \frac{\partial^2 G(x,\xi)}{\partial x\, \partial \xi} = \mathcal{K}(x,\xi) \tag{2.1.10}$$

we get a homogeneous Fredholm integral equation:

$$y(x) = \mathcal{N} \int_0^\ell \mathcal{K}(x,\xi)\, y(\xi)\, d\xi \tag{2.1.11}$$

In this way the eigenvalue problems are reduced to eigenvalue problems governed by homogeneous Fredholm integral equations. The above steps are based on [**19**]. Differential equation (2.1.9) can be rewritten in the form

$$K(w) = \lambda M(w); \qquad K(w) = w^{(4)}, \quad M(w) = -w^{(2)}, \quad \lambda = \mathcal{N}\,. \tag{2.1.12}$$

The exact solution $w(x)$ is a comparative function, while the differential operator $K(w)$ and the eigenvalue problems mentioned are self-adjoint.

## 2.2. Green function definition and construction for three-point BVPs

**2.2.1. Definition.** We shall consider the inhomogeneous ordinary differential equation

$$L[y(x)] = r(x)\,, \tag{2.2.1}$$

where the differential operator of order $2k$ is defined by

$$L[y(x)] = \sum_{n=0}^{2k} p_n(x) y^{(n)}(x). \tag{2.2.2}$$

Here, $k$ is a natural number, the functions $p_n(x)$ and $r(x)$ are continuous and $p_{2k}(x) \neq 0$ if $x \in [0, \ell]$ ($\ell > 0$). Moreover let $b$ an inner point in the interval $[0, \ell]$: $b = \ell_1$, $\ell - b = \ell_2$ and $\ell_1 + \ell_2 = \ell$.

We assume the inhomogeneous differential equation (2.2.1) is paired with the homogeneous boundary and continuity conditions:

$$\begin{aligned} \sum_{n=0}^{2k} \alpha_{nrI} y_I^{(n-1)}(0) = 0\,, \qquad & r = 1, 2, \ldots, k \\ \sum_{n=0}^{2k} \beta_{nrI} y_I^{(n-1)}(b) - \sum_{n=0}^{2k} \beta_{nrII} y_{II}^{(n-1)}(b) = 0\,, \qquad & r = 1, 2, ...., 2k \\ \sum_{n=0}^{2k} \gamma_{nrII} y_{II}^{(n-1)}(\ell) = 0\,. \qquad & r = 1, 2, \ldots, k \end{aligned} \tag{2.2.3}$$

The Latin subscripts $I$ and $II$ refer successively to the intervals $[0, b]$ and $[b, \ell]$: $y_I$ and $y_{II}$ are the solutions to the differential equation in the interval $I$ and $II$. While $\alpha_{nrI}$, $\beta_{nrI}$, $\beta_{nrII}$ and $\gamma_{nrII}$ are arbitrary constants.

Solution of (2.2.1), (2.2.2) and (2.2.3) is sought as

$$y(x) = \int_0^\ell G(x, \xi) r(\xi) d\xi\,, \tag{2.2.4}$$

where the function $G(x, \xi)$ is the Green function defined by the following formulas and properties [**76**, **77**]:
Formulae:

$$G(x, \xi) = \begin{cases} G_{1I}(x, \xi) & \text{if } x, \xi \in [0, \ell], \\ G_{2I}(x, \xi) & \text{if } x \in [b, \ell] \text{ and } \xi \in [0, \ell], \\ G_{1II}(x, \xi) & \text{if } x \in [0, b] \text{ and } \xi \in [b, \ell], \\ G_{2II}(x, \xi) & \text{if } x, \xi \in [b, \ell]. \end{cases} \tag{2.2.5}$$

Properties:
1. The function $G_{1I}(x, \xi)$ is a continuous function of $x$ and $\xi$ if $0 \leq x \leq \xi \leq b$ and $0 \leq \xi \leq x \leq b$. In addition it is $2k$ times differentiable with respect to $x$ and the derivatives

$$\frac{\partial^n G_{1I}(x, \xi)}{\partial x^n} = G_{1I}(x, \xi)^{(n)}(x, \xi)\,, \qquad n = 1, 2, \ldots, 2k \tag{2.2.6}$$

are also continuous functions of $x$ and $\xi$ in the triangles $0 \leq x \leq \xi \leq b$ and $0 \leq \xi \leq x \leq b$.
2. Let $\xi$ be fixed in $[0, b]$. The function $G_{1I}(x, \xi)$ and its derivatives

$$G_{1I}^{(n)}(x, \xi) = \frac{\partial^n G_{1I}(x, \xi)}{\partial x^n}\,, \qquad n = 1, 2, \ldots, 2k - 2 \tag{2.2.7}$$

should be continuous for $x = \xi$:

$$\begin{aligned} \lim_{\varepsilon \to 0} \left[ G_{1I}^{(n)}(\xi + \varepsilon, \xi) - G_{1I}^{(n)}(\xi - \varepsilon, \xi) \right] = \\ = \left[ G_{1I}^{(n)}(\xi + 0, \xi) - G_{1I}^{(n)}(\xi - 0, \xi) \right] = 0\,, \quad n = 0, 1, 2, \ldots 2k - 2 \end{aligned} \tag{2.2.8a}$$

The derivative $G_{1I}^{(2k-1)}(x, \xi)$ should, however, have a jump if $x = \xi$:

$$\begin{aligned} \lim_{\varepsilon \to 0} \left[ G_{1I}^{(2k-1)}(\xi + \varepsilon, \xi) - G_{1I}^{(2k-1)}(\xi - \varepsilon, \xi) \right] = \\ = \left[ G_{1I}^{(2k-1)}(\xi + 0, \xi) - G_{1I}^{(2k-1)}(\xi - 0, \xi) \right] = \frac{1}{p_{2k}(\xi)}\,. \end{aligned} \tag{2.2.8b}$$

In contrast to this, $G_{2I}(x,\xi)$ and its derivatives

$$G_{2I}^{(n)}(x,\xi) = \frac{\partial^n G_{2I}(x,\xi)}{\partial x^n}\,, \qquad n = 1,2,\ldots,2k \tag{2.2.9}$$

are all continuous functions for any $x$ in $[b,\ell]$.
3. Let $\xi$ be fixed in $[b,\ell]$. The function $G_{1II}(x,\xi)$ and its derivatives

$$G_{1II}^{(n)}(x,\xi) = \frac{\partial^n G_{1II}(x,\xi)}{\partial x^n}\,, \qquad n = 1,2,\ldots,2k \tag{2.2.10}$$

are all continuous functions for any $x$ in $[0,b]$.
4. Though the function $G_{2II}(x,\xi)$ and its derivatives

$$G_{2II}^{(n)}(x,\xi) = \frac{\partial^n G_{2II}(x,\xi)}{\partial x^n}\,, \qquad n = 1,2,\ldots,2k-2 \tag{2.2.11}$$

are also continuous for $x = \xi$:

$$\begin{aligned}\lim_{\varepsilon\to 0}\Big[G_{2II}^{(n)}(\xi+\varepsilon,\xi) - G_{2II}^{(n)}(\xi-\varepsilon,\xi)\Big] = \\ = \Big[G_{2II}^{(n)}(\xi+0,\xi) - G_{2II}^{(n)}(\xi-0,\xi)\Big] = 0\,, \quad n = 0,1,2,\ldots 2k-2\end{aligned} \tag{2.2.12a}$$

the derivative $G_{2II}^{(2k-1)}(x,\xi)$ should, however, have a jump if $x = \xi$:

$$\begin{aligned}\lim_{\varepsilon\to 0}\Big[G_{2II}^{(2k-1)}(\xi+\varepsilon,\xi) - G_{21I}^{(2k-1)}(\xi-\varepsilon,\xi)\Big] = \\ = \Big[G_{2II}^{(2k-1)}(\xi+0,\xi) - G_{2II}^{(2k-1)}(\xi-0,\xi)\Big] = \frac{1}{p_{2k}(\xi)}\,.\end{aligned} \tag{2.2.12b}$$

5. Let $\alpha$ be an arbitrary but finite non-zero constant. For a fixed $\xi \in [0,\ell]$ the product $G(x,\xi)\alpha$ as a function of $x$ ($x \neq \xi$) should satisfy the homogeneous differential equation

$$L\left[G(x,\xi)\alpha\right] = 0\,.$$

6. The product $G(x,\xi)\alpha$ as a function of $x$ should satisfy both the boundary conditions and the continuity conditions

$$\begin{aligned}\textstyle\sum_{n=1}^{2k} \alpha_{nrI}\, G^{(n-1)}(0) = 0\,, &\qquad r = 1,\ldots,k \\ \textstyle\sum_{n=1}^{2\kappa} \left(\beta_{nrI}\, G^{(n-1)}(b-0) - \beta_{nrII}\, G^{(n-1)}(b+0)\right) = 0\,, &\qquad r = 1,\ldots,2k \\ \textstyle\sum_{n=1}^{2k} \gamma_{nrII}\, G^{(n-1)}(\ell) = 0\,. &\qquad r = 1,\ldots,k\end{aligned} \tag{2.2.13}$$

The above continuity conditions should be satisfied by the function pairs $G_{1I}(x,\xi)$, $G_{2I}(x,\xi)$ and $G_{1II}(x,\xi)$, $G_{2II}(x,\xi)$ as well.

Integral (2.2.4) satisfies differential equation and boundary conditions (2.2.3). Because the BVP (2.2.1) and (2.2.3) is self-adjoint, the Green function is symmetric [**76**]:

$$G(x,\xi) = G(\xi,x)\,. \tag{2.2.14}$$

In Subsections 2.2.2, 2.2.3 and 2.2.4 we present the Green functions for the boundary conditions of Table 21. The calculations are detailed for FssF case only.

### 2.2.2. Green function for FssF beams.

2.2.2.1. *Calculation of the Green function if* $\xi \in [0, b]$. As regards the form $G_{1I}(x, \xi)$, it is distinguished as

$$\begin{aligned} G_{1I}(x,\xi) &= \sum_{m=1}^{4} (a_{mI}(\xi) + b_{mI}(\xi)) w_m(x), \qquad x \le \xi \\ G_{1I}(x,\xi) &= \sum_{m=1}^{4} (a_{mI}(\xi) - b_{mI}(\xi)) w_m(x), \qquad x \ge \xi \end{aligned} \tag{2.2.15}$$

if $x \in [0, b]$. Otherwise, it has the structure

$$G_{2I}(x,\xi) = \sum_{m=1}^{4} c_{mI}(\xi) w_m(x), \tag{2.2.16}$$

if $x \in [b, \ell]$. The coefficients $a_{mI}(\xi), b_{mI}(\xi)$ and $c_{mI}(\xi)$ are unknown functions, $w_m(x)$ is defined in Eq. (2.1.6b).

This representation for $G_{1I}(x, \xi)$ and $G_{2I}(x, \xi)$ ensures the fulfillment of the above listed properties.

The related continuity and discontinuity conditions (2.2.8) return

$$\sum_{m=1}^{4} b_{mI}(\xi) w_m^{(n)}(\xi) = 0, \qquad n = 0, 1, 2 \tag{2.2.17a}$$

$$\sum_{m=1}^{4} b_{mI}(\xi) w_m^{(3)}(\xi) = -\frac{1}{2}. \tag{2.2.17b}$$

For FssF beams equations (2.2.17a) and (2.2.17b) are

$$\begin{bmatrix} 1 & \xi & \xi^2 & \xi^3 \\ 0 & 1 & 2\xi & 3\xi^2 \\ 0 & 0 & 2 & 6\xi \\ 0 & 0 & 0 & 6 \end{bmatrix} \begin{bmatrix} b_{1I} \\ b_{2I} \\ b_{3I} \\ b_{4I} \end{bmatrix} = \begin{bmatrix} 0 \\ 0 \\ 0 \\ -\frac{1}{2} \end{bmatrix}, \tag{2.2.18}$$

yielding

$$b_{1I} = \frac{\xi^3}{12}, \quad b_{2I} = -\frac{\xi^2}{4}, \quad b_{3I} = \frac{\xi}{4}, \quad b_{4I} = \frac{1}{12}. \tag{2.2.19}$$

Note that the results for $b_{mI}$ are independent of the boundary conditions.

As per Property 6, $G_{1I}(x, \xi)$ and $G_{2I}(x, \xi)$ should satisfy the boundary and continuity conditions. This condition returns the following equations:

(i) Boundary conditions at $x = 0$:

$$\begin{aligned} a_{1I} w_1(0) + a_{2I} w_2(0) + a_{3I} w_3(0) + a_{4I} w_4(0) = \\ = -b_{1I} w_1(0) - b_{2I} w_2(0) - b_{3I} w_3(0) - b_{4I} w_4(0), \end{aligned} \tag{2.2.20a}$$

$$\begin{aligned} a_{1I} w_1^{(1)}(0) + a_{2I} w_{2I}^{(1)}(0) + a_{3I} w_3^{(1)}(0) + a_{4I} w_4^{(1)}(0) = \\ = -b_{1I} w_1^{(1)}(0) - b_{2I} w_2^{(1)}(0) - b_{3I} w_3^{(1)}(0) - b_{4I} w_4^{(1)}(0). \end{aligned} \tag{2.2.20b}$$

(ii) Continuity conditions at $x = b$:

$$\begin{aligned} a_{1I} w_1(b) + a_{2I} w_2(b) + a_{3I} w_3(b) + a_{4I} w_4(b) = \\ = b_{1I} w_1(b) + b_{2I} w_2(b) + b_{3I} w_3(b) + b_{4I} w_4(b), \end{aligned} \tag{2.2.20c}$$

$$c_{1I} w_1(b) + c_{2I} w_2(b) + c_{3I} w_3(b) + c_{4I} w_4(b) = 0, \tag{2.2.20d}$$

$$a_{1I}w_1^{(1)}(b)+a_{2I}w_{2I}^{(1)}(b)+a_{3I}w_3^{(1)}(b)+a_{4I}w_4^{(1)}(b)- \\ -c_{1I}w_1^{(1)}(b)-c_{2I}w_2^{(1)}(b)-c_{3I}w_3^{(1)}(b)-c_{4I}w_4^{(1)}(b)= \\ =b_{1I}w_1^{(1)}(b)+b_{2I}w_2^{(1)}(b)+b_{3I}w_3^{(1)}(b)+b_{4I}w_4^{(1)}(b)\,, \quad (2.2.20e)$$

$$a_{1I}w_1^{(3)}(b)+a_{2I}w_{2I}^{(3)}(b)+a_{3I}w_3^{(3)}(b)+a_{4I}w_4^{(3)}(b)- \\ -c_{1I}w_1^{(3)}(b)-c_{2I}w_2^{(3)}(b)-c_{3I}w_3^{(3)}(b)-c_{4I}w_4^{(3)}(b)- \\ -\chi(c_{1I}w_1(b)+c_{2I}w_2(b)+c_{3I}w_3(b)+c_{4I}w_4(b))= \\ =b_{1I}w_1^{(3)}(b)+b_{2I}w_2^{(3)}(b)+b_{3I}w_3^{(3)}(b)+b_{4I}w_4^{(3)}(b) \quad (2.2.20f)$$

(iii) Boundary conditions at $x=\ell$:

$$c_{1I}w_1(\ell)+c_{2I}w_2(\ell)+c_{3I}w_3(\ell)+c_{4I}w_4(\ell)=0\,, \quad (2.2.20g)$$

$$c_{1I}w_1^{(1)}(\ell)+c_{2I}w_2^{(1)}(\ell)+c_{3I}w_3^{(1)}(\ell)+c_{4I}w_4^{(1)}(\ell)=0\,. \quad (2.2.20h)$$

After the solutions are found for the linear system of equations, they are plugged back to the formula for $G_{1I}(x,\xi)$ so that

$$G_{1I}(x,\xi)=\sum_{\ell=1}^{4}\left(a_{\ell I}(\xi)\pm b_{\ell I}(\xi)\right)w_\ell(x)=\left(-\frac{\xi^3}{12}\pm\frac{1}{12}\xi^3\right)+\left(\frac{3}{12}\xi^2\pm\left(-\frac{3\xi^2}{12}\right)\right)x+ \\ +\left(\frac{3}{12}\xi\frac{3\ell^4-12\ell^3\xi+6\ell^2\xi^2+\chi b\left(\ell-b\right)^3\left(b^2\ell-3b\ell\xi+\ell\xi^2+\xi^2b-\xi b^2\right)}{\ell\left(\chi b^3\left(\ell-b\right)^3+3\ell^3\right)}\pm\frac{3\xi}{12}\right)x^2+ \\ +\left(-\frac{1}{12}\frac{12\ell\xi^3-18\ell^2\xi^2+3\ell^4+\chi\left(\ell-b\right)^3\left(b^3\ell+\ell\xi^3-3b^2\xi^2-3b\ell\xi^2+3\xi^3b\right)}{\ell\left(\chi b^3\left(\ell-b\right)^3+3\ell^3\right)}\pm\frac{-1}{12}\right)x^3 \quad (2.2.21a)$$

As regards $G_{2I}(x,\xi)$ the result is

$$G_{2I}(x,\xi)=\sum_{\ell=1}^{4}c_{\ell I}(\xi)w_\ell(x)= \\ =-\frac{1}{4}\frac{\xi^2}{\ell}\frac{\left(x-\ell\right)^2}{\chi b^3\left(\ell-b\right)^3+3\ell^3}\left(2\xi\ell^2-6x\ell^2+4x\xi\ell+\chi b^2\left(\ell-b\right)^2\left(b-x\right)\left(\xi-b\right)\right) \quad (2.2.21b)$$

2.2.2.2. *Calculation of the Green function if* $\xi\in[b,\ell]$. The following notations are applied:

If $x\in[b,\ell]$ then

$$G_{2II}(x,\xi)=\sum_{m=1}^{4}(a_{mII}(\xi)+b_{mII}(\xi))w_m(x), \qquad x\le\xi \\ G_{2II}(x,\xi)=\sum_{m=1}^{4}(a_{mII}(\xi)-b_{mII}(\xi))w_m(x), \qquad x\ge\xi \quad (2.2.22)$$

however, if $x\in[0,b]$ then

$$G_{1II}(x,\xi)=\sum_{m=1}^{4}c_{mII}(\xi)w_m(x), \quad (2.2.23)$$

where the coefficients $a_{mII}(\xi), b_{mII}(\xi)$ and $c_{mII}(\xi)$ are unknown. Continuity and discontinuity conditions (2.2.12) determine an equation system for the unknowns $b_{mII}(\xi)$, $c_{mII}(\xi)$

$m = 1, 2, 3, 4$. It holds that $b_{mII}(\xi) = b_{mI}(\xi)$.

(i) Boundary conditions at $x = 0$:

$$c_{1II}w_1(0) + c_{2II}w_2(0) + c_{3II}w_3(0) + c_{4II}w_4(0) = 0\,. \tag{2.2.24a}$$

$$c_{1II}w_1^{(1)}(0) + c_{2II}w_2^{(1)}(0) + c_{3II}w_3^{(1)}(0) + c_{4II}w_4^{(1)}(0) = 0\,, \tag{2.2.24b}$$

(ii) Continuity conditions at $x = b$:

$$c_{1II}w_1(b) + c_{2II}w_2(b) + c_{3II}w_3(b) + c_{4II}w_4(b) = 0\,, \tag{2.2.24c}$$

$$\begin{aligned} a_{1II}w_1(b) + a_{2II}w_2(b) + a_{3II}w_3(b) + a_{4II}w_4(b) = \\ = -b_{1II}w_1(b) - b_{2II}w_2(b) - b_{3II}w_3(b) - b_{4II}w_4(b), \end{aligned} \tag{2.2.24d}$$

$$\begin{aligned} a_{1II}w_1^{(1)}(b) + a_{2II}w_{2I}^{(1)}(b) + a_{3II}w_3^{(1)}(b) + a_{4II}w_4^{(1)}(b) - \\ - c_{1II}w_1^{(1)}(b) - c_{2II}w_2^{(1)}(b) - c_{3II}w_3^{(1)}(b) - c_{4II}w_4^{(1)}(b) \\ = -b_{1II}w_1^{(1)}(b) - b_{2II}w_2^{(1)}(b) - b_{3II}w_3^{(1)}(b) - b_{4II}w_4^{(1)}(b)\,, \end{aligned} \tag{2.2.24e}$$

$$\begin{aligned} - a_{1II}w_1^{(3)}(b) - a_{2II}w_{2I}^{(3)}(b) - a_{3II}w_3^{(3)}(b) - a_{4II}w_4^{(3)}(b) - \\ + c_{1II}w_1^{(3)}(b) + c_{2II}w_2^{(3)}(b) + c_{3II}w_3^{(3)}(b) + c_{4II}w_4^{(3)}(b)) + \\ + \chi\left(c_{1II}w_1(b) + c_{2II}w_2(b) + c_{3II}w_3(b) + c_{4II}w_4(b)\right) = \\ = b_{1II}w_1^{(3)}(b) + b_{2II}w_2^{(3)}(b) + b_{3II}w_3^{(3)}(b) + b_{4II}w_4^{(3)}(b)\,. \end{aligned} \tag{2.2.24f}$$

(iii) Boundary conditions at $x = \ell$:

$$\begin{aligned} a_{1II}w_1(\ell) + a_{2II}w_2(\ell) + a_{3II}w_3(\ell) + a_{4II}w_4(\ell) - \\ - b_{1II}w_1(\ell) - b_{2II}w_2(\ell) - b_{3II}w_3(\ell) - b_{4II}w_4(\ell) = 0\,, \end{aligned} \tag{2.2.24g}$$

$$\begin{aligned} a_{1II}w_1^{(1)}(\ell) + a_{2II}w_2^{(1)}(\ell) + a_{3II}w_3^{(1)}(\ell) + a_{4II}w_4^{(1)}(\ell) - \\ - b_{1II}w_1^{(1)}(\ell) - b_{2II}w_2^{(1)}(\ell) - b_{3II}w_3^{(1)}(\ell) - b_{4II}w_4^{(1)}(\ell) = 0\,. \end{aligned} \tag{2.2.24h}$$

Since $c_{1II} = c_{2II} = 0$ the last equation system has the following form:

$$\begin{bmatrix} 1 & b & b^2 & b^3 & -b^2 & -b^3 \\ 0 & 1 & 2b & 3b^2 & -2b & -3b^2 \\ 0 & 0 & 2 & 6b & -2 & -6b \\ 0 & 0 & 0 & -6 & -\chi b^2 & -\chi b^3 + 6 \\ 1 & \ell & \ell^2 & \ell^3 & 0 & 0 \\ 0 & 1 & 2\ell & 3\ell^2 & 0 & 0 \end{bmatrix} \begin{bmatrix} a_{1II} \\ a_{2II} \\ a_{3II} \\ a_{4II} \\ c_{3II} \\ c_{4II} \end{bmatrix} = \frac{1}{12} \begin{bmatrix} -\xi^3 + 3b\xi^2 - 3b^2\xi + b^3 \\ 3\xi^2 - 6b\xi + 3b^2 \\ -6\xi + 6b \\ -6 \\ \xi^3 - 3\xi^2\ell + 3\xi\ell^2 - \ell^3 \\ -3\xi^2 + 6\xi\ell - 3\ell^2 \end{bmatrix} \tag{2.2.25}$$

Solution of the above yields the coefficients, that makes it possible to construct the terms $G_{1II}(x, \xi)$ and $G_{2II}(x, \xi)$ as

$$\begin{aligned} G_{1II}(x, \xi) &= \sum_{\ell=1}^{4} c_{\ell I}(\xi) w_\ell(x) = \\ &= -\frac{1}{4}\frac{x^2}{\ell}\frac{(\xi - \ell)^2}{\chi b^3 (\ell - b)^3 + 3\ell^3}\left(2x\ell^2 - 6\xi\ell^2 + 4x\xi\ell + b^2\chi (b - \ell)^2 (\xi - b)(b - x)\right) \end{aligned} \tag{2.2.26a}$$

and

$$
\begin{aligned}
G_{2II}(x,\xi) &= \sum_{\ell=1}^{4} \left(a_{\ell II}(\xi) \pm b_{\ell II}(\xi)\right) w_\ell(x) = \\
&= -\frac{1}{12}\frac{3\ell^3\xi^3 + \chi b^3\left(\ell^3\xi^3 + \ell^3 b^3 + b^3\xi^3 - 3b^3\xi^2\ell - 3b^2\ell^3\xi - 3b\ell^2\xi^3 + 6b^2\xi^2\ell^2\right)}{\chi b^3\left(\ell - b\right)^3 + 3\ell^3} \pm \frac{\xi^3}{12} + \\
&+ \left(\frac{3}{12}\frac{3\ell^3\xi^2 + \chi b^3\left(b^2\ell^3 + 2b^2\xi^3 + 3b\xi^2\ell^2 - 3b\ell\xi^3 + \ell^3\xi^2 - 3b\ell^3\xi - b^3\xi^2\right)}{\chi b^3\left(\ell - b\right)^3 + 3\ell^3} \pm \frac{-3\xi^2}{12}\right) x + \\
&+ \left(\frac{3}{12}\frac{3\ell^4\xi - 12\ell^3\xi^2 + 6\ell^2\xi^3}{\ell\left(\chi b^3\left(\ell - b\right)^3 + 3\ell^3\right)} + \right. \\
&\left. + \frac{3}{12}\frac{\chi b^3\left(\ell^4\xi - 4\ell^3\xi^2 + 2\ell^2\xi^3 - 2b^2\ell^3 - b^3\ell\xi - b^2\xi^3 + b^3\xi^2 + \ell^2 b^3 + 3b\ell^3\xi\right)}{\ell\left(\chi b^3\left(\ell - b\right)^3 + 3\ell^3\right)} \pm \frac{3\xi}{12}\right) x^2 + \\
&+ \left(\frac{1}{12}\frac{18\xi^2\ell^2 - 3\ell^4 - 12\ell\xi^3}{\ell\left(\chi b^3\left(\ell - b\right)^3 + 3\ell^3\right)} x^3 + \right. \\
&\left. + \frac{1}{12}\frac{\chi b^3\left(3b\xi^3 - 3b^2\xi^2 + 3b\ell^3 - 9b\ell^2\xi + 6\xi^2\ell^2 - 4\ell\xi^3 + 6b^2\xi\ell - b^3\ell - \ell^4\right)}{\ell\left(\chi b^3\left(\ell - b\right)^3 + 3\ell^3\right)} \pm \frac{-1}{12}\right) x^3
\end{aligned}
\tag{2.2.26b}
$$

Figure 2.2 displays the Green function of an FssF beam if $L = 100$ mm, $\hat{\xi} = 75$ mm as function of the dimensionless spring constant $\chi$. If $(\chi = 0)$ $[\chi \to \infty]$ the beam behaves as if it were a (fixed-fixed beam,see Table 8.1 in [**78**]) [fixed-fixed beam with an intermediate roller support, see Fig. 2 in paper [**77**]for a comparison]. The graphs that show the Green function are the continuous lines, and the markers are the computed values.

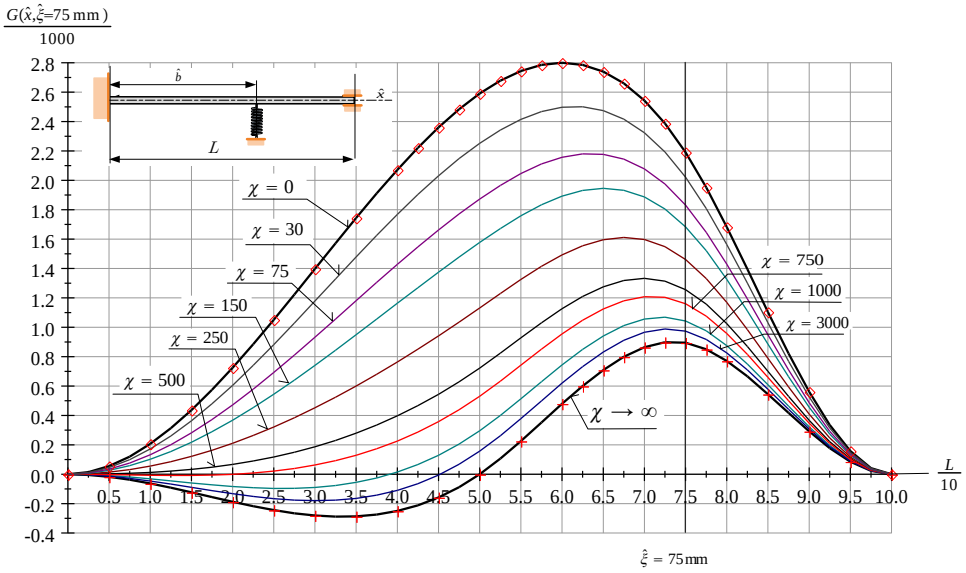


FIGURE 2.2. The Green function of an FssF beam.

**2.2.3. Green function for FssP beams.** Repeating the calculation steps detailed in Subsection 2.2.2 but now for FssP beams, it is now simple to find the following four elements of the Green function:

$$G_{1I}(x,\xi)=\sum_{\ell=1}^{4}\left(a_{\ell I}(\xi)\pm b_{\ell I}(\xi)\right)w_\ell(x)=\left(-\frac{\xi^3}{12}\pm\frac{\xi^3}{12}\right)+\left(\frac{3\xi}{12}\pm\left(-\frac{3\xi^2}{12}\right)\right)x+$$
$$+\left(\frac{3}{12}\xi\frac{12\ell\left(\ell^2+\xi^2-3\xi\ell\right)-\chi b\left(b-\ell\right)^2\left(b^3-4b^2\ell-2\xi^2b+12b\ell\xi-4\ell\xi^2\right)}{\chi b^3\left(4\ell-b\right)\left(b-\ell\right)^2+12\ell^3}\pm\frac{3\xi}{12}\right)x^2+$$
$$+\left(\frac{1}{12}\frac{12\xi^2\left(3\ell-\xi\right)-12\ell^3}{\chi b^3\left(4\ell-b\right)\left(b-\ell\right)^2+12\ell^3}+\right.$$
$$\left.+\frac{1}{12}\frac{\chi\left(b-\ell\right)^2\left(b^4-4b^3\ell+6b^2\xi^2-8\xi^3b+12\xi^2b\ell-4\xi^3\ell\right)}{\chi b^3\left(4\ell-b\right)\left(b-\ell\right)^2+12\ell^3}\pm\frac{-1}{12}\right)x^3, \tag{2.2.27a}$$

$$G_{2I}(x,\xi)=\sum_{m=1}^{4}c_{mI}(\xi)w_m(x)=\frac{1}{2}\left(\ell-x\right)\xi^2\left(\frac{2\left(6x\ell^2-2\ell^2\xi-3x^2\ell-2\ell\xi x+\xi x^2\right)}{\chi b^3\left(4\ell-b\right)\left(\ell-b\right)^2+12\ell^3}+\right.$$
$$\left.+\frac{\chi b^2\left(b-x\right)\left(\ell-b\right)\left(2\ell-b-x\right)\left(b-\xi\right)}{\chi b^3\left(4\ell-b\right)\left(\ell-b\right)^2+12\ell^3}\right), \tag{2.2.27b}$$

$$G_{1II}(x,\xi)=\sum_{m=1}^{4}c_{mII}(\xi)w_m(x)=\frac{1}{2}\left(\ell-\xi\right)x^2\left(\frac{2\left(6\xi\ell^2-2\ell^2x-3\xi^2\ell-2\ell x\xi+x\xi^2\right)}{\chi b^3\left(4\ell-b\right)\left(\ell-b\right)^2+12\ell^3}+\right.$$
$$\left.+\frac{\chi b^2\left(b-\xi\right)\left(\ell-b\right)\left(2\ell-b-\xi\right)\left(b-x\right)}{\chi b^3\left(4\ell-b\right)\left(\ell-b\right)^2+12\ell^3}\right), \tag{2.2.27c}$$

$$G_{2II}(x,\xi)=\sum_{\ell=1}^{4}\left(a_{\ell II}(\xi)\pm b_{\ell II}(\xi)\right)w_\ell(x)=$$
$$=-\frac{1}{12}\frac{12\ell^3\xi^3+\chi b^3\left(b^3\xi^3-9b\ell^2\xi^3-6b^3\xi^2\ell-12b^2\xi\ell^3+4\ell^3\xi^3+18b^2\ell^2\xi^2+4b^3\ell^3\right)}{\chi b^3\left(4\ell-b\right)\left(\ell-b\right)^2+12\ell^3}\pm\frac{\xi^3}{12}+$$
$$+\left(\frac{3}{12}\frac{12\ell^3\xi^2+\chi b^3\left(4b^2\ell^3-12b\xi\ell^3+4\ell^3\xi^2+9b\ell^2\xi^2+2b^2\xi^3-b^3\xi^2-6b\ell\xi^3\right)}{\chi b^3\left(4\ell-b\right)\left(\ell-b\right)^2+12\ell^3}\pm\frac{-3\xi^2}{12}\right)x+$$
$$+\left(\frac{3}{12}\frac{12\ell\xi\left(\xi^2-3\ell\xi+\ell^2\right)}{\chi b^3\left(4\ell-b\right)\left(\ell-b\right)^2+12\ell^3}+\right.$$
$$\left.+\frac{3}{12}\frac{\chi b^3\left(9b\xi\ell^2-12\ell^2\xi^2+4\ell\xi^3+2b^3\ell-b^3\xi+4\xi\ell^3-6b^2\ell^2\right)}{\chi b^3\left(4\ell-b\right)\left(\ell-b\right)^2+12\ell^3}\pm\frac{3\xi}{12}\right)x^2+$$
$$+\left(-\frac{1}{12}\frac{12\left(\xi^3-3\ell\xi^2+\ell^3\right)}{\chi b^3\left(4\ell-b\right)\left(\ell-b\right)^2+12\ell^3}-\right.$$
$$\left.-\frac{1}{12}\frac{\chi b^3\left(4\ell^3-9b\ell^2+18b\xi\ell-12\xi^2\ell-6b^2\xi+4\xi^3+b^3\right)}{\chi b^3\left(4\ell-b\right)\left(\ell-b\right)^2+12\ell^3}\pm\frac{-1}{12}\right)x^3. \tag{2.2.27d}$$

**2.2.4. Green function for PssP beams.** As regards PssP beams the following equations constitute the Green functions:

$$G_{1I}(x,\xi)=\sum_{\ell=1}^{4}\left(a_{\ell I}(\xi)\pm b_{\ell I}(\xi)\right)w_\ell(x)=\left(-\frac{\xi^3}{12}\pm\frac{\xi^3}{12}\right)+$$

$$+\left(\frac{1}{12}\xi\frac{12\ell^3+6\xi^2\ell-9\ell^2\xi+\chi b\left(\ell-b\right)^2\left(4b^2\ell-3b\ell\xi+2\xi^2\ell+\xi^2b-b^3\right)}{\ell\left(\chi b^2\left(\ell-b\right)^2+3\ell\right)}\pm\left(-\frac{3\xi^2}{12}\right)\right)x+$$
$$+\left(-\frac{3\xi}{12}\pm\frac{3\xi}{12}\right)x^2+\left(-\frac{1}{12}\frac{3\ell^2-6\ell\xi+\chi\left(\ell-b\right)^2\left(b^2\ell-2b\ell\xi-\xi b^2+\xi^3\right)}{\ell\left(\chi b^2\left(\ell-b\right)^2+3\ell\right)}\pm\frac{-1}{12}\right)x^3, \tag{2.2.28a}$$

$$G_{2I}(x,\xi)=\sum_{\ell=1}^{4}c_{\ell I}(\xi)w_\ell(x)=\frac{\xi}{12}\frac{1}{\ell\left(\chi b^2\left(\ell-b\right)^2+3\ell\right)}\Big(6\ell\left(\ell-x\right)\left(2x\ell-x^2-\xi^2\right)+$$
$$+\chi b\left(b-x\right)\left(\ell-x\right)\left(\ell-b\right)\left(2\ell-b-x\right)\left(b^2-\xi^2\right)\Big), \tag{2.2.28b}$$

$$G_{1II}(x,\xi)=\sum_{\ell=1}^{4}c_{\ell II}(\xi)w_\ell(x)=\frac{x}{12}\frac{1}{\ell\left(\chi b^2\left(\ell-b\right)^2+3\ell\right)}\Big(6\ell\left(\ell-\xi\right)\left(2\xi\ell-\xi^2-x^2\right)+$$
$$+\chi b\left(b-\xi\right)\left(\ell-\xi\right)\left(\ell-b\right)\left(2\ell-b-\xi\right)\left(b^2-x^2\right)\Big) \tag{2.2.28c}$$

$$G_{2II}(x,\xi)=\sum_{\ell=1}^{4}\left(a_{\ell II}(\xi)\pm b_{\ell II}(\xi)\right)w_\ell(x)=$$
$$=-\frac{1}{12}\frac{3\ell\xi^3-\chi b^2\left(2b^2\ell^2\xi-\ell^2\xi^3-3\ell b^2\xi^2+2b\ell\xi^3-\ell b^4+b^4\xi\right)}{\chi b^2\left(\ell-b\right)^2+3\ell}\pm\frac{\xi^3}{12}+$$
$$+\left(\frac{1}{12}\frac{3\ell\xi\left(2\xi^2-3\ell\xi+4\ell^2\right)}{\ell\left(\chi b^2\left(\ell-b\right)^2+3\ell\right)}+\right.$$
$$\left.+\frac{1}{12}\frac{\chi b^2\left(3\ell^3\xi^2-8b\ell^3\xi+2\ell^3b^2+6b\xi^2\ell^2-4b\ell\xi^3+\ell b^4-b^4\xi+b^2\xi^3\right)}{\ell\left(\chi b^2\left(\ell-b\right)^2+3\ell\right)}\pm\frac{-3\xi^2}{12}\right)x+$$
$$+\left(\frac{3}{12}\frac{-3\ell\xi+\chi b^2\left(\xi^3+2b\xi\ell-3\xi^2\ell+\xi\ell^2-b^2\ell\right)}{\chi b^2\left(\ell-b\right)^2+3\ell}\pm\frac{3\xi}{12}\right)x^2+$$
$$+\left(-\frac{1}{12}\frac{3\ell^2-6\ell\xi+\chi b^2\left(-b^2\xi+\xi^3+\ell^3-2b\ell^2+4b\xi\ell-3\xi^2\ell\right)}{\ell\left(\chi b^2\left(\ell-b\right)^2+3\ell\right)}\pm\frac{-1}{12}\right)x^3. \tag{2.2.28d}$$

Note that the Green functions given by equations (2.2.21) and (2.2.26) (FssF beams), (2.2.27) (FssP beams), (2.2.28) (PssP beams) are dimensionless quantities. However, if we write $\hat{b}$, $L$, $\hat{x}$, $\hat{\xi}$ and $\hat{\chi}$ for $b$, $\ell$, $x$, $\xi$ and $\chi$ in these formulae we obtain the Green function for the case when we use a selected length unit. Then the unit of the Green function is the cube of the length unit selected and the displacement field $\hat{w}(\hat{x})$ due to the distributed load $f_z(\hat{x})$ is given by the relation

$$\hat{w}(\hat{x})=\frac{1}{I_{ey}}\int_0^L G(\hat{x},\hat{\xi})f_z(\hat{\xi})\mathrm{d}\xi\,. \tag{2.2.29}$$

## 2.3. Stability problem of beams

**2.3.1. Solution procedure.** There are several methods to find the critical loads. Likewise, one can solve the eigenvalue problem numerically with, e.g., the boundary element

technique, or alternatively, one can find the related characteristic equations to be solved numerically. The use of the boundary element technique is preferred hereinafter while the characteristic equation will serve as benchmark. The solution procedure is detailed in book [**78**]. It is noted that the interval $[0, 1]$ was divided into 40 quadratic elements. A Fortran 90 code was developed. The resulting algebraic eigenvalue problem was solved with the subroutine DGVLRG.

The kernel in equation (2.1.11) takes the structure

$$\mathcal{K}(x,\xi) = \begin{cases} \mathcal{K}_{1I}(x,\xi) & \text{if } x,\xi \in [0,\ell], \\ \mathcal{K}_{2I}(x,\xi) & \text{if } x \in [b,\ell] \text{ and } \xi \in [0,\ell], \\ \mathcal{K}_{1II}(x,\xi) & \text{if } x \in [0,b] \text{ and } \xi \in [b,\ell], \\ \mathcal{K}_{2II}(x,\xi) & \text{if } x,\xi \in [b,\ell], \end{cases} \tag{2.3.1a}$$

where

$$\begin{aligned} \mathcal{K}_{1I}(x,\xi) &= \frac{\partial^2 G_{1I}(x,\xi)}{\partial x\,\partial\xi}, \qquad & \mathcal{K}_{2I}(x,\xi) &= \frac{\partial^2 G_{2I}(x,\xi)}{\partial x\,\partial\xi}, \\ \mathcal{K}_{1II}(x,\xi) &= \frac{\partial^2 G_{1II}(x,\xi)}{\partial x\,\partial\xi}, \qquad & \mathcal{K}_{2II}(x,\xi) &= \frac{\partial^2 G_{2II}(x,\xi)}{\partial x\,\partial\xi}. \end{aligned} \tag{2.3.1b}$$

### 2.3.2. Numerical results.

2.3.2.1. *FssF beams.* Figure 2.3 illustrates the dimensionless critical force $\sqrt{\mathcal{N}_{\text{crit}}}/\pi$ of a FssF beam for multiple values of $b$, and $\chi$. The graph shows that when $\chi = 0$, so there is no middle support, the beam behaves as a standard fixed-fixed beam, yielding a constant critical force of 2.0. As $\chi$ increases, indicating a stiffer intermediate support, the critical force rises continuously and significantly. Peak values are found at $b = 0.5$. For very high values of $\chi$, the beam behaves as if it had a nearly rigid support at the midpoint, substantially increasing the critical force the beam can withstand.

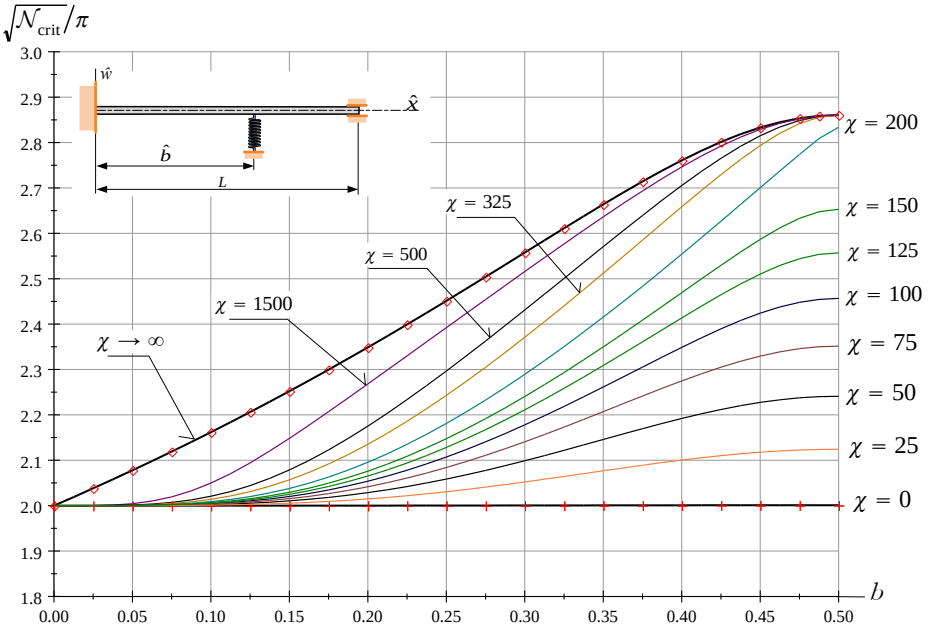


FIGURE 2.3. The dimensionless critical force for an FssF beam.

2.3.2.2. *FssP beams.* Figure 2.4 shows the dimensionless critical force for FssP beams against $b$. Unlike FssF beams, which exhibit symmetric behavior around $b = 0.5$, fixed-pinned beams show that the critical buckling force is influenced by the position of the intermediate support $b$, with the maximum resistance to buckling occurring when $b$ is placed around 0.63. For $\chi = 0$, the results for fixed-pinned beam are retrieved, with a constant

critical force of 1.4303. As $\chi$ approaches infinity, the beam behaves as if it has a rigid intermediate support, with the critical force peaking at approximately 2.458 (see Figure 7 in [**77**] for comparison). This trend reflects that intermediate supports, particularly at mid-span, can drastically enhance the buckling resistance.

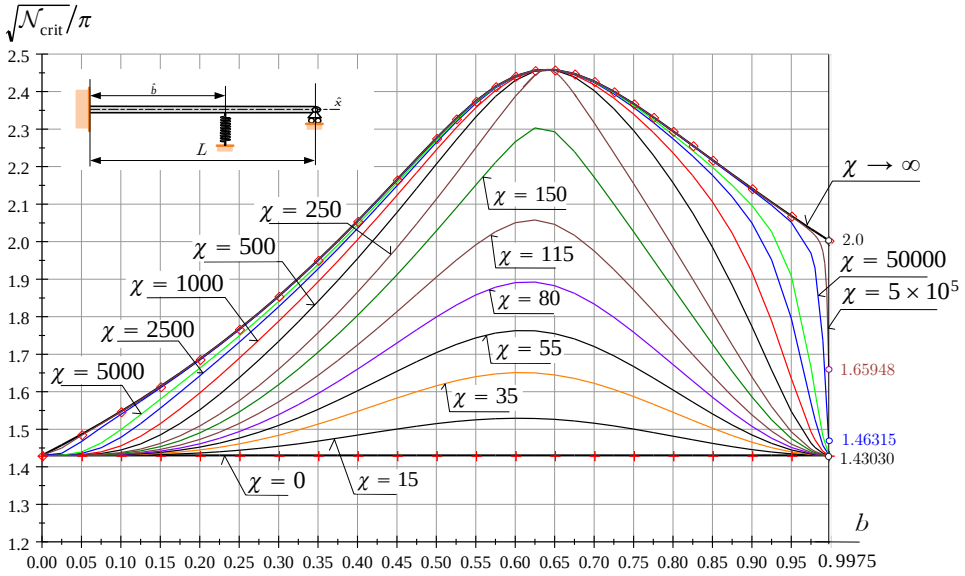


FIGURE 2.4. The dimensionless critical force for an FssP beam.

2.3.2.3. *PssP beams.* Figure 2.5 illustrates the dimensionless critical force for PssP beams as a function of the support position $b$. When $\chi = 0$, the beam behaves as a simple pinned-pinned beam, yielding a dimensionless critical force of $\sqrt{\mathcal{N}_{\text{crit}}}/\pi = 1.0$. In this configuration, the dimensionless critical force reaches its maximum at $b = 0.5$. As $\chi$ approaches infinity, the beam behaves as if it had a rigid intermediate support, yielding a critical force peak at approximately 2.0.

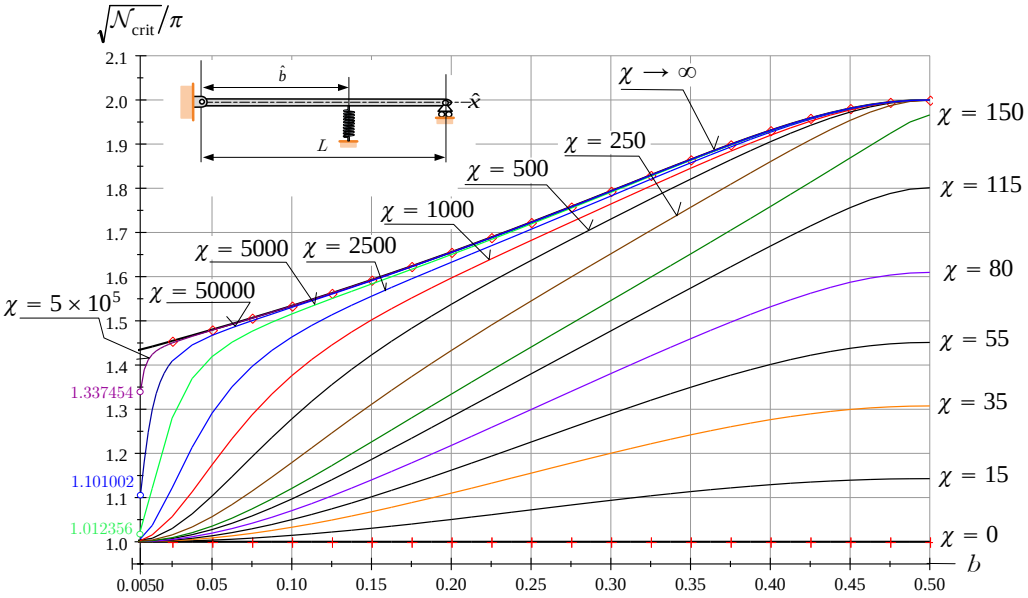


FIGURE 2.5. The dimensionless critical force for a PssP beam.

**2.3.3. Example.** Consider now a PssP beam with a rectangular cross-section as shown in Figure 2.6. It is assumed that $a = c = 100$ mm, $a_1 = a_2 = a/3$, $L = 2$ m, $E_1 = E_{\text{aluminium}} \approx 7.0 \cdot 10^4$ N/mm$^2$ while $E_2 = E_{\text{steal}} \approx 2.1 \cdot 10^5$ N/mm$^2$. The length $L$ of the beam is 2000 mm.

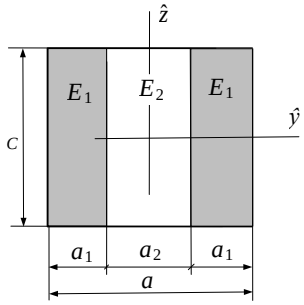


FIGURE 2.6. The cross-section of an FssF beam

Under these conditions

$$I_{ey} = \frac{c^3}{12}(2a_1E_1 + a_2E_2) = 9.722\,222 \times 10^{11}\ \mathrm{N/mm^2} \tag{2.3.2}$$

It will also be assumed that $k = 12.0 \times 10^3$ N/mm. Then

$$\chi = \frac{k}{I_{ey}}L^3 = \frac{12.0 \times 10^3}{9.722\,222 \times 10^{11}} \times 2000^3 = 98.7.$$

The dimensionless critical force for $b = 0.5$ is given by $\sqrt{\mathcal{N}_{\text{crit}}}/\pi = 1.722880$ from where, it is $\mathcal{N}_{\text{crit}} \cong 29.3$.

With $\mathcal{N}_{\text{crit}}$, equation (2.1.8) yields $N_{\text{crit}} = 7.1211 \times 10^7$ N.

TABLE 22. finite element results for PssP beams

| 3D Homogeneous beam(*Alum*) | | | 3D Heterogenous beam(*Steel* – *Alum*) | |
|---|---|---|---|---|
| | *New model*($10^5N$) | *FEM*($10^5N$) | *New model*($10^5N$) | *FEM*($10^5N$) |
| $b$ | $\chi = 165$ | | $\chi = 100$ | |
| 0 | 1.437 | 1.456 | 2.396 | 2.331 |
| 0.25 *or* 0.75 | 3.072 | 3.050 | 4.355 | 4.357 |
| 0.5 | 5.751 | 5.677 | 7.121 | 7.066 |

Table 22 compares the results of the boundary element method to commercial finite element program solutions by Ansys. In the finite element code, the beam was mapped with 480 uniform hexahedral elements (SOLID185). As per the table, there is an excellent agreement between the two sets of results.

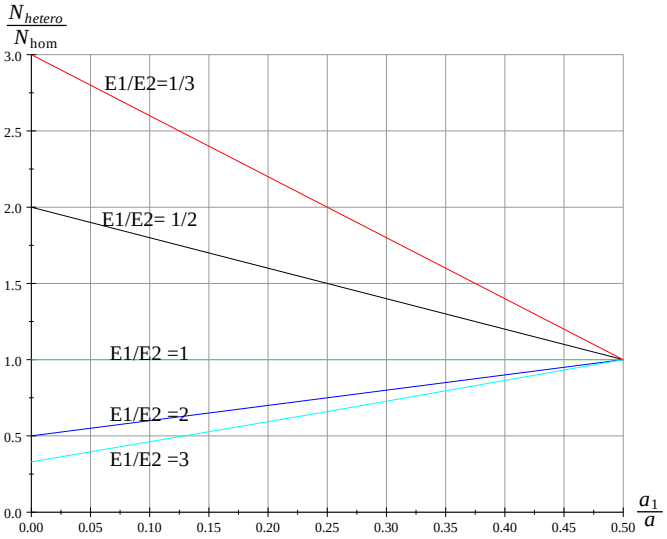


FIGURE 2.7. The effect of heterogeneity on the critical force.

Finally, Figure 2.7 illustrates the influence of cross-sectional heterogeneity shown in Figure 2.6, on the critical force. The critical load $\mathcal{N}_{\text{crit}}$ for the three-layered beam increases as the ratio $E_1/E_2$ decreases. By strategically selecting the material distribution, it is possible to improve the stiffness of the structure. It is noted this Chapter was based on the Author's publication {6}.

CHAPTER 3

# Examination of four-point boundary value problems with the Green function

## 3.1. Four-point boundary value problems

Let us consider the ordinary differential equation

$$L[y(x)] = r(x)\,. \tag{3.1.1a}$$

The order of the differential operator is $2\kappa$. The operator is defined by the following equation:

$$L[y(x)] = \sum_{n=0}^{2\kappa} p_n(x)\, y^{(n)}(x)\,. \tag{3.1.1b}$$

Here $\kappa \geq 1$ is a natural number, the functions $p_n(x)$ and $r(x)$ are continuous if $x \in [0, \ell = 1]$ ($\ell > 0$) and $p_{2\kappa}(x) \neq 0$. Further, let $b$ and $c$ be an inner points in the interval $[0, \ell = 1]$ where $0 < b < c < \ell$, $b = \ell_1$, $c - b = \ell_2$, $\ell - c = \ell_3$ and $\ell_1 + \ell_2 + \ell_3 = \ell = 1$.

The linearly independent particular solutions of (3.1.1b) are $y_\ell(x)$ ($\ell = 1, 2, \ldots, 2\kappa$). Here the $y_\ell(x)$ the general solution has the form

$$\begin{aligned}
y_I(x) &= \sum_{\ell=1}^{2\kappa} \mathcal{A}_{\ell I} y_{\ell I}(x), && \text{if } \; x \in [0, b]; \\
y_{II}(x) &= \sum_{\ell=1}^{2\kappa} \mathcal{A}_{\ell II} y_{\ell II}(x), && \text{if } \; x \in [b, c]; \\
y_{III}(x) &= \sum_{\ell=1}^{2\kappa} \mathcal{A}_{\ell III} y_{\ell III}(x), && \text{if } \; x \in [c, \ell].
\end{aligned} \tag{3.1.2}$$

$y_\ell(x) = y_{\ell I}(x) = y_{\ell_{II}}(x) = y_{\ell_{III}}(x)$. Further, $\mathcal{A}_{\ell I}$, $\mathcal{A}_{\ell II}$ and $\mathcal{A}_{\ell III}$ are undetermined constants.

The differential equation (4.1.1) is paired with the boundary and continuity conditions

$$U_{0r}[y] = \sum_{n=1}^{2\kappa} \alpha_{nrI}\, y_I^{(n-1)}(0) = 0\,, \qquad r = 1, 2, \ldots, \kappa \tag{3.1.3a}$$

$$\begin{aligned}
U_{br}[y] &= U_{brI}[y_I] - U_{brII}[y_{II}] = \\
&= \sum_{n=1}^{2\kappa} \Big( \beta_{nrI}\, y_I^{(n-1)}(b) - \beta_{nrII}\, y_{II}^{(n-1)}(b) \Big) = 0\,, \qquad r = 1, 2, \ldots, 2\kappa
\end{aligned} \tag{3.1.3b}$$

$$\begin{aligned}
U_{cr}[y] &= U_{crI}[y_{II}] - U_{crII}[y_{III}] = \\
&= \sum_{n=1}^{2\kappa} \Big( \gamma_{nrI}\, y_I^{(n-1)}(c) - \gamma_{nrII}\, y_{II}^{(n-1)}(c) \Big) = 0\,, \qquad r = 1, 2, \ldots, 2\kappa
\end{aligned} \tag{3.1.3c}$$

$$U_{1r}[y] = \sum_{n=1}^{2\kappa} \delta_{nrII}\, y_{II}^{(n-1)}(\ell) = 0\,, \qquad r = 1, 2, \ldots, \kappa \tag{3.1.3d}$$

where $\alpha_{nrI}$, $\beta_{nrI}$, $\beta_{nrII}$, $\gamma_{nrI}$, $\gamma_{nrII}$ and $\delta_{nrII}$ are real constants.

The above mentioned integration constants $\mathcal{A}_{\ell I}$, $\mathcal{A}_{\ell II}$ and $\mathcal{A}_{\ell III}$ can be found from the boundary and continuity conditions:

$$\sum_{\ell=1}^{2\kappa} \mathcal{A}_{\ell I} U_{0r}[y_{\ell I}] = 0, \qquad r = 1, 2, \ldots, \kappa \tag{3.1.4a}$$

$$\sum_{\ell=1}^{2\kappa} \left(\mathcal{A}_{\ell I} U_{brI}[y_{\ell I}] - \mathcal{A}_{\ell II} U_{brII}[y_{\ell II}]\right) = 0, \qquad r = 1, 2, \ldots, 2\kappa \tag{3.1.4b}$$

$$\sum_{\ell=1}^{2\kappa} \left(\mathcal{A}_{\ell II} U_{crI}[y_{\ell II}] - \mathcal{A}_{\ell III} U_{crII}[y_{\ell III}]\right) = 0, \qquad r = 1, 2, \ldots, 2\kappa \tag{3.1.4c}$$

$$\sum_{\ell=1}^{2\kappa} \mathcal{A}_{\ell III} U_{1r}[z_{\ell II}] = 0, \qquad r = 1, 2, \ldots, \kappa \tag{3.1.4d}$$

If the Green function $G(x, \xi)$ of the selected BVP is known, the solution can be given as

$$y(x) = \int_{\xi=0}^{\ell=1} G(x, \xi)\, r(\xi)\, \mathrm{d}\xi\,. \tag{3.1.5}$$

### 3.2. Definition of the Green function for four point BVP

The $G(x, \xi)$ Green function is defined in the forthcoming. Although the definition is similar to what was given in the former Chapter, but now there are more intervals and for this reason, it is detailed.
Formulas:

$$G(x,\xi) = \begin{cases} G_{1I}(x,\xi) & \text{if } x, \xi \in [0, b], \\ G_{2I}(x,\xi) & \text{if } x \in [b, c] \text{ and } \xi \in [0, b], \\ G_{3I}(x,\xi) & \text{if } x \in [b, \ell] \text{ and } \xi \in [0, b], \\ G_{1II}(x,\xi) & \text{if } x \in [0, b] \text{ and } \xi \in [b, c], \\ G_{2II}(x,\xi) & \text{if } x, \xi \in [b, c], \\ G_{3II}(x,\xi) & \text{if } x \in [c, \ell] \text{ and } \xi \in [b, c], \\ G_{1III}(x,\xi) & \text{if } x \in [0, b] \text{ and } \xi \in [c, \ell], \\ G_{2III}(x,\xi) & \text{if } x \in [b, c] \text{ and } \xi \in [c, \ell], \\ G_{3III}(x,\xi) & \text{if } x, \xi \in [c, \ell]. \end{cases} \tag{3.2.1}$$

Properties:
1. Let $\xi$ be fixed in $[0, b]$.
(i) The function $G_{1I}(x, \xi)$ is continuous of $x$ and $\xi$ if $0 \le x \le \xi \le b$ and $0 \le \xi \le x \le b$ – see Figure 3.1. Additionally, it is $2\kappa$ times differentiable with respect to $x$. The derivatives

$$\frac{\partial^n G_{1I}(x,\xi)}{\partial x^n} = G_{1I}(x,\xi)^{(n)}(x,\xi)\,, \qquad n = 1, 2, \ldots, 2\kappa \tag{3.2.2a}$$

are also continuous in $x$ and $\xi$ in the triangular domains $0 \le x \le \xi \le b$ and $0 \le \xi \le x \le b$.

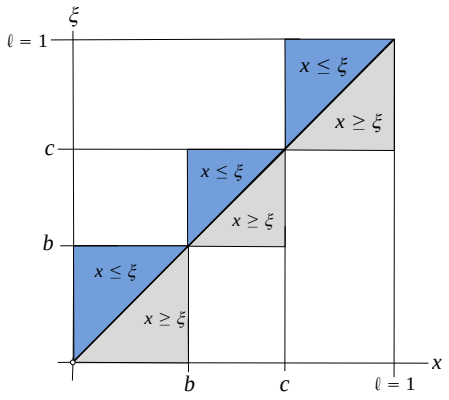


FIGURE 3.1. Triangular domains

The function $G_{1I}(x,\xi)$ and its derivatives

$$G_{1I}^{(n)}(x,\xi) = \frac{\partial^n G_{1I}(x,\xi)}{\partial x^n}\,, \qquad n = 1,2,\dots,2\kappa-2 \tag{3.2.2b}$$

are continuous for $x = \xi$:

$$\lim_{\varepsilon\to 0}\left[G_{1I}^{(n)}(\xi+\varepsilon,\xi) - G_{1I}^{(n)}(\xi-\varepsilon,\xi)\right] = \\ = \left[G_{1I}^{(n)}(\xi+0,\xi) - G_{1I}^{(n)}(\xi-0,\xi)\right] = 0 \quad n = 0,1,2,\dots 2\kappa-2. \tag{3.2.2c}$$

The derivative $G_{1I}^{(2\kappa-1)}(x,\xi)$ has a jump at $x = \xi$:

$$\lim_{\varepsilon\to 0}\left[G_{1I}^{(2\kappa-1)}(\xi+\varepsilon,\xi) - G_{1I}^{(2\kappa-1)}(\xi-\varepsilon,\xi)\right] = \\ = \left[G_{1I}^{(2\kappa-1)}(\xi+0,\xi) - G_{1I}^{(2\kappa-1)}(\xi-0,\xi)\right] = \frac{1}{p_{2\kappa}(\xi)}. \tag{3.2.2d}$$

(ii) In contrast, the function $G_{2I}(x,\xi)$ and its derivatives

$$G_{2I}^{(n)}(x,\xi) = \frac{\partial^n G_{2I}(x,\xi)}{\partial x^n}\,, \qquad n = 1,2,\dots,2\kappa \tag{3.2.2e}$$

are all continuous functions for any $x$ in $[b,c]$

(iii) The function $G_{3I}(x,\xi)$ and its derivatives

$$G_{3I}^{(n)}(x,\xi) = \frac{\partial^n G_{3I}(x,\xi)}{\partial x^n}\,, \qquad n = 1,2,\dots,2\kappa \tag{3.2.2f}$$

are also continuous for any $x$ in $[c,\ell]$.

2. Let $\xi$ be fixed in $[b,c]$.

(i) The function $G_{1II}(x,\xi)$ and its derivatives

$$G_{1II}^{(n)}(x,\xi) = \frac{\partial^n G_{1II}(x,\xi)}{\partial x^n}\,, \qquad n = 1,2,\dots,2\kappa \tag{3.2.3a}$$

are continuous for any $x$ in $[0,b]$.

(ii) The function $G_{2II}(x,\xi)$ is a continuous function of $x$ and $\xi$ if $b \le x \le \xi \le c$ and $b \le \xi \le x \le c$ – see Figure 3.1. In addition it is $2\kappa$ times differentiable with respect to $x$. The derivatives

$$\frac{\partial^n G_{2II}(x,\xi)}{\partial x^n} = G_{2II}(x,\xi)^{(n)}(x,\xi)\,, \qquad n = 1,2,\dots,2\kappa \tag{3.2.3b}$$

are also continuous in $x$ and $\xi$ in the triangular domains $b \le x \le \xi \le c$ and $b \le \xi \le x \le c$.

The function $G_{2II}(x,\xi)$ and its derivatives

$$G_{2II}^{(n)}(x,\xi) = \frac{\partial^n G_{2II}(x,\xi)}{\partial x^n}\,, \qquad n = 1,2,\ldots,2\kappa-2 \tag{3.2.3c}$$

are continuous for $x = \xi$:

$$\lim_{\varepsilon\to 0}\left[G_{2II}^{(n)}(\xi+\varepsilon,\xi) - G_{2II}^{(n)}(\xi-\varepsilon,\xi)\right] = \\ = \left[G_{2II}^{(n)}(\xi+0,\xi) - G_{2II}^{(n)}(\xi-0,\xi)\right] = 0\,, \quad n = 0,1,2,\ldots 2\kappa-2. \tag{3.2.3d}$$

The derivative $G_{2II}^{(2\kappa-1)}(x,\xi)$ has a jump at $x = \xi$:

$$\lim_{\varepsilon\to 0}\left[G_{2II}^{(2\kappa-1)}(\xi+\varepsilon,\xi) - G_{2II}^{(2\kappa-1)}(\xi-\varepsilon,\xi)\right] = \\ = \left[G_{2II}^{(2\kappa-1)}(\xi+0,\xi) - G_{2II}^{(2\kappa-1)}(\xi-0,\xi)\right] = \frac{1}{p_{2\kappa}(\xi)}. \tag{3.2.3e}$$

(iii) The function $G_{3II}(x,\xi)$ and its derivatives

$$G_{3II}^{(n)}(x,\xi) = \frac{\partial^n G_{1II}(x,\xi)}{\partial x^n}\,, \qquad n = 1,2,\ldots,2\kappa \tag{3.2.3f}$$

are continuous functions for any $x$ in $[c,\ell]$.

3. Let $\xi$ be fixed in the interval $[c,\ell]$.

(i) The function $G_{1III}(x,\xi)$ and its derivatives

$$G_{1III}^{(n)}(x,\xi) = \frac{\partial^n G_{1III}(x,\xi)}{\partial x^n}\,, \qquad n = 1,2,\ldots,2\kappa \tag{3.2.4a}$$

are continuous functions for any $x$ in $[0,b]$.

(ii) The function $G_{2III}(x,\xi)$ and its derivatives

$$G_{2III}^{(n)}(x,\xi) = \frac{\partial^n G_{2III}(x,\xi)}{\partial x^n}\,, \qquad n = 1,2,\ldots,2\kappa \tag{3.2.4b}$$

are also continuous for any $x$ in $[b,c]$.

(iii) The function $G_{3III}(x,\xi)$ is a continuous function of $x$ and $\xi$ if $c \le x \le \xi \le \ell$ and $c \le \xi \le x \le \ell$ – see Figure 3.1. In addition it is $2\kappa$ times differentiable with respect to $x$ and the derivatives

$$\frac{\partial^n G_{3III}(x,\xi)}{\partial x^n} = G_{3III}(x,\xi)^{(n)}(x,\xi)\,, \qquad n = 1,2,\ldots,2\kappa \tag{3.2.4c}$$

are also continuous functions of $x$ and $\xi$ in the triangles $c \le x \le \xi \le \ell$ and $c \le \xi \le x \le \ell$.

The function $G_{3III}(x,\xi)$ and its derivatives

$$G_{3III}^{(n)}(x,\xi) = \frac{\partial^n G_{3III}(x,\xi)}{\partial x^n}\,, \qquad n = 1,2,\ldots,2\kappa-2 \tag{3.2.4d}$$

are continuous for $x = \xi$:

$$\lim_{\varepsilon\to 0}\left[G_{3III}^{(n)}(\xi+\varepsilon,\xi) - G_{3III}^{(n)}(\xi-\varepsilon,\xi)\right] = \\ = \left[G_{3III}^{(n)}(\xi+0,\xi) - G_{3III}^{(n)}(\xi-0,\xi)\right] = 0 \quad n = 0,1,2,\ldots 2\kappa-2. \tag{3.2.4e}$$

The derivative $G_{3III}^{(2k-1)}(x,\xi)$ has a jump if $x = \xi$:

$$\lim_{\varepsilon\to 0}\left[G_{3III}^{(2\kappa-1)}(\xi+\varepsilon,\xi) - G_{3III}^{(2\kappa-1)}(\xi-\varepsilon,\xi)\right] =$$

$$= \left[G_{3III}^{(2\kappa-1)}(\xi+0,\xi) - G_{3III}^{(2\kappa-1)}(\xi-0,\xi)\right] = \frac{1}{p_{2\kappa}(\xi)}\,.$$

4. Let $\alpha$ be an arbitrary non-zero constant. For a fixed $\xi \in [0,\ell]$ value, the term $G(x,\xi)\alpha$ as a function of $x \neq \xi$ should satisfy the homogeneous differential equation

$$L\left[G(x,\xi)\alpha\right] = 0\,.$$

5. The product $G(x,\xi)\alpha$ as a function of $x$ should satisfy the boundary conditions and the continuity conditions

$$\begin{aligned}
&\sum_{n=1}^{2\kappa} \alpha_{nrI}\, G^{(n-1)}(0) = 0\,, && r = 1,\dots,\kappa\\
&\sum_{n=1}^{2\kappa} \left(\beta_{nrI}\, G^{(n-1)}(b-0) - \beta_{nrII}\, G^{(n-1)}(b+0)\right) = 0\,, && r = 1,\dots,2\kappa\\
&\sum_{n=1}^{2\kappa} \left(\gamma_{nrII}\, G^{(n-1)}(c-0) - \gamma_{nrIII}\, G^{(n-1)}(c+0)\right) = 0\,, && r = 1,\dots,2\kappa\\
&\sum_{n=1}^{2\kappa} \delta_{nrIII}\, G^{(n-1)}(\ell) = 0\,. && r = 1,\dots,\kappa
\end{aligned} \tag{3.2.5}$$

The above boundary and continuity conditions should be satisfied by the functions triplets

$$\begin{aligned}
&\{G_{1I}(x,\xi), G_{2I}(x,\xi), G_{3I}(x,\xi)\}\,,\\
&\{G_{1II}(x,\xi), G_{2II}(x,\xi), G_{3II}(x,\xi)\}\,,\\
&\{G_{1III}(x,\xi), G_{2III}(x,\xi), G_{3III}(x,\xi)\}
\end{aligned}$$

### 3.3. The Green function – calculation

**3.3.1. Elements if $\xi \in (0,b)$.** As per $G_{1I}(x,\xi)$, it is assumed that

$$\begin{aligned}
G_{1I}(x,\xi) &= \sum_{m=1}^{2\kappa} (a_{mI}(\xi) + b_{mI}(\xi)) y_m(x), && x \le \xi;\\
& && x \in [0,b].\\
G_{1I}(x,\xi) &= \sum_{m=1}^{2\kappa} (a_{mI}(\xi) - b_{mI}(\xi)) y_m(x), && x \ge \xi;
\end{aligned} \tag{3.3.1a}$$

For $G_{2I}(x,\xi)$ and $G_{3I}(x,\xi)$ the forms are

$$G_{2I}(x,\xi) = \sum_{m=1}^{2\kappa} c_{mI}(\xi) y_m(x), \qquad x \in [b,c] \tag{3.3.1b}$$

and

$$G_{3I}(x,\xi) = \sum_{m=1}^{2\kappa} d_{mI}(\xi) y_m(x) \qquad x \in [c,\ell]. \tag{3.3.1c}$$

Here the coefficients $a_{mI}(\xi), b_{mI}(\xi), c_{mI}(\xi), d_{mI}(\xi)$ are the unknown.

The corresponding continuity and discontinuity equations (3.2.2c) and (3.2.2d) yield

$$\sum_{m=1}^{2\kappa} b_{mI}(\xi) y_m^{(n)}(\xi) = 0, \quad n = 0,1,2,\dots,2\kappa-2 \tag{3.3.2a}$$

and

$$\left[G_{1I}^{(2\kappa-1)}(\xi+0,\xi)-G_{1I}^{(2\kappa-1)}(\xi-0,\xi)\right]=\frac{1}{p_{2\kappa}(\xi)}=-\sum_{m=1}^{2\kappa}b_{mI}(\xi)y_m^{(2\kappa-1)}(\xi)$$

or

$$\sum_{m=1}^{2\kappa}b_{mI}(\xi)y_m^{(2\kappa-1)}(\xi)=-\frac{1}{p_{2\kappa}(\xi)} \tag{3.3.2b}$$

The determinant of the inhomogeneous linear equation system (4.2.2) has the form:

$$\begin{vmatrix} y_1(\xi) & y_2(\xi) & \dots & y_{2\kappa}(\xi) \\ y_1^{(1)}(\xi) & y_2^{(1)}(\xi) & \dots & y_{2\kappa}^{(1)}(\xi) \\ \dots & \dots & \dots & \dots \\ y_1^{(2\kappa-1)}(\xi) & y_2^{(2\kappa-1)}(\xi) & \dots & y_{2\kappa}^{(2\kappa-1)}(\xi) \end{vmatrix}. \tag{3.3.3}$$

It represents the Wronskian of (4.1.1), which is non-zero because the particular solutions are linearly independent **[79]**. It means there exists a unique solution for the unknowns. These unknowns can be found from (3.2.5) as

$$\sum_{n=1}^{2\kappa}\alpha_{nrI}\sum_{m=1}^{2\kappa}(a_{mI}(\xi)+b_{mI}(\xi))y_m(0)=0\,,\qquad r=1,2,3,\dots,\kappa; \tag{3.3.4a}$$

$$\sum_{n=1}^{2\kappa}\left(\beta_{nrI}\sum_{m=1}^{2\kappa}(a_{mI}(\xi)-b_{mI}(\xi))y_m^{(n-1)}(b)-\beta_{nrII}\sum_{m=1}^{2\kappa}c_{mI}(\xi)y_m^{(n-1)}(b)\right)=0\,,$$
$$r=1,2,3,\dots,2\kappa; \tag{3.3.4b}$$

$$\sum_{n=1}^{2\kappa}\left(\gamma_{nrII}\sum_{m=1}^{2\kappa}c_{mI}(\xi)y_m^{(n-1)}(c)-\gamma_{nrIII}\sum_{m=1}^{2\kappa}d_{mI}(\xi)y_m^{(n-1)}(c)\right)=0\,,$$
$$r=1,2,3,\dots,2\kappa; \tag{3.3.4c}$$

$$\sum_{n=1}^{2\kappa}\left(\delta_{nrIII}\sum_{m=1}^{2\kappa}d_{mI}(\xi)y_m^{(n-1)}(\ell)\right)=0\,,\qquad r=1,2,3,\dots,\kappa. \tag{3.3.4d}$$

**3.3.2. The elements of the Green function if $\xi\in(b,c)$.** The Green function this time is given as

$$G_{1II}(x,\xi)=\sum_{m=1}^{2\kappa}c_{mII}(\xi)y_m(x),\qquad x\in[0,b]; \tag{3.3.5a}$$

$$\begin{aligned} G_{2II}(x,\xi)&=\sum_{m=1}^{2\kappa}(a_{mII}(\xi)+b_{mII}(\xi))y_m(x),\qquad x\le\xi \\ G_{2II}(x,\xi)&=\sum_{m=1}^{2\kappa}(a_{mII}(\xi)-b_{mII}(\xi))y_m(x),\qquad x\ge\xi \end{aligned}\qquad x\in[b,c]; \tag{3.3.5b}$$

$$G_{3II}(x,\xi)=\sum_{m=1}^{2\kappa}d_{mII}(\xi)y_m(x),\qquad x\in[c,\ell\,]. \tag{3.3.5c}$$

with unknowns $a_{mII}(\xi), b_{mII}(\xi)$, $c_{mII}(\xi), d_{mII}(\xi)$.

Substituting to Eqs. (3.2.3d) and (3.2.3e) yields

$$\sum_{m=1}^{2\kappa}b_{mII}(\xi)y_m^{(n)}(\xi)=0,\quad n=0,1,2,\dots,2\kappa-2 \tag{3.3.6a}$$

and

$$\sum_{m=1}^{2\kappa} b_{mII}(\xi) y_m^{(2\kappa-1)}(\xi) = -\frac{1}{p_{2\kappa}(\xi)}\,. \tag{3.3.6b}$$

This system coincides formally with (4.2.2), so it is solvable with $b_{mII}(\xi) = b_{mI}(\xi)$. Recalling the conditions (3.2.5), it becomes possible to find $a_{mII}(\xi)$, $c_{mII}(\xi)$, and $d_{mII}(\xi)$:

$$\sum_{n=1}^{2\kappa} \left( \alpha_{nrI} \sum_{m=1}^{2\kappa} c_{mII}(\xi) y_m^{(n-1)}(0) \right) = 0\,, \qquad r = 1, 2, 3, \ldots, \kappa; \tag{3.3.7a}$$

$$\sum_{n=1}^{2\kappa} \left( \beta_{nrI} \sum_{m=1}^{2\kappa} c_{mII}(\xi) y_m^{(n-1)}(b) - \beta_{nrII} \sum_{m=1}^{2\kappa} (a_{mII}(\xi) + b_{mII}(\xi)) y_m^{(n-1)}(b) \right) = 0\,,$$
$$r = 1, 2, 3, \ldots, 2\kappa; \tag{3.3.7b}$$

$$\sum_{n=1}^{2\kappa} \left( \gamma_{nrII} \sum_{m=1}^{2\kappa} (a_{mII}(\xi) - b_{mII}(\xi)) y_m^{(n-1)}(c) - \gamma_{nrIII} \sum_{m=1}^{2\kappa} d_{mII}(\xi) y_m^{(n-1)}(c) \right) = 0\,,$$
$$r = 1, 2, 3, \ldots, 2\kappa; \tag{3.3.7c}$$

$$\sum_{n=1}^{2\kappa} \left( \delta_{nrIII} \sum_{m=1}^{2\kappa} d_{mII}(\xi) y_m^{(n-1)}(\ell) \right) = 0\,, \qquad r = 1, 2, 3, \ldots, \kappa. \tag{3.3.7d}$$

**3.3.3. Elements if $\xi \in (c, \ell)$.** The elements of the Green function is collected below:

$$G_{1III}(x, \xi) = \sum_{m=1}^{2\kappa} c_{mIII}(\xi) y_m(x), \qquad x \in [0, b]; \tag{3.3.8a}$$

$$G_{2III}(x, \xi) = \sum_{m=1}^{4} d_{mIII}(\xi) y_m(x), \qquad x \in [b, c]; \tag{3.3.8b}$$

and

$$\begin{aligned} G_{3III}(x, \xi) &= \sum_{m=1}^{4} (a_{mIII}(\xi) + b_{mIII}(\xi)) y_m(x), \qquad x \le \xi \\ &\qquad\qquad\qquad\qquad\qquad\qquad\qquad\qquad , \qquad x \in [b, \ell]. \\ G_{3III}(x, \xi) &= \sum_{m=1}^{4} (a_{mIII}(\xi) - b_{mIII}(\xi)) y_m(x), \qquad x \ge \xi \end{aligned} \tag{3.3.8c}$$

$a_{mIII}(\xi)$, $a_{mIII}(\xi)$, $c_{mIII}(\xi)$ and $d_{mIII}(\xi)$ are unknowns, while $b_{mIII}(\xi) = b_{mII}(\xi) = b_{mI}(\xi)$.

Conditions (3.2.5) yield

$$\sum_{n=1}^{2\kappa} \left( \alpha_{nrI} \sum_{m=1}^{2\kappa} c_{mIII}(\xi) y_m^{(n-1)}(0) \right) = 0\,, \qquad r = 1, 2, 3, \ldots, \kappa; \tag{3.3.9a}$$

$$\sum_{n=1}^{2\kappa} \left( \beta_{nrI} \sum_{m=1}^{2\kappa} c_{mIII}(\xi) y_m^{(n-1)}(b) - \beta_{nrII} \sum_{m=1}^{2\kappa} d_{mIII}(\xi) y_m^{(n-1)}(b) \right) = 0\,,$$
$$r = 1, 2, 3, \ldots, 2\kappa; \tag{3.3.9b}$$

$$\sum_{n=1}^{2\kappa}\left(\gamma_{nrII}\sum_{m=1}^{2\kappa}d_{mI}(\xi)y_m^{(n-1)}(c)-\gamma_{nrIII}\sum_{m=1}^{2\kappa}(a_{mIII}(\xi)+b_{mIII}(\xi))y_m^{(n-1)}(c)\right)=0\,,$$
$$r=1,2,3,\ldots,2\kappa;\quad (3.3.9c)$$

$$\sum_{n=1}^{2\kappa}\left(\delta_{nrIII}\sum_{m=1}^{2\kappa}(a_{mIII}(\xi)-b_{mIII}(\xi))y_m^{(n-1)}(\ell)\right)=0\,,\qquad r=1,2,3,\ldots,\kappa.\qquad (3.3.9d)$$

### 3.4. Further properties of the Green function

**3.4.1. Self-Adjointness.** The comparison functions $u(x)\neq 0$ and $v(x)\neq 0$ satisfy the boundary and continuity conditions (3.1.3). Similarly, the solution of the four-point boundary value problem is as well comparison function. Let us define the product on operator $L$:

$$(u,v)_L=\int_a^c u(x)\,L[v(x)]\,\mathrm{d}x \qquad (3.4.1)$$

The four point BVP (4.1.1), (3.1.3) is self-adjoint if the product (4.3.2) is commutative, i.e.,

$$(u,v)_L=(v,u)_L\,. \qquad (3.4.2)$$

**3.4.2. Symmetry of the Green function.** Consider now two inhomogeneous four-point boundary value problems

$$L[u(x)]=r(x)\,,\qquad L[v(x)]=s(x) \qquad (3.4.3)$$

and

$$\begin{array}{lll} U_{0r}[u]=0, & U_{0r}[v]=0, & r=1,2,\ldots,\kappa;\\ U_{br}[u]=0, & U_{br}[v]=0, & r=1,2,\ldots,2\kappa;\\ U_{cr}[u]=0, & U_{cr}[v]=0, & r=1,2,\ldots,2\kappa;\\ U_{1r}[u]=0, & U_{1r}[v]=0, & r=1,2,\ldots,\kappa; \end{array} \qquad (3.4.4)$$

In this case, $u(x)$ and $v(x)$ are the unknown functions. It is assumed the BVPs (4.3.3), (4.3.4) are self-adjoint. Then it holds that

$$(u,v)_L-(v,u)_L=0,$$

where

$$u(x)=\int_0^\ell G(x,\xi)r(\xi)\,\mathrm{d}\xi\qquad\text{and}\qquad v(x)=\int_0^\ell G(x,\xi)s(\xi)\,\mathrm{d}\xi\,.$$

It, therefore, follows

$$(u,v)_L-(v,u)_L=\int_0^\ell(u\,L[v]-v\,L[u])\,\mathrm{d}x=$$
$$=\int_0^\ell\int_0^\ell[G(x,\xi)-G(\xi,x)]\,r(\xi)s(x)\,\mathrm{d}\xi\mathrm{d}x=0\,. \qquad (3.4.5)$$

Since both $r(x)$ and $s(x)$ are arbitrary continuous and non-zero functions in the interval $[0,\ell]$, the last integral in this equation can be zero if and only if the Green function is symmetric:

$$G(x,\xi)=G(\xi,x)\ . \qquad (3.4.6)$$

### 3.5. Four-point eigenvalue problems

The generalization of several concepts introduced in the likes of [**19**] and [**76**] are given hereinafter, which are valid for two- and three-point boundary value problems. Consider ODE

$$K\,[y] = \lambda\, M\,[y] \tag{3.5.1a}$$

where $y = y(x)$ is again the unknown function while the unknown $\lambda$ is actually the eigenvalue sought. Differential operators $K\,[y]$ and $M\,[y]$ are defined by the equations

$$\begin{aligned} K\,[y] &= \sum_{n=0}^{\kappa} (-1)^n \left[f_n(x) y^{(n)}(x)\right]^{(n)}\,, \qquad \frac{\mathrm{d}^n(\ldots)}{\mathrm{d}x^n} = (\ldots)^{(n)}\,; \\ M\,[y] &= \sum_{n=0}^{\mu} (-1)^n \left[g_n(x) y^{(n)}(x)\right]^{(n)}\,, \qquad \kappa > \mu \geq 1 \end{aligned} \tag{3.5.1b}$$

in which the real function $(f_\nu(x))$ $[g_\nu(x)]$ is assumed to be differentiable continuously $(\kappa)$ $[\mu]$ times and

$$f_\kappa(x) \neq 0\,, \qquad g_\mu(x) \neq 0 \qquad \text{if } \; x \in [0, \ell\,]\,. \tag{3.5.1c}$$

It is noticed that the order of the differential operator on the left of (4.4.1a) is greater than the order on the right. Let $x \in (0, \ell]$ be the interval where solution is sought, while $b < c$ and $c$ denote inner points in $[0, \ell]$. The typical quantities in the subintervals $[0, b]$, $[b, c]$, and $[c, \ell]$ are denoted similarly as beforehand, with indices $I$, $II$, and $III$. Some quantities within the intervals $[0, b]$, $[b, c]$, and $[c, \ell]$ are denoted in the same manner as before—see equation (4.1.2)—using the Roman subscripts $I$, $II$, and $III$.

If we perform partial integrations using the comparison functions $u(x)$ and $v(x)$ $x \in [0, \ell]$, we get

$$\begin{aligned} (u, v)_K = &\left[\sum_{n=0}^{\kappa}\sum_{r=0}^{n-1} (-1)^{(n+r)} u(x)^{(r)} \left[f_n(x)\, v^{(n)}(x)\right]^{(n-1-r)}\right]_0^{b-0} + \\ &+ \left[\sum_{n=0}^{\kappa}\sum_{r=0}^{n-1} (-1)^{(n+r)} u(x)^{(r)} \left[f_n(x)\, v^{(n)}(x)\right]^{(n-1-r)}\right]_{b+0}^{c-0} + \\ &+ \left[\sum_{n=0}^{\kappa}\sum_{r=0}^{n-1} (-1)^{(n+r)} u(x)^{(r)} \left[f_n(x)\, v^{(n)}(x)\right]^{(n-1-r)}\right]_{c+0}^{\ell} + \\ &+ \sum_{n=0}^{\kappa} \int_0^{\ell} u^{(n)}(x) f_n(x) v^{(n)}(x)\,\mathrm{d}x = \\ &= K_0(u, v) + \sum_{n=0}^{\kappa} \int_0^{\ell} u^{(n)}(x) f_n(x) v^{(n)}(x)\,\mathrm{d}x\,, \end{aligned} \tag{3.5.2a}$$

and

$$\begin{aligned} (u, v)_M = &\left[\sum_{n=0}^{\mu}\sum_{r=0}^{n-1} (-1)^{(n+r)} u(x)^{(r)} \left[g_n(x)\, v^{(n)}(x)\right]^{(n-1-r)}\right]_0^{b-0} + \\ &+ \left[\sum_{n=0}^{\mu}\sum_{r=0}^{n-1} (-1)^{(n+r)} u(x)^{(r)} \left[g_n(x)\, v^{(n)}(x)\right]^{(n-1-r)}\right]_{b+0}^{c-0} + \\ &+ \left[\sum_{n=0}^{\mu}\sum_{r=0}^{n-1} (-1)^{(n+r)} u(x)^{(r)} \left[g_n(x)\, v^{(n)}(x)\right]^{(n-1-r)}\right]_{c+0}^{\ell} + \end{aligned}$$

$$+\sum_{n=0}^{\mu}\int_0^{\ell} u^{(n)}(x)g_n(x)v^{(n)}(x)\,\mathrm{d}x =$$

$$= M_0(u,v)+\sum_{n=0}^{\mu}\int_0^{\ell} u^{(n)}(x)g_n(x)v^{(n)}(x)\,\mathrm{d}x. \tag{3.5.2b}$$

$K_0(u,v)$ and $M_0(u,v)$ are boundary and continuity expressions. If

$$K_0(u,v)=K_0(v,u) \qquad \text{and} \qquad M_0(u,v)=M_0(v,u) \tag{3.5.3}$$

then the four-point eigenvalue problem is self-adjoint. Let the $k$-th eigenvalue be $\lambda_k$ ($k=1,2,3,\ldots$). The related eigenfunction is, therefore,

$$y_k(x)=\begin{cases} y_{Ik}(x) & \text{if } x\in[0,b],\\ y_{IIk}(x) & \text{if } x\in[b,c],\\ y_{IIIk}(x) & \text{if } x\in[c,\ell]. \end{cases} \tag{3.5.4}$$

For self-adjoint BVPs, the eigenfunctions are orthogonal:

$$(y_k,y_n)_K=\begin{cases} \lambda_n\,(y_k,y_n)_M & \text{if } k=n,\\ 0 & \text{if } k\neq n. \end{cases} \qquad k,n=1,2,3\ldots\ . \tag{3.5.5}$$

The proof to this is similar as published in [**19**]. After setting $k$ and $n$ equal, we get

$$\lambda_n=\frac{(y_n,y_n)_K}{(y_n,y_n)_M} \tag{3.5.6}$$

therefore sign of the eigenvalues depends on the products $(y_n,y_n)_K$ and $(y_n,y_n)_M$. If

$$(u,u)_K>0\,, \quad \text{and} \quad (u,u)_M>0 \tag{3.5.7}$$

are satisfied for any $u$, it means that the four-point eigenvalue problem (4.4.1), (3.1.3) is positive definite.

Assuming the eigenvalue problem to be simple – that is, $M[y]=g_0(x)y(x)$ – and the Green function that belongs to the differential operator $K[y]$ is known, then

$$y(x)=\lambda\int_0^{\ell} G(x,\xi)g_0(\xi)y(\xi)\,\mathrm{d}\xi\,. \tag{3.5.8}$$

So the eigenvalue problem is replaced in this way by a homogeneous Fredholm integral equation. Given that the original eigenvalue problem is self-adjoint and positive definite, the related Fredholm integral equation becomes:

$$\mathcal{Y}(x)=\lambda\int_0^{\ell}\mathcal{K}(x,\xi)\mathcal{Y}(\xi)\,\mathrm{d}\xi\,, \tag{3.5.9}$$

where

$$\mathcal{Y}(x)=\sqrt{g_0(x)}y(x), \qquad \mathcal{K}(x,\xi)=\sqrt{g_0(x)}G(x,\xi)\sqrt{g_0(\xi)}. \tag{3.5.10}$$

Here, $\mathcal{Y}(x)$ is a new unknown with the kernel $\mathcal{K}(x,\xi)$ being symmetric.

## 3.6. Application to heterogeneous beams

**3.6.1. Governing equations.** Let us consider two uniform beams of length $L$ as shown in Figure 3.2. The notations and not specifically mentioned assumptions are the same as in the previous Chapter. This time. the beams have four supports: the first beam (FrrF) is fixed at $\hat{x}=0$ and has a slider at $\hat{x}=L$. The next beam (PrrP) is pinned at the left end and has a roller support at the right end. The two intermediate supports are rollers, identically.

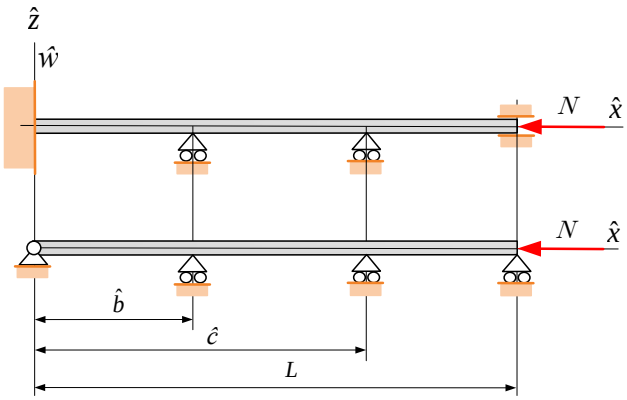


FIGURE 3.2. Heterogeneous FrrF and PrrP beams.

Traditional equilibrium problems of Euler-Bernoulli beams under a constant axial force are determined by

$$\frac{\mathrm{d}^4\hat{w}}{\mathrm{d}\hat{x}^4} \pm \hat{\mathcal{N}}\frac{\mathrm{d}^2\hat{w}}{\mathrm{d}\hat{x}^2} = \frac{\hat{f}_z}{I_{ey}}, \qquad \hat{\mathcal{N}} = \frac{N}{I_{ey}}, \tag{3.6.1}$$

Each quantity in the above equation is well defined in Chapter 2—see 2.1.1, 2.1.2, and 2.1.3. We use the dimensionless quantities defined in (2.1.4). The selected problems to be solved are the following:

(a) In case of equilibrium problems, the axial load is zero. Then Eq. (3.6.1) becomes:

$$K(w) = \frac{\mathrm{d}^4 w}{\mathrm{d}x^4} = f_z\,. \tag{3.6.2}$$

(b) In case of free vibrations, the related equation is

$$K(w) = \frac{\mathrm{d}^4 w}{\mathrm{d}x^4} = \lambda w = \lambda M(w)\,, \qquad \lambda = \frac{\rho_a A \omega^2 L^4}{I_{ey}}\,, \tag{3.6.3}$$

with $w$ as the the dimensionless amplitude and $\lambda$ as the unknown eigenvalue.

$$\rho_a = \frac{1}{A}\int_A \rho\,\mathrm{d}A \tag{3.6.4}$$

defines the average surface density and $\omega$ is the natural circular frequency.

(c) The static stability issue is formulated by

$$\frac{\mathrm{d}^4 w}{\mathrm{d}x^4} + \mathcal{N}\frac{\mathrm{d}^2 w}{\mathrm{d}x^2} = 0\,. \tag{3.6.5}$$

The dimensionless buckling load (the critical load) $\mathcal{N}$ is the unknown.

The related boundary and continuity conditions are gathered in Table 31.

TABLE 31. Boundary and Continuity conditions.

| Boundary conditions | |
|---|---|
| Fixed-fixed beam | Pinned-pinned beam |
| with two intermediate roller supports | |
| (FrrF beam) | (PrrP beam) |
| $w(0)=0\,,\quad w^{(1)}(0)=0$ | $w(0)=0\,,\ w^{(2)}(0)=0$ |
| $w(\ell)=0\,,\ w^{(1)}(\ell)=0$ | $w(\ell)=0\,,\ w^{(2)}(\ell)=0$ |
| Continuity conditions | |
| $w(b-0)=0\,,\qquad w(b+0)=0\,,$ | |
| $w^{(1)}(b-0)=w^{(1)}(b+0)\,,$ | |
| $w^{(2)}(b-0)=w^{(2)}(b+0)\,,$ | |
| $w(c-0)=0\,,\qquad w(c+0)=0\,,$ | |
| $w^{(1)}(c-0)=w^{(1)}(c+0)\,,$ | |
| $w^{(2)}(c-0)=w^{(2)}(c+0)\,.$ | |

Utilizing (3.6.3) and (4.4.2a), while accounting for the boundary and continuity conditions in Table 31, we can conclude that $(u,v)_K=(v,u)_K$. This confirms that the four-point boundary problems of equations (3.6.2) and the conditions in Table 31 are self-adjoint.

Furthermore, for equation (3.6.3), $(u,u)_K>0$ and $(u,u)_M>0$, meaning the four-point eigenvalue problems governed by equations (3.6.3) and the conditions in Table 31 are not only self-adjoint but also positive definite.

By employing the Green's functions $G(x,\xi)$ of the BVP defined by the (3.6.2), the closed-form solutions for $w(x)$ can be expressed by

$$w(x)=\int_{\xi=0}^{\ell=1} G(x,\xi)\,f(\xi)\,\mathrm{d}\xi\,. \tag{3.6.6}$$

Replacing $f(\xi)$ with $\lambda w(\xi)$ in (3.6.6) yields the homogeneous Fredholm integral equation as an alternative to (3.6.3)

$$w(x)=\lambda\int_{\xi=0}^{\ell=1} G(x,\xi)\,w(\xi)\,\mathrm{d}\xi\,. \tag{3.6.7}$$

With Eq. (2.1.10), eigenvalue problems (3.6.5) and Table 31 can be reduced to an eigenvalue problems governed by the homogeneous Fredholm integral equations of (2.1.11). As regards the details the reader is referred to 2.1.2 in Chapter 2.

### 3.6.2. Green function for FrrF beams.

3.6.2.1. *Elements of the Green function when* $\xi\in(0,b)$. The sought elements can be given in the forms (3.3.1) where $y_m(x)=w_m(x)$ stands for the particular solutions, that are

$$w_1=1,\quad w_2=x,\quad w_3=x^2,\quad w_4=x^3\,. \tag{3.6.8}$$

Equations (4.2.2) return

$$\sum_{m=1}^{4} b_{mI}(\xi)w_m^{(n)}(\xi)=0,\qquad n=0,1,2 \tag{3.6.9a}$$

$$\sum_{m=1}^{4} b_{mI}(\xi)w_m^{(3)}(\xi)=-\frac{1}{2} \tag{3.6.9b}$$

from where

$$\begin{bmatrix} 1 & \xi & \xi^2 & \xi^3 \\ 0 & 1 & 2\xi & 3\xi^2 \\ 0 & 0 & 2 & 6\xi \\ 0 & 0 & 0 & 6 \end{bmatrix} \begin{bmatrix} b_{1I} \\ b_{2I} \\ b_{3I} \\ b_{4I} \end{bmatrix} = \begin{bmatrix} 0 \\ 0 \\ 0 \\ -\frac{1}{2} \end{bmatrix}.$$

It results in the solutions

$$\begin{bmatrix} b_{1I} \\ b_{2I} \\ b_{3I} \\ b_{4I} \end{bmatrix} = \frac{1}{12} \begin{bmatrix} \xi^3 \\ -3\xi^2 \\ 3\xi \\ -1 \end{bmatrix}. \tag{3.6.10}$$

As per equations (4.2.5) $b_{mIII}(\xi) = b_{mII}(\xi) = b_{mI}(\xi)$

With Eq. (4.2.3) and the boundary and continuity conditions, unknowns $a_{mI}(\xi)$, $c_{mI}(\xi)$ and $d_{mI}(\xi)$ can be found in the following steps:

(a) Boundary conditions at $x = 0$:

$$\sum_{m=1}^{4} a_{mI} w_m(0) = -\sum_{m=1}^{4} b_{mI}(\xi)\, w_m(0)\,, \tag{3.6.11a}$$

$$\sum_{m=1}^{4} a_{mI} w_m^{(1)}(0) = -\sum_{m=1}^{4} b_{mI}(\xi)\, w_m^{(1)}(0)\,. \tag{3.6.11b}$$

(b) Continuity conditions at $x = b$:

$$\sum_{m=1}^{4} a_{mI} w_m(b) = \sum_{m=1}^{4} b_{mI}(\xi)\, w_m(b)\,, \tag{3.6.12a}$$

$$\sum_{m=1}^{4} c_{mI} w_m(b) = 0\,, \tag{3.6.12b}$$

$$\sum_{m=1}^{4} a_{mI} w_m^{(1)}(b) - \sum_{m=1}^{4} c_{mI} w_m^{(1)}(b) = \sum_{m=1}^{4} b_{mI}(\xi)\, w_m^{(1)}(b)\,, \tag{3.6.12c}$$

$$\sum_{m=1}^{4} a_{mI} w_m^{(2)}(b) - \sum_{m=1}^{4} c_{mI} w_m^{(2)}(b) = \sum_{m=1}^{4} b_{mI}(\xi)\, w_m^{(2)}(b). \tag{3.6.12d}$$

(c) Continuity conditions at $x = c$:

$$\sum_{m=1}^{4} c_{mI} w_m(c) = 0\,, \tag{3.6.13a}$$

$$\sum_{m=1}^{4} d_{mI} w_m(c) = 0\,, \tag{3.6.13b}$$

$$\sum_{m=1}^{4} c_{mI} w_m^{(1)}(c) = \sum_{m=1}^{4} d_{mI} w_m^{(1)}(c)\,, \tag{3.6.13c}$$

$$\sum_{m=1}^{4} c_{mI} w_m^{(2)}(b) = \sum_{m=1}^{4} d_{mI} w_m^{(2)}(b)\,. \tag{3.6.13d}$$

(d) Boundary conditions at $x = \ell$:

$$\sum_{m=1}^{4} d_{mI} w_m(\ell) = 0\,, \tag{3.6.14a}$$

$$\sum_{m=1}^{4} d_{mI} w_m^{(1)}(\ell) = 0\,. \tag{3.6.14b}$$

Since closed-form solutions are available for $a_{1I}, \ldots, d_{4I}$, the $G_{1I}(x,\xi)$, $G_{2I}(x,\xi)$ and $G_{3I}(x,\xi)$ elements are (3.3.1):

$$\begin{aligned} G_{1I}(x,\xi) = {} & \left(-\frac{1}{12}\xi^3 \pm \frac{1}{12}\xi^3\right) + \left(\frac{3\xi^2}{12} \pm \left(-\frac{3\xi^2}{12}\right)\right) x + \\ & + \left\{ \frac{3\xi}{12b^2 D}\left[2\xi^2\left(2b^2 - b\ell + bc - 2c\ell\right) - 4b\xi\left(2bc + b^2 - 3c\ell\right) + 3b^3 c + b^3\ell - 4b^2 c\ell\right] \pm \frac{3\xi}{12}\right\} x^2 + \\ & + \left\{ -\frac{1}{12b^3 D}\left[4\xi^3\left(3b^2 - c\ell - 2b\ell\right) - 6b\xi^2\left(2b^2 - b\ell + bc - 2c\ell\right) - \right.\right. \\ & \left.\left. - 4b^3 c\ell + b^4\ell + 3b^4 c\right] \pm \frac{-1}{12}\right\} x^3 \end{aligned} \tag{3.6.15a}$$

$$G_{2I}(x,\xi) = -\frac{1}{2b}\frac{\xi^2}{D\,(b-c)}\,(b-x)\,(c-x)\,(b-\xi)\,(cx - 2bx + b\ell - 2c\ell + x\ell + bc)\,, \tag{3.6.15b}$$

$$G_{3I}(x,\xi) = \frac{1}{2b}\frac{\xi^2}{(c-\ell)\,D}\,(b-c)\,(b-\xi)\,(c-x)\,(x-\ell)^2\,, \tag{3.6.15c}$$

where

$$D = b\ell - 4c\ell + 3bc\,. \tag{3.6.16}$$

3.6.2.2. *Elements of the Green function if* $\xi \in (b,c)$. As per Eqs. (4.2.4), the following equation system can be set up to find $a_{mII}(\xi)$, $c_{mII}(\xi)$ and $d_{mII}(\xi)$:
(a) Boundary conditions at $x = 0$:

$$\sum_{m=1}^{4} c_{mII} w_m(0) = 0\,, \tag{3.6.17a}$$

$$\sum_{m=1}^{4} c_{mII} w_1^{(1)}(0) = 0\,. \tag{3.6.17b}$$

(b) Continuity conditions at $x = b$:

$$\sum_{m=1}^{4} c_{mII} w_m(b) = 0\,, \tag{3.6.18a}$$

$$\sum_{m=1}^{4} a_{mII} w_m(b) = -\sum_{m=1}^{4} b_{mII}(\xi) w_m(b)\,, \tag{3.6.18b}$$

$$\sum_{m=1}^{4} a_{mII} w_m^{(1)}(b) - \sum_{m=1}^{4} c_{1II} w_m^{(1)}(b) = -\sum_{m=1}^{4} b_{1II}(\xi) w_m^{(1)}(b)\,, \tag{3.6.18c}$$

$$\sum_{m=1}^{4} a_{mII} w_m^{(1)}(b) - \sum_{m=1}^{4} c_{1II} w_m^{(1)}(b) = -\sum_{m=1}^{4} b_{1II}(\xi) w_m^{(1)}(b)\,. \tag{3.6.18d}$$

(c) Continuity conditions at $x = c$:

$$\sum_{m=1}^{4} a_{mII} w_m(c) = \sum_{m=1}^{4} b_{1II}(\xi) w_m(b)\,, \tag{3.6.19a}$$

$$\sum_{m=1}^{4} d_{mII} w_m(c) = 0\,, \tag{3.6.19b}$$

$$\sum_{m=1}^{4} a_{mII} w_m^{(1)}(c) - \sum_{m=1}^{4} d_{1II} w_m^{(1)}(c) = \sum_{m=1}^{4} b_{1II}(\xi) w_m^{(1)}(c)\,, \tag{3.6.19c}$$

$$\sum_{m=1}^{4} a_{mII} w_m^{(2)}(c) - \sum_{m=1}^{4} d_{1II} w_m^{(2)}(c) = \sum_{m=1}^{4} b_{1II}(\xi) w_m^{(2)}(c)\,. \tag{3.6.19d}$$

(d) Boundary conditions at $x = \ell$:

$$\sum_{m=1}^{4} d_{mII} w_m(\ell) = 0\,, \tag{3.6.20a}$$

$$\sum_{m=1}^{4} d_{mII} w_m^{(1)}(\ell) = 0\,. \tag{3.6.20b}$$

Since $c_{1II} = c_{2II} = 0$, the remaining equations make it possible to find the unknowns. Thus, one can find that

$$G_{1II}(x,\xi) = -\frac{1}{2b}\frac{x^2}{D\,(b-c)}\,(b-\xi)\,(c-\xi)\,(b-x)\,(c\xi - 2b\xi + b\ell - 2c\ell + \xi\ell + bc)\,, \tag{3.6.21a}$$

$$\begin{aligned} G_{2II}(x,\xi) = \frac{1}{12D_1}\Big[&\xi^3\left(3b^3c - 3bc^3 + b^3\ell + 4c^3\ell - 9bc^2\ell\right) - \\ &-6b^2c\xi^2\left(b\ell - 3c\ell + bc - c^2\right) - 12\ell b^2c^3\xi + 4\ell b^3c^3\Big] \pm \frac{1}{12}\xi^3 + \\ &+\left\{\frac{1}{4D_1}\Big[2b\xi^3\left(3c^2 - b\ell + 3c\ell - 3bc\right) + \xi^2\left(b^3\ell - 3bc^3 + 3b^3c - 4c^3\ell - 9bc^2\ell\right) + \right. \\ &\left. +12\ell bc^3\xi - 4\ell b^2c^3\Big] \pm \frac{-3}{12}\xi^2\right\} x + \\ &+\left\{\frac{1}{4D_1}\left[4\xi^3\left(b^2 - c\ell - c^2\right) - 4\xi^2\left(b^3 - 3c^2\ell - c^3\right) - \xi\left(3bc^3 - 3b^3c - b^3\ell + 4c^3\ell + 9bc^2\ell\right) + \right.\right. \\ &\left.\left. +2b^2c^3 + 6\ell b^2c^2 - 2b^3c^2 - 2\ell b^3c\right] \pm \frac{3}{12}\xi\right\} x^2 + \\ &+\left\{\frac{1}{12D_1}\left[4\xi^3\left(3c + \ell - 3b\right) + 12\xi^2\left(b^2 - c\ell - c^2\right) - 6b\xi\left(b\ell - 3c\ell + 3bc - 3c^2\right) + \right.\right. \\ &\left.\left. +4\ell c^3 - 9\ell bc^2 + 3b^3c - 3bc^3 + \ell b^3\right] \pm \frac{-1}{12}\right\} x^3, \end{aligned} \tag{3.6.21b}$$

$$G_{3II}(x,\xi) = -\frac{1}{2D_1\,(c-\ell)}\,(b-\xi)\,(c-x)\,(c-\xi)\,(x-\ell)^2\,(b\xi - 2c\xi + bc)\,, \tag{3.6.21c}$$

$$-\frac{1}{2D_1}\,(c-x)\,(b-\xi)\,\frac{c-\xi}{c-\ell}\,(x-\ell)^2\,(b\xi - 2c\xi + bc)$$

where

$$D_1 = (b-c)^2\,(b\ell - 4c\ell + 3bc)\,. \tag{3.6.22}$$

3.6.2.3. *Elements of the Green function if* $\xi \in (c, \ell)$. Similarly as beforehand, the functions $a_{mIII}(\xi)$, $c_{mIII}(\xi)$ and $d_{mIII}(\xi)$ can be expressed by considering:
(a) Boundary conditions at $x = 0$:

$$\sum_{m=1}^{4} c_{mIII} w_m(0) = 0\,, \tag{3.6.23a}$$

$$\sum_{m=1}^{4} c_{mIII} w_1^{(1)}(0) = 0\,. \tag{3.6.23b}$$

(b) Continuity conditions at $x = b$:

$$\sum_{m=1}^{4} c_{mIII} w_m(b) = 0\,, \tag{3.6.24a}$$

$$\sum_{m=1}^{4} d_{mIII} w_m(b) = 0\,, \tag{3.6.24b}$$

$$\sum_{m=1}^{4} c_{mIII} w_m^{(1)}(b) - \sum_{m=1}^{4} d_{1III} w_m^{(1)}(b) = 0, \tag{3.6.24c}$$

$$\sum_{m=1}^{4} c_{mIII} w_m^{(2)}(b) - \sum_{m=1}^{4} d_{1III} w_m^{(2)}(b) = 0\,. \tag{3.6.24d}$$

(c) Continuity conditions at $x = c$:

$$\sum_{m=1}^{4} d_{mIII} w_m(c) = 0\,, \tag{3.6.25a}$$

$$\sum_{m=1}^{4} a_{mIII} w_m(c) = -\sum_{m=1}^{4} b_{1III}(\xi) w_m(c)\,, \tag{3.6.25b}$$

$$\sum_{m=1}^{4} a_{mIII} w_m^{(1)}(c) - \sum_{m=1}^{4} d_{1III} w_m^{(1)}(c) = -\sum_{m=1}^{4} b_{1III}(\xi) w_m^{(1)}(c)\,, \tag{3.6.25c}$$

$$\sum_{m=1}^{4} a_{mIII} w_m^{(2)}(c) - \sum_{m=1}^{4} d_{1III} w_m^{(2)}(c) = -\sum_{m=1}^{4} b_{1III}(\xi) w_m^{(2)}(c)\,. \tag{3.6.25d}$$

(d) Boundary conditions at $x = c$:

$$\sum_{m=1}^{4} a_{mIII} w_m(c) = \sum_{m=1}^{4} b_{1III}(\xi) w_m(c)\,, \tag{3.6.26a}$$

$$\sum_{m=1}^{4} a_{mIII} w_m^{(1)}(c) = -\sum_{m=1}^{4} b_{1III}(\xi) w_m^{(1)}(c)\,. \tag{3.6.26b}$$

Since $c_{1III} = c_{2III} = 0$, the remaining unknowns can be expressed. Thus, the Green functions are

$$G_{1III}(x, \xi) = \frac{1}{2b} \frac{x^2}{(c - \ell)\, D} (b - c)(b - x)(c - \xi)(\xi - \ell)^2\,, \tag{3.6.27a}$$

$$G_{2III}(x, \xi) = -\frac{1}{2D_1 (c - \ell)} (b - x)(c - \xi)(c - x)(\xi - \ell)^2 (bx - 2cx + bc)\,, \tag{3.6.27b}$$

$G_{3III}(x, \xi) =$

$$= \frac{1}{12D_2}\left[\xi^3\left(12c^2\ell^3+3bc^4+b\ell^4-4c\ell^4-4c^4\ell-8bc^3\ell\right)+12c^2\xi^2\ell^2\left(2bc-b\ell-2c\ell+c^2\right)+\right.$$
$$\left.+\xi\left(6bc^2\ell^4+12c^3\ell^4-18bc^4\ell^2\right)+4c^3\ell^3\left(3bc-2b\ell-c\ell\right)\right]\pm\frac{1}{12}\xi^3+$$
$$+\left\{\frac{1}{4D_2}\left[4c^2\xi^3\ell\left(b+2c-3\ell\right)+\xi^2\left(12c^2\ell^3-3bc^4-b\ell^4+4c\ell^4-4c^4\ell-8bc^3\ell\right)+\right.\right.$$
$$\left.\left.+12c^2\xi\ell\left(-\ell^3+bc^2\right)-2c^2\ell^2\left(3bc^2-b\ell^2-2c\ell^2\right)\right]\pm\frac{-3\xi^2}{12}\right\}x+$$
$$+\left\{\frac{1}{4D_2}\left[2\xi^3\left(4c\ell^2-bc^2-b\ell^2-2c^3\right)+4\xi^2\left(2bc^3+b\ell^3-4c\ell^3+c^4\right)-\right.\right.$$
$$\left.\left.-\xi\left(b\ell-12c^2\ell^3+3bc^4-4c\ell^4+4c^4\ell+8bc^3\ell\right)+4c^2\ell^2\left(2bc-b\ell-2c\ell+c^2\right)\right]\pm\frac{3\xi}{12}\right\}x^2+$$
$$+\left(\left\{\frac{1}{12D_2}\left[4\xi^3\left(b\ell-4c\ell+3c^2\right)-6\xi^2\left(bc^2+b\ell^2-4c\ell^2+2c^3\right)+\right.\right.\right.$$
$$\left.\left.\left.+12c^2\xi\ell\left(b+2c-3\ell\right)+3bc^4-4c^4\ell+b\ell^4-8bc^3\ell-4c\ell^4+12c^2\ell^3\right]\pm\frac{-1}{12}\right\}x^3, \quad (3.6.27c)$$

where

$$D_2 = (c-\ell)^3\left(b\ell-4c\ell+3bc\right). \quad (3.6.28)$$

The four-point boundary value problem defined by (3.6.2) and the boundary and continuity conditions is self-adjoint. Consequently, the Green function is symmetric.

In the integral

$$G(x,\xi_P) = \int_0^\ell G(x,\xi)\,\delta(\xi-\xi_P)\,\mathrm{d}\xi \quad (3.6.29)$$

$\xi_P \in (0,\ell)$ is an arbitrary but fixed point and $\delta(\xi-\xi_P)$ is the Dirac delta, representing a dimensionless vertical load of unit magnitude applied at $\xi_P$. Accordingly, $G(x,\xi_P)$ is the dimensionless vertical displacement at $x$ due to this load. Maxwell's reciprocity theorem states that the vertical displacement at $x$ on account to a unit load at $\xi_P$ is equal to the vertical displacement at $\xi_P$ due to the unit load at $x$. Hence the Green function is a symmetric function of $x$ and $\xi$:

$$G(x,\xi_P) = G(\xi_P,x). \quad (3.6.30)$$

If we consider that $b=0.3$, $c=0.6$ and $\xi=0.8$, then Figure 3.3 shows the Green function for FrrF case.

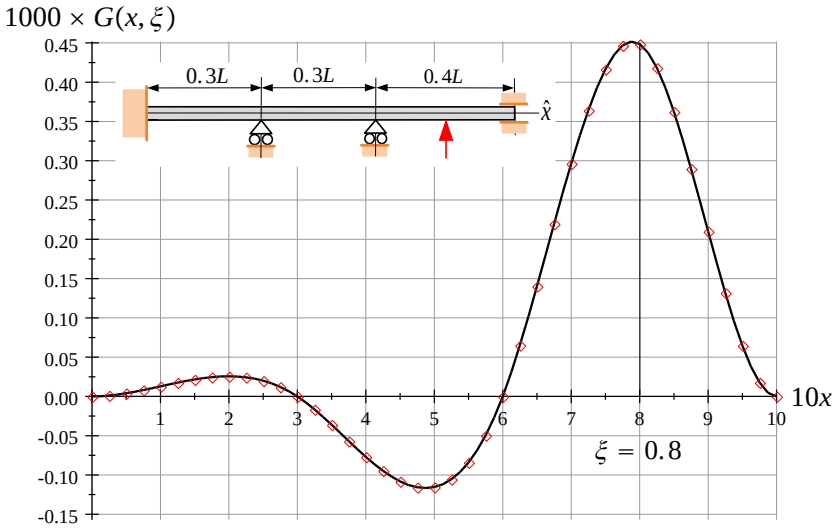


FIGURE 3.3. The Green function of FrrF beams

**3.6.3. Green function of PrrP beams.** The elements of the Green function for PrrP beams are given here without details. The formal calculation steps are identical to that given in Section 3.6.2.

(a) If $\xi \in (0, b)$:

$$G_{1I}(x,\xi) = \left(-\frac{1}{12}\xi^3 \pm \frac{1}{12}\xi^3\right) + \left\{\frac{1}{12bD_3}\left[2\xi^3\left(3b^2-2b\ell-4c\ell+2bc+c^2\right)-3bc\xi^2\left(2b+c-4\ell\right)+\right.\right.$$
$$\left.\left.+b^2\xi\left(4b\ell-3b\xi-16c\ell+8bc+4c^2\right)\right] \pm \left(-\frac{3\xi^2}{12}\right)\right\} x + \left(-\frac{3}{12}\xi \pm \frac{3\xi}{12}\right) x^2 +$$
$$+\left\{\frac{1}{12b^2D}\left[4\xi^3\left(\ell-b\right)+2b\xi\left(2bc-2b\ell-4c\ell+3b^2+c^2\right)-\right.\right.$$
$$\left.\left.-b^2\left(2bc-4c\ell+b^2+c^2\right)\right] \pm \frac{-1}{12}\right\} x^3, \quad (3.6.31a)$$

$$G_{2I}(x,\xi) = \frac{1}{6b}\frac{\xi}{D_3\left(b-c\right)}\left(b-x\right)\left(c-x\right)\left(\xi^2-b^2\right)\left(2x\ell-3bx+cx+2b\ell-4c\ell+bc+c^2\right) \quad (3.6.31b)$$

and

$$G_{3I}(x,\xi) = \frac{1}{6b}\frac{\xi}{D_3\left(c-\ell\right)}\left(c-b\right)\left(c-x\right)\left(x-\ell\right)\left(c+x-2\ell\right)\left(\xi^2-b^2\right), \quad (3.6.31c)$$

where

$$D_3 = b^2+2bc+c^2-4\ell c\,. \quad (3.6.32)$$

(b) If $\xi \in (b, c)$:

$$G_{1II}(x,\xi) = \frac{1}{6b}\frac{x}{D_4\left(b-c\right)}\left(b-\xi\right)\left(c-\xi\right)\left(x^2-b^2\right)\left(2\xi\ell-3b\xi+c\xi+2b\ell-4c\ell+bc+c^2\right), \quad (3.6.33a)$$

$$G_{2II}(x,\xi) = \frac{1}{12D_4\left(b-c\right)}\left[\xi^3\left(b^4-8\ell bc^2-c^4+4\ell c^3\right)-\right.$$

$$
\begin{aligned}
&-2b^2c\xi\left(b^2c+2b^2\ell+4c^2\ell-c^3\right)+12b^2c^2\xi^2\ell+4b^4c^2\ell\big]\pm\frac{1}{12}\xi^3+\\
&+\left\{\frac{1}{12D_4\,(b-c)}\left[4b\xi^3\left(4c\ell-b\ell-2bc+2c^2\right)-3\xi^2\left(4c^3\ell+b^4-c^4+8bc^2\ell\right)+\right.\right.\\
&\left.\left.+4b\xi\left(2b^3c+b^3\ell+8c^3\ell-2c^4\right)-2b^2c\left(b^2c+2b^2\ell+4c^2\ell-c^3\right)\right]\pm\frac{-3}{12}\xi^2\right\}x+\\
&+\left\{\frac{1}{4D_4\,(b-c)}\left[2\xi^3\left(-2c\ell+b^2-c^2\right)+12c^2\xi^2\ell-\right.\right.\\
&\left.\left.-\xi\left(4c^3\ell+b^4-c^4+8bc^2\ell\right)+4\ell b^2c^2\right]\pm\frac{3}{12}\xi\right\}x^2+\\
&+\left\{\frac{1}{12\,(b-c)\,D_4}\left[4\xi^3\,(2c+\ell-2b)+6\xi^2\left(b^2-2c\ell-c^2\right)-\right.\right.\\
&\left.\left.-4b\xi\left(b\ell-4c\ell+2bc-2c^2\right)+\left(4c^3\ell+b^4-c^4-8bc^2\ell\right)\right]\pm\frac{-1}{12}\right\}x^3
\end{aligned}
\tag{3.6.33b}
$$

and

$$
\begin{aligned}
&G_{3II}(x,\xi)=\\
&=-\frac{1}{6D_4\,(c-\ell)}\,(c-x)\,(b-\xi)\,(c-\xi)\,(x-\ell)\,(c+x-2\ell)\left(b\xi-3c\xi+bc+b^2\right)\,,
\end{aligned}
\tag{3.6.33c}
$$

where

$$
D_4=(b-c)\left(b^2+2bc+c^2-4\ell c\right)\,. \tag{3.6.34}
$$

(b) If $\xi\in(c,\ell)$:

$$
G_{1III}(x,\xi)=\frac{1}{6b}\frac{x}{D_3\,(c-\ell)}\,(c-b)\,(c-\xi)\,(\xi-\ell)\,(c+\xi-2\ell)\left(x^2-b^2\right)\,, \tag{3.6.35a}
$$

$$
\begin{aligned}
&G_{2III}(x,\xi)=\\
&=-\frac{1}{6D_4\,(c-\ell)}\,(c-\xi)\,(b-x)\,(c-x)\,(\xi-\ell)\,(c+\xi-2\ell)\left(bx-3cx+bc+b^2\right)
\end{aligned}
\tag{3.6.35b}
$$

and

$$
\begin{aligned}
G_{3III}(x,\xi)=\frac{1}{12D_5}&\left[\xi^3\left(c^4-b^2\ell^2-9c^2\ell^2+2bc^3+4c\ell^3+b^2c^2-2bc\ell^2\right)-\right.\\
&-6c\xi^2\ell\left(2bc^2+b^2c-b^2\ell-3c^2\ell+c^3-2bc\ell\right)+\\
&+4c\xi\ell\left(2bc^3-b^2\ell^2-3c^2\ell^2+b^2c^2-2bc\ell^2\right)-\\
&\left.-4c^2\ell^2\left(2bc^2+b^2c-b^2\ell-c^2\ell-2bc\ell\right)\right]\pm\frac{1}{12}\xi^3+\\
&+\left\{-\frac{1}{12D_5}\left[2\xi^3\left(2bc^2+b^2c-b^2\ell-9c^2\ell+3c^3-2bc\ell\right)-\right.\right.\\
&-3\xi^2\left(-b^2\ell^2-9c^2\ell^2+2bc^3-4c\ell^3+b^2c^2+c^4-2bc\ell^2\right)+\\
&+4\xi\left(-b^2\ell^3-9c^2\ell^3+2bc^4+b^2c^3-2bc\ell^3\right)-\\
&\left.\left.-4c\ell\left(-b^2\ell^2-3c^2\ell^2+2bc^3+b^2c^2-2bc\ell^2\right)\pm\frac{-3\xi^2}{12}\right\}x+\right.
\end{aligned}
$$

$$
\begin{aligned}
&+\left\{-\frac{1}{4D_5}\left[4c\xi^3\ell-12c\xi^2\ell^2-\right.\right.\\
&-\xi\left(-b^2\ell^2-9c^2\ell^2+2bc^3-4c\ell^3+b^2c^2+c^4-2bc\ell^2\right)+\\
&\left.\left.+2c\ell\left(2bc^2+b^2c-b^2\ell-3c^2\ell+c^3-2bc\ell\right)\right]\pm\frac{3\xi}{12}\right\}x^2+\\
&+\left\{\frac{1}{12D_5}\left[4c\xi^3-12c\xi^2\ell-2\xi\left(2bc^2+b^2c-b^2\ell-9c^2\ell+3c^3-2bc\ell\right)+\right.\right.\\
&\left.\left.+(-b^2\ell^2-9c^2\ell^2+2bc^3+4c\ell^3+b^2c^2+c^4-2bc\ell^2)\right]\pm\frac{-1}{12}\right\}x^3\,, \qquad (3.6.35c)
\end{aligned}
$$

where

$$D_5=(c-\ell)^2\left(b^2+2bc+c^2-4\ell c\right)\,. \qquad (3.6.36)$$

## 3.7. Eigenvalues for free vibrations

**3.7.1. Integral equation formulation.** An algorithm to solve the eigenvalue problems in Fredholm integral equation form (3.6.7) is published in **[76]**. This is based on the boundary element method. The integral equation (3.6.7) is replaced by an algebraic eigenvalue problem that can be solved numerically. A Fortran 90 program was developed for this aim and was used to compute numerical solutions. The interval $[0,\ell=1]$ was mapped by 60 elements, with a quadratic isoparametric approximation employed to approximate the unknown vibration amplitude $w$. The resulting algebraic eigenvalue problem was solved with the DGVLRG subroutine.

**3.7.2. Results for FrrF beams.** Figure 3.4 shows the function $\sqrt{\lambda_1}/4.73004^2$ against $c$, with $b$ as parameter. If $b$ is identical to $c$, the coefficient matrix in the algebraic eigenvalue problem becomes singular, as this follows from relation (3.6.15b), where the term $b-c$ is in the denominator.

The step size for $c$ was 0.0125 in our calculations. In Figure 3.4, we plotted all data pairs $c,\sqrt{\lambda_1}/4.73004^2(c)$ for multiple values of $b$.

Likewise, if $c-b=0.0001$, the two intermediate roller supports are very close, preventing rigid body rotation. When $b$ is zero, the beam behaves as if it were fixed-fixed, with one intermediate roller support at $c$, and the results agree with at least four decimal accuracy with **[80]**. Similarly, if $c=b+0.00001$, the section of the beam in the interval $[b,\ell]$ behaves like a fixed-fixed one with length $\ell-c$. Hence, the numerical results should satisfy the relation

$$\sqrt{\lambda_1}(b,c=b+0.0001)=\frac{\sqrt{\lambda_1}(b=0,c=b+0.0001)}{(\ell-b)^2} \qquad (3.7.1)$$

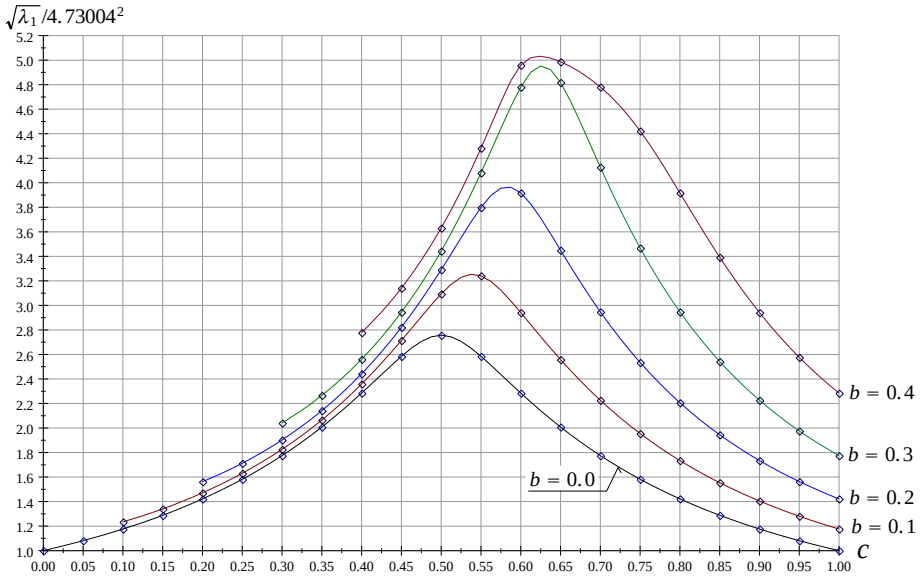


FIGURE 3.4. The first eigenvalue against $c$ for FrrF beams

Table 32 shows some computational results for FrrF beams. The point pairs $c, \sqrt{\lambda_1}/4.73004^2(c)$ in this table are drawn by diamond markers in Figure 3.4.

TABLE 32. Eigenvalues for FrrF beams

| | $b = 0.0$ | $b = 0.1$ | $b = 0.2$ | $b = 0.3$ | $b = 0.4$ |
|---|---|---|---|---|---|
| $c$ | $\sqrt{\lambda_1}/4.73004^2$ | | | | |
| 0.000 | 1.00018 | | | | |
| 0.0500 | 1.08109 | | | | |
| 0.1000 | 1.17608 | 1.23475 | | | |
| 0.1500 | 1.28825 | 1.34004 | | | |
| 0.2000 | 1.42173 | 1.47116 | 1.56276 | | |
| 0.2500 | 1.58179 | 1.63091 | 1.71215 | | |
| 0.3000 | 1.77484 | 1.82594 | 1.90263 | 2.04121 | |
| 0.3500 | 2.00789 | 2.06529 | 2.14189 | 2.26609 | |
| 0.4000 | 2.28463 | 2.35937 | 2.44281 | 2.56109 | 2.77840 |
| 0.4500 | 2.58411 | 2.71417 | 2.82181 | 2.94455 | 3.14045 |
| 0.5000 | 2.75695 | 3.09419 | 3.29103 | 3.44316 | 3.63104 |
| 0.5500 | 2.58465 | 3.24126 | 3.79877 | 4.08139 | 4.28243 |
| 0.6000 | 2.28519 | 2.94116 | 3.91744 | 4.78102 | 4.95962 |
| 0.6500 | 2.00837 | 2.55784 | 3.44989 | 4.81778 | 4.98735 |
| 0.7000 | 1.77525 | 2.22636 | 2.94691 | 4.12708 | 4.78102 |
| 0.7500 | 1.58212 | 1.95508 | 2.53420 | 3.46813 | 4.42276 |
| 0.8000 | 1.42201 | 1.73435 | 2.20617 | 2.94691 | 3.91744 |
| 0.8500 | 1.28848 | 1.55374 | 1.94478 | 2.54247 | 3.39276 |
| 0.9000 | 1.17628 | 1.40468 | 1.73444 | 2.22636 | 2.94116 |
| 0.9500 | 1.08125 | 1.28049 | 1.56296 | 1.97598 | 2.57613 |
| 0.9999 | 1.00018 | 1.17626 | 1.42198 | 1.77520 | 2.28513 |

**3.7.3. Results for PrrP case.** Figure 3.5 shows the function $\sqrt{\lambda_1}/\pi^2$ in terms of $c$. The coordinate $b$ is, again, a parameter. The step in $c$ was again selected to be 0.0125. The curves $\sqrt{\lambda_1}/\pi^2(c)$ against $c$ are drawn in Figure 3.5.

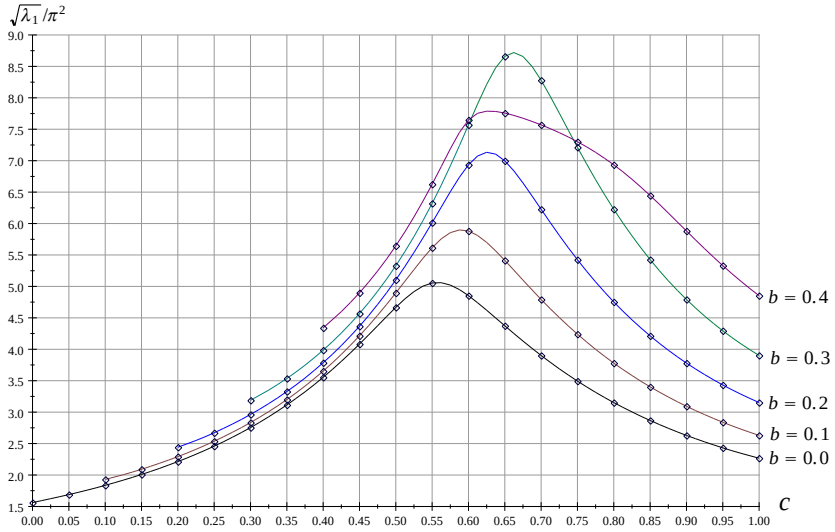


FIGURE 3.5. The first eigenvalue against $c$ for PrrP beams

In case $c-b=0.0001$, the two intermediate roller supports are very close so they prevent rotation at $b$. If $b=0$, there is a fixed-pinned beam with one intermediate roller support at $c$. If $c=b+0.00001$ the beam part in the interval $[b,\ell]$ behaves again as if it were a fixed-pinned of length $\ell-c$.

Table 33 contains come computational results for PrrP case.

TABLE 33. Eigenvalues for PrrP beams

| | $b=0.0$ | $b=0.1$ | $b=0.2$ | $b=0.3$ | $b=0.4$ |
|---|---|---|---|---|---|
| $c$ | $\sqrt{\lambda_1}/\pi^2$ | | | | |
| 0.0001 | 1.56219 | | | | |
| 0.0500 | 1.68846 | | | | |
| 0.1000 | 1.83560 | 1.92892 | | | |
| 0.1500 | 2.00849 | 2.09141 | | | |
| 0.2000 | 2.21344 | 2.29250 | 2.44133 | | |
| 0.2500 | 2.45863 | 2.53688 | 2.67205 | | |
| 0.3000 | 2.75465 | 2.83472 | 2.96334 | 3.18875 | |
| 0.3500 | 3.11478 | 3.20047 | 3.32785 | 3.53609 | |
| 0.4000 | 3.55416 | 3.65311 | 3.78606 | 3.98641 | 4.34038 |
| 0.4500 | 4.08271 | 4.21452 | 4.36642 | 4.56914 | 4.89916 |
| 0.5000 | 4.66648 | 4.89618 | 5.10347 | 5.32852 | 5.64511 |
| 0.5500 | 5.05444 | 5.61582 | 6.01520 | 6.32092 | 6.62657 |
| 0.6000 | 4.85258 | 5.88174 | 6.93406 | 7.56998 | 7.64802 |
| 0.6500 | 4.37349 | 5.41365 | 6.99743 | 8.65966 | 7.75661 |
| 0.7000 | 3.90174 | 4.79210 | 6.22702 | 8.27915 | 7.56998 |
| 0.7500 | 3.49401 | 4.24033 | 5.42411 | 7.21298 | 7.30172 |
| 0.8000 | 3.15205 | 3.78027 | 4.75338 | 6.22702 | 6.93406 |
| 0.8500 | 2.86727 | 3.40276 | 4.21318 | 5.42610 | 6.44601 |
| 0.9000 | 2.63014 | 3.09342 | 3.78027 | 4.79300 | 5.88174 |
| 0.9500 | 2.43232 | 2.83936 | 3.43248 | 4.29466 | 5.33130 |
| 0.9999 | 2.26722 | 2.63049 | 3.15250 | 3.90236 | 4.85336 |

**3.7.4. FEM verification.** Let us consider an FrrF beam with the rectangular cross-section illustrated in Figure 2.6. The length of the beam is now set to 4000mm. The surface densities are given as follows: $\rho_1=\rho_{\text{Aluminium}}=2710/10^9$ kg/mm$^2$ and $\rho_2=\rho_{\text{steel}}=7850/10^9$ kg/mm$^2$.

Under these conditions:

$$\begin{aligned} I_{ey} &= 9.5 \times 10^{14}\,\mathrm{kg\,mm^3}/s^2, \\ \rho_a &= 4.423333 \times 10^{-6}\ \mathrm{kg/mm^3}. \end{aligned} \tag{3.7.2}$$

Let us select that $b = 0.2$ and $c = 0.8$. Thus, the intermediate roller supports are symmetrically arranged. As per Table 32, for FrrF beams

$$\sqrt{\lambda_1|_{b=0.2,c=0.8}} = 2.20617 \times 4.73004^2 = 49.\,359\,255. \tag{3.7.3}$$

Using equation (3.6.3) we find

$$\omega_1|_{b=0.2,c=0.8} = \frac{\sqrt{\lambda_1|_{b=0.2,c=0.8}}}{L^2}\sqrt{\frac{I_{ey}}{\rho_a A}} = 452.\,101\ \frac{\mathrm{r}}{s}. \tag{3.7.4}$$

For PrrP beams, we get from Table 33:

$$\sqrt{\lambda_1|_{b=0.2,c=0.8}} = 4.75338 \times \pi^2 = 46.913\,98017 \tag{3.7.5}$$

Thus

$$\breve{\omega}_1|_{b=0.2,c=0.8} = \frac{46.913\,980\,17}{4000^2} \times \sqrt{\frac{9.5 \times 10^{14}}{4.423333 \times 10^{-6} \times 100^2}} = 429.704\,\frac{\mathrm{rad}}{s}. \tag{3.7.6}$$

These numerical findings were validated using the commercial finite element software Ansys. A total of 480 uniform SOLID185 hexahedral elements were used to map the geometry. Table 34 presents the validation of the results. When calculating the relative error, the solutions of the novel model were used as the denominator. It is clear that that there is a strong agreement between the solutions, indicating the accuracy of our approach. It is noted that this Chapter is based on Author publication {3}.

TABLE 34. Comparison with FEM results

| | FrrF beam | PrrP beam |
|---|---|---|
| | $\breve{\omega}_1\|_{b=0.2,c=0.8}/2\pi$ 1/s | |
| New model | 71.95 | 68.38 |
| Ansys solution | 71.24 | 67.94 |
| Relative error % | 0.9867 | 0.6565 |

CHAPTER 4

# The Green function for some coupled boundary value problems

## 4.1. Coupled BVPs

**4.1.1. Definition.** The definition, in certain ways, is similar to that in the previous section for four-point BVPs. In the forthcoming, the differences will be emphasised. Assume there are two inhomogeneous ordinary differential equations, whose operators $L_i[y_i(x)]$ have the same order, that is $2\kappa \geq 2$:

$$L_i[y_i(x)] = \sum_{n=0}^{2\kappa} p_{ni}(x)\, y_i^{(n)}(x) = r_i(x), \quad i = 1, 2. \tag{4.1.1}$$

A coordinate at in inner point in $x \in [0, \ell = 1]$ is $b$, that makes two sub-intervals. Their ranges are $0 < \ell_1 = b < 1$ and $\ell_2 = 1 - \ell_1$. Functions ($p_{n1}(x)$ and $r_1(x)$) $\{p_{n2}(x)$ and $r_2(x)\}$ are continuous in the intervals ($x \in [0, b)$) $\{x \in (b, \ell = 1]\}$ and $p_{2\kappa i}(x) \neq 0$.

The particular solutions of Eqs. (4.1.1) are noted by $y_{mi}(x)$ $(m = 1, 2, \ldots, 2\kappa)$ and the general solutions

$$y_1 = \sum_{m=1}^{2\kappa} \mathcal{A}_{m1} y_{m1}(x), \quad y_2 = \sum_{\ell=1}^{2\kappa} \mathcal{A}_{m2} y_{m2}(x), \tag{4.1.2}$$

with unknowns $\mathcal{A}_{m1}$ and $\mathcal{A}_{m2}$.

Equations (4.1.1) are paired with boundary and continuity conditions, similarly to Eq. (3.1.3), but now there is only one intermediate point.

The integration constants, like in Chapter 3, can be found from the boundary conditions.

**4.1.2. Green functions for CBVPs.** If the Green function $G(x, \xi)$ of the given coupled boundary value problem (CBVP) is known, the solution can be found in a similar way as in Chapter 3 in the two subdomains with

$$y(x) = \begin{cases} y_1(x) & \text{if } x \in [0, b) \\ y_2(x) & \text{if } x \in (b, \ell = 1] \end{cases} \quad \text{and} \quad r(\xi) = \begin{cases} r_1(\xi) & \text{if } \xi \in [0, b) \\ r_2(\xi) & \text{if } \xi \in (b, \ell = 1] \end{cases} \tag{4.1.3}$$

while $G(x, \xi)$ has the structure

$$G(x, \xi) = \begin{cases} G_{11}(x, \xi) & \text{if } x, \xi \in [0, b], \\ G_{21}(x, \xi) & \text{if } x \in [b, \ell] \text{ and } \xi \in [0, b], \\ G_{12}(x, \xi) & \text{if } x \in [0, b] \text{ and } \xi \in [b, \ell], \\ G_{22}(x, \xi) & \text{if } x, \xi \in [b, \ell], \end{cases} \tag{4.1.4}$$

Property 1 and 2 are identical to what is in Chapter 2. Property 3 and 4 are identical with the subscripts $I$ and $II$ be replaced by 1 and 2.

Property 5 needs modifications. Let $\alpha$ be an arbitrary finite non-zero constant. For a given $\xi \in [0, \ell]$, the term $G(x, \xi)\alpha$ as a function of $x \neq \xi$ should satisfy the homogeneous differential equations

$$\begin{aligned} L_1\left[G(x, \xi)\alpha\right] &= 0, \quad \text{if} \quad x \in [0, b]; \\ L_2\left[G(x, \xi)\alpha\right] &= 0, \quad \text{if} \quad x \in [b, \ell]. \end{aligned} \tag{4.1.5}$$

Property 6 is also the same as in Chapter 2.

### 4.2. Calculation of the Green function

**4.2.1. Elements $G_{11}$ and $G_{21}$ ($\xi \in [0,b)$).** The element $G_{11}(x,\xi)$ ($x \in [0,b]$) is sought as

$$\begin{aligned} G_{11}(x,\xi) &= \sum_{m=1}^{2\kappa}(a_{m1}(\xi)+b_{m1}(\xi))y_{m1}(x), \qquad x<\xi \\ G_{11}(x,\xi) &= \sum_{m=1}^{2\kappa}(a_{m1}(\xi)-b_{m1}(\xi))y_{m1}(x), \qquad x\geq\xi \end{aligned} \tag{4.2.1a}$$

while element $G_{21}(x,\xi)$ ($x \in [b,\ell]$) has the structure

$$G_{21}(x,\xi) = \sum_{m=1}^{4} c_{m1}(\xi)y_{m2}(x). \tag{4.2.1b}$$

The unknown coefficients are $a_{m1}(\xi), b_{m1}(\xi)$ and $c_{m1}(\xi)$. Continuity and discontinuity conditions of Property 1 yield equations

$$\sum_{m=1}^{2\kappa} b_{m1}(\xi)y_{m1}^{(n)}(\xi) = 0, \quad n = 0,1,2,\ldots,2\kappa-2 \tag{4.2.2a}$$

and

$$\sum_{m=1}^{2\kappa} b_{m1}(\xi)y_{m1}^{(2\kappa-1)}(\xi) = -\frac{1}{p_{2\kappa 1}(\xi)} \tag{4.2.2b}$$

Applying now the boundary and continuity conditions results the equation system

$$\sum_{n=1}^{2\kappa}\alpha_{nr1}\sum_{m=1}^{2\kappa}(a_{m1}(\xi)+b_{m1}(\xi))y_{m1}(0) = 0\,, \qquad r = 1,2,3,\ldots,\kappa; \tag{4.2.3a}$$

$$\sum_{n=1}^{2\kappa}\left(\beta_{nr1}\sum_{m=1}^{2\kappa}(a_{m1}(\xi)-b_{m1}(\xi))y_{m1}^{(n-1)}(b) - \beta_{nr2}\sum_{m=1}^{2\kappa} c_{m1}(\xi)y_{m2}^{(n-1)}(b)\right) = 0\,, \qquad r = 1,2,3,\ldots,2\kappa; \tag{4.2.3b}$$

$$\sum_{n=1}^{2\kappa}\left(\gamma_{nr2}\sum_{m=1}^{2\kappa} c_{m1}(\xi)y_{m2}^{(n-1)}(\ell)\right) = 0\,, \qquad r = 1,2,3,\ldots,\kappa. \tag{4.2.3c}$$

**4.2.2. Elements $G_{12}$; $G_{22}$ ($\xi \in (b,\ell]$).** The following representations are used this time:

$$G_{12}(x,\xi) = \sum_{m=1}^{2\kappa} c_{m2}(\xi)y_{m1}(x), \qquad x \in [0,b]; \tag{4.2.4a}$$

$$\begin{aligned} G_{22}(x,\xi) &= \sum_{m=1}^{2\kappa}(a_{m2}(\xi)+b_{m2}(\xi))y_{m2}(x), \qquad x<\xi \\ G_{22}(x,\xi) &= \sum_{m=1}^{2\kappa}(a_{m2}(\xi)-b_{m2}(\xi))y_{m2}(x), \qquad x>\xi \end{aligned} \qquad x \in [b,\ell]. \tag{4.2.4b}$$

Here the unknowns are $b_{m2}(\xi)$, $a_{m2}(\xi)$ and $c_{m2}(\xi)$. Similarly as in Subsection 4.2.2 the equations for $b_{m2}(\xi)$ are:

$$\sum_{m=1}^{2\kappa} b_{m2}(\xi) y_{m2}^{(n)}(\xi) = 0, \quad n = 0, 1, 2, \ldots, 2\kappa - 2 \tag{4.2.5a}$$

and

$$\sum_{m=1}^{2\kappa} b_{m2}(\xi) y_{m2}^{(2\kappa-1)}(\xi) = -\frac{1}{p_{2\kappa 2}(\xi)}\,. \tag{4.2.5b}$$

As for $a_{m2}(\xi)$ and $c_{m2}(\xi)$, the related boundary and continuity conditions yield

$$\sum_{n=1}^{2\kappa} \left( \alpha_{nr1} \sum_{m=1}^{2\kappa} c_{m2}(\xi) y_{m1}^{(n-1)}(0) \right) = 0\,, \qquad r = 1, 2, 3, \ldots, \kappa; \tag{4.2.6a}$$

$$\sum_{n=1}^{2\kappa} \left( \beta_{nr1} \sum_{m=1}^{2\kappa} c_{m2}(\xi) y_{m1}^{(n-1)}(b) - \beta_{nr2} \sum_{m=1}^{2\kappa} (a_{m2}(\xi) + b_{m2}(\xi)) y_{m2}^{(n-1)}(b) \right) = 0\,, \quad r = 1, 2, 3, \ldots, 2\kappa; \tag{4.2.6b}$$

$$\sum_{n=1}^{2\kappa} \left( \gamma_{nr2} \sum_{m=1}^{2\kappa} (a_{m2}(\xi) - b_{m2}(\xi)) y_{m2}^{(n-1)}(b) \right) = 0\,, \qquad r = 1, 2, 3, \ldots, \kappa. \tag{4.2.6c}$$

## 4.3. Self-adjointness and symmetry of the Green function

**4.3.1. Self-adjointness.** Assume that there are the comparison functions

$$u(x) = \begin{cases} u_1(x) & \text{if } x \in [0, b] \\ u_2(x) & \text{if } x \in [b, \ell] \end{cases}$$

and

$$v(x) = \begin{cases} v_1(x) & \text{if } x \in [0, b] \\ v_2(x) & \text{if } x \in [b, \ell] \end{cases}\,.$$

Let us define the operations

$$(u, v)_L = \int_0^b u_1(x)\, L_1[v_1(x)]\, \mathrm{d}x + \int_b^\ell u_2(x)\, L_2[v_2(x)]\, \mathrm{d}x \tag{4.3.2}$$

on $L_1$ and $L_2$. The coupled boundary value problem is self-adjoint if the product (4.3.2) is commutative.

**4.3.2. Symmetry of the Green function.** Let us consider now the following two inhomogeneous coupled boundary value problems

$$\begin{aligned} L_1[u_1(x)] &= r_1(x)\,, \qquad L_2[u_2(x)] = r_2(x) \\ L_1[v_1(x)] &= s_1(x)\,, \qquad L_2[v_2(x)] = s_2(x) \end{aligned} \tag{4.3.3}$$

and the associated conditions:

$$\begin{aligned} U_{0r}[u_1] &= 0, & U_{0r}[v_1] &= 0, & r &= 1, 2, \ldots, \kappa; \\ U_{br}[u_1, u_2] &= 0, & U_{br}[v_1, v_2] &= 0, & r &= 1, 2, \ldots, 2\kappa; \\ U_{1r}[u_2] &= 0, & U_{2r}[v_2] &= 0, & r &= 1, 2, \ldots, \kappa. \end{aligned} \tag{4.3.4}$$

Here $u_1(x)$, $u_2(x)$, $v_1(x)$, $v_2(x)$ are now the unknowns, $r_1(x)$, $r_2(x)$ and $s_1(x)$, $s_2(x)$ are continuous inhomogeneities in $x \in [0, b]$, $x \in [b, \ell]$. For such self-adjoint BVPs, it holds that

$$(u, v)_L - (v, u)_L = 0,$$

where $u(x)$ and $v(x)$ can be given as

$$u(x) = \int_0^\ell G(x,\xi) r(\xi)\,\mathrm{d}\xi \qquad \text{and} \qquad v(x) = \int_0^\ell G(x,\xi) s(\xi)\,\mathrm{d}\xi\,,$$

in which

$$r(\xi) = \begin{cases} r_1(\xi) & \text{if } x \in [0,b) \\ r_2(\xi) & \text{if } x \in (b, \ell = 1] \end{cases} \quad \text{and} \quad s(\xi) = \begin{cases} s_1(\xi) & \text{if } \xi \in [0,b) \\ s_2(\xi) & \text{if } \xi \in (b, \ell = 1] \end{cases} \tag{4.3.5}$$

Hence

$$\begin{aligned}(u,v)_L - (v,u)_L &= \int_0^\ell (u\,L[v] - v\,L[u])\,\mathrm{d}x = \\ &= \int_0^\ell \int_0^\ell [G(x,\xi) - G(\xi,x)]\, r(\xi) s(x)\,\mathrm{d}\xi\mathrm{d}x = 0\,. \end{aligned} \tag{4.3.6}$$

As both $r(x)$ and $s(x)$ are arbitrary continuous functions, the last integral in the former equation is zero if and only if the Green function is symmetric in $\xi$ and $x$.

### 4.4. Coupled eigenvalue problems

There are the differential equations

$$K_i\,[y_i] = \lambda\, M_i\,[y_i]\,, \qquad i = 1,2 \tag{4.4.1a}$$

where $y_1(x),\ x \in [0,b]$ and $y_2(x),\ x \in [b,\ell];(0 < b < \ell = 1)$ are unknowns while $\lambda$ is the unknown eigenvalue. Differential operators $K_i\,[y_i]$ and $M_i\,[y_i]$ are detailed by

$$\begin{aligned} K_i\,[y_i] &= \sum_{n=0}^{\kappa} (-1)^n \left[ f_{ni}(x) y_i^{(n)}(x) \right]^{(n)}\,, \\ M_i\,[y_i] &= \sum_{n=0}^{\mu} (-1)^n \left[ g_{ni}(x) y_i^{(n)}(x) \right]^{(n)}\,, \qquad \kappa > \mu \geq 1 \end{aligned} \tag{4.4.1b}$$

in which the real function $(f_{ni}(x))$ $[g_{ni}(x)]$ is continuously differentiable $(\kappa)$ $[\mu]$ times and

$$f_{\kappa i}(x) \neq 0 \qquad \text{if } x \in [0,b] \tag{4.4.1c}$$

$$g_{\mu i}(x) \neq 0 \qquad \text{if } x \in [b,\ell]\,. \tag{4.4.1d}$$

This time, the order of the operator on the left side of (4.4.1a) is greater than the order on the right side.

Equation (4.4.1) and the homogeneous boundary conditions define a coupled eigenvalue problem (CEP). After performing partial integrations, the following formulae are found for the products $(u,v)_K$ and $(u,v)_M$:

$$\begin{aligned}(u,v)_K = &\left[ \sum_{n=0}^{\kappa} \sum_{r=0}^{n-1} (-1)^{(n+r)} u_1^{(r)}(x) \left[ f_{n1}(x)\, v_1^{(n)}(x) \right]^{(n-1-r)} \right]_0^{b-0} + \\ &+ \left[ \sum_{n=0}^{\kappa} \sum_{r=0}^{n-1} (-1)^{(n+r)} u_2^{(r)}(x) \left[ f_{n2}(x)\, v_2^{(n)}(x) \right]^{(n-1-r)} \right]_{b+0}^{\ell} + \\ &+ \sum_{n=0}^{\kappa} \int_0^b u_1^{(n)}(x) f_n(x) v_1^{(n)}(x)\,\mathrm{d}x + \sum_{n=0}^{\kappa} \int_b^\ell u_2^{(n)}(x) f_n(x) v_2^{(n)}(x)\,\mathrm{d}x = \end{aligned}$$

$$= K_0(u,v) + \sum_{n=0}^{\kappa} \int_0^b u_1^{(n)}(x) f_n(x) v_1^{(n)}(x)\,\mathrm{d}x + \sum_{n=0}^{\kappa} \int_b^{\ell} u_2^{(n)}(x) f_n(x) v_2^{(n)}(x)\,\mathrm{d}x\,, \tag{4.4.2a}$$

and

$$\begin{aligned}(u,v)_M = &\left[\sum_{n=0}^{\mu}\sum_{r=0}^{n-1}(-1)^{(n+r)} u_1^{(r)}(x)\left[g_{n1}(x)\, v_1^{(n)}(x)\right]^{(n-1-r)}\right]_0^{b-0} + \\ &+ \left[\sum_{n=0}^{\mu}\sum_{r=0}^{n-1}(-1)^{(n+r)} u_2^{(r)}(x)\left[g_{n2}(x)\, v_2^{(n)}(x)\right]^{(n-1-r)}\right]_{b+0}^{\ell} + \\ &+ \sum_{n=0}^{\mu}\int_0^b u_1^{(n)}(x) g_{n1}(x) v_1^{(n)}(x)\,\mathrm{d}x + \sum_{n=0}^{\mu}\int_b^{\ell} u_2^{(n)}(x) g_{n2}(x) v_2^{(n)}(x)\,\mathrm{d}x = \\ &= M_0(u,v) + \sum_{n=0}^{\mu}\int_0^b u_1^{(n)}(x) g_{n1}(x) v_1^{(n)}(x)\,\mathrm{d}x + \sum_{n=0}^{\mu}\int_b^{\ell} u_2^{(n)}(x) g_{n2}(x) v_2^{(n)}(x)\,\mathrm{d}x.\end{aligned} \tag{4.4.2b}$$

If

$$K_0(u,v) = K_0(v,u) \qquad \text{and} \qquad M_0(u,v) = M_0(v,u) \tag{4.4.3}$$

then the problem is self-adjoint.

The $n$-th eigenvalue is $\lambda_n$ $(n = 1, 2, 3, \ldots)$ and the related eigenfunction is

$$y_n(x) = \begin{cases} y_{1n}(x) & \text{if } x \in [0,b], \\ y_{2n}(x) & \text{if } x \in [b,\ell], \end{cases} \tag{4.4.4}$$

Because of the self-adjointness, the eigenfunctions are orthogonal:

$$(y_n, y_m)_K = \begin{cases} \lambda_n (y_k, y_n)_M & \text{if } n = m, \\ 0 & \text{if } n \neq m. \end{cases} \qquad n, m = 1, 2, 3 \ldots\,. \tag{4.4.5}$$

If we set $n$ and $m$ equal, there is

$$\lambda_n = \frac{(y_n, y_n)_K}{(y_n, y_n)_M} \tag{4.4.6}$$

If

$$(u,u)_K > 0\,, \quad \text{and} \quad (u,u)_M > 0 \tag{4.4.7}$$

is fulfilled for any $u$ then the CEP is positive definite.

The eigenvalue problem is simple in case

$$M_1[y] = g_{01}(x) y_1(x) \qquad \text{and} \qquad M_2[y] = g_{02}(x) y_2(x). \tag{4.4.8}$$

Assume that the eigenvalue problem is simple and the Green function of the problem is known. Then

$$y(x) = \lambda \int_0^{\ell} G(x,\xi) g_0(\xi) y(\xi)\,\mathrm{d}\xi\,, \tag{4.4.9}$$

where

$$y(x) = \begin{cases} y_1(x) & \text{if } \xi \in [0,b)\,, \\ y_2(x) & \text{if } \xi \in (b,\ell] \end{cases} \qquad \text{and} \qquad g_0(x) = \begin{cases} g_{01}(x) & \text{if } \xi \in [0,b)\,, \\ g_{02}(x) & \text{if } \xi \in (b,\ell] \end{cases}$$

The structure of $G(x,\xi)$ is given by Eq. (4.1.4). In this way the CEP is replaced by a homogeneous Fredholm integral equation. When that the original eigenvalue problem is self-adjoint, and positive definite, i.e. it holds $g_0(\xi) > 0$ $(\xi \in [0,\ell])$. In such case, the previous

Fredholm integral equation can be rewritten by

$$\mathcal{Y}(x) = \lambda \int_0^{\ell} \mathcal{K}(x,\xi)\mathcal{Y}(\xi)\,\mathrm{d}\xi\,, \tag{4.4.10}$$

where

$$\mathcal{Y}(x) = \sqrt{g_0(x)}y(x), \qquad \mathcal{K}(x,\xi) = \sqrt{g_0(x)}G(x,\xi)\sqrt{g_0(\xi)}. \tag{4.4.11}$$

Here, $\mathcal{Y}(x)$ is the unknown while the kernel $\mathcal{K}(x,\xi)$ is symmetric.

## 4.5. Stepped beams

**4.5.1. Governing equations for heterogeneous stepped beam problems.** Figure 4.1 shows a fixed-fixed (fixed - slider supported) heterogeneous stepped (FFStp) beam and a pinned-pinned stepped (PPStp) beam under the action of an axial force. The arrangement, assumptions and notations are the same as in the previous chapters. The cross-sectional areas $A_i$, $(i = 1, 2)$ are constant and there is cross-sectional heterogeneity. The discontinuity in the cross-sections occurs at coordinate $\hat{b}$.

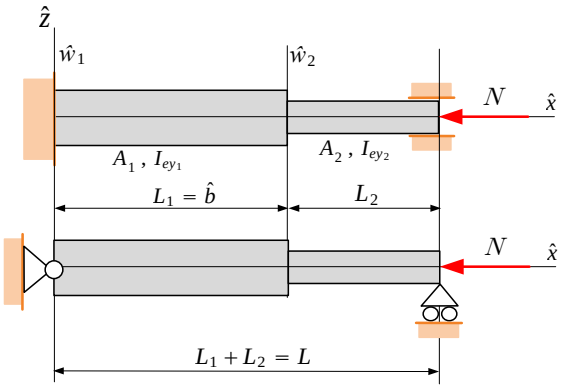


FIGURE 4.1. Heterogeneous stepped beams.

Equilibrium problems of such beams are governed by **[75]**:

$$\begin{aligned} \hat{K}_1(\hat{w}_1(x)) &= I_{ey_1}\frac{\mathrm{d}^4\hat{w}_1}{\mathrm{d}\hat{x}^4} = \hat{f}_{y1}(\hat{x}), \;\; \hat{x} \in [0,\hat{b}]; \\ \hat{K}_2(\hat{w}_2(x)) &= I_{ey_2}\frac{\mathrm{d}^4\hat{w}_2}{\mathrm{d}\hat{x}^4} = \hat{f}_{y2}(\hat{x}), \;\; \hat{x} \in [\hat{b},L] \end{aligned} \tag{4.5.1}$$

The former equation with dimensionless quantities are

$$\begin{gathered} K_i(w_i(x)) = I_{ey_i}w_i^{(4)} = f_{zi}(x)\,, \quad f_{zi} = L^3\hat{f}_{zi}, \quad x \in \begin{cases} [0,b] & \text{if } i=1 \\ [b,\ell] & \text{if } i=2 \end{cases} \\ \frac{\mathrm{d}^k w_i}{\mathrm{d}x^k} = w_i^{(k)}, \;\; (k = 1,\ldots,4) \end{gathered} \tag{4.5.2}$$

The related boundary and continuity conditions are detailed in Table 41.

TABLE 41. Boundary and continuity conditions

| Boundary conditions | |
|---|---|
| (FFStp beams) | (PPStp beams) |
| $w_1(0)=0\,,\ w_1^{(1)}(0)=0$ | $w_1(0)=0\,,\ w_1^{(2)}(0)=0$ |
| $w_2(\ell)=0\,,\ w_2^{(1)}(\ell)=0$ | $w_2(\ell)=0\,,\ w_2^{(2)}(\ell)=0$ |
| Continuity conditions | |
| $w_1(b-0)=w_2(b+0)$ | |
| $w_1^{(1)}(b-0)=w_2^{(1)}(b+0)$ | |
| $I_{ey_1}w_1^{(2)}(b-0)=I_{ey_2}w_2^{(2)}(b+0)$ | |
| $I_{ey_1}w_1^{(3)}(b-0)=I_{ey_2}w_2^{(3)}(b+0)$ | |

If the Green function of the coupled boundary value problem is known, the solution to the dimensionless deflection $w(x)$ ($w(x)=w_1(x)$ if $x\in[0,b]$; $w(x)=w_2(x)$ if $x\in[b,\ell]$), is given by

$$w(x)=\int_0^\ell G(x,\xi)f(\xi)\mathrm{d}\xi,\qquad f(\xi)=\begin{cases} f_{z1}(\xi) & \text{if } \xi\in[0,b],\\ f_{z2}(\xi) & \text{if } \xi\in[b,\ell].\end{cases} \tag{4.5.3}$$

Moving on now to the free vibrations, the loading in this case is

$$f(\xi)=\begin{cases} \rho_{a1}A_1L^4\omega^2w_1(x) & \text{if } \xi\in[0,b],\\ \rho_{a2}A_2L^4\omega^2w_2(x) & \text{if } \xi\in[b,\ell].\end{cases} =\underbrace{\rho_{a1}A_1L^4\omega^2}_{\lambda_d}w(\xi)\begin{cases} 1 & \text{if } \xi\in[0,b],\\ \dfrac{\rho_{a2}A_2}{\rho_{a1}A_1} & \text{if } \xi\in[b,\ell].\end{cases} \tag{4.5.4}$$

in which $w_i(x)$ is the dimensionless vibration amplitude, $\rho_{ai}$ is the average density of $A_i$ while $\omega$ is the natural circular frequency. Hence

$$\begin{aligned} K_1(w_1(x))&=I_{ey_1}w_1^{(4)}=\underbrace{\rho_{a1}A_1L^4\omega^2}_{\lambda_d}w_1(x)\,,\\ K_2(w_1(x))&=I_{ey_2}w_2^{(4)}=\lambda_d\frac{\rho_{a2}A_2}{\rho_{a1}A_1}w_2(x)\end{aligned} \tag{4.5.5}$$

are the equations to be satisfied by $w_i(x)$ to get the $\lambda_d$ eigenvalues. Recalling Eq. (4.5.3) in case the corresponding Green function is known, this eigenvalue problem can be replaced by the Fredholm integral equation:

$$w(x)=\lambda_d\int_0^\ell G(x,\xi)w(\xi)\left\{\begin{array}{ll} 1 & \text{if } \xi\in[0,b],\\ \dfrac{\rho_{a2}A_2}{\rho_{a1}A_1} & \text{if } \xi\in[b,\ell].\end{array}\right\}\mathrm{d}\xi. \tag{4.5.6}$$

**4.5.2. Calculation of the Green function – FFStep.**

4.5.2.1. *Particular solutions.* The linearly independent particular solutions of the corresponding differential equation $K_i(w_i(x),i=1,2)=0$ are

$$w_{11}=w_{12}=1\,,\quad w_{21}=w_{22}=x\,,\quad w_{31}=w_{32}=x^2\,,\quad w_{41}=w_{42}=x^3\,. \tag{4.5.7}$$

4.5.2.2. *Calculations if* $\xi\in(0,b)$. Here we seek the unknown coefficients $a_{m1}(\xi),b_{m1}(\xi)$ and $c_{m1}(\xi)$ for the Green function. To do so, equations (4.2.2) yield

$$\begin{bmatrix} b_{11}\\ b_{21}\\ b_{31}\\ b_{41}\end{bmatrix}=\frac{1}{12I_{ey_1}}\begin{bmatrix} \xi^3\\ -3\xi^2\\ 3\xi\\ -1\end{bmatrix}. \tag{4.5.8}$$

Boundary and continuity conditions of Table 41 determine the following equation system:

Boundary conditions at $x = 0$:

$$\sum_{m=1}^{4} a_{mi} w_{m1}(0) = -\sum_{m=1}^{4} b_{mi} w_{m1}(0)\,, \tag{4.5.9a}$$

$$\sum_{m=1}^{4} a_{mi} w_{m1}^{(1)}(0) = -\sum_{m=1}^{4} b_{mi} w_{m1}^{(1)}(0)\,. \tag{4.5.9b}$$

Continuity conditions at $x = b$:

$$\sum_{m=1}^{4} a_{mi} w_{m1}(b) - \sum_{m=1}^{4} c_{mi} w_{m2}(b) = \sum_{m=1}^{4} b_{mi} w_{m1}(b)\,, \tag{4.5.9c}$$

$$\sum_{m=1}^{4} a_{mi} w_{m1}^{(1)}(b) - \sum_{m=1}^{4} c_{mi} w_{m2}^{(1)}(b) = \sum_{m=1}^{4} b_{mi} w_{m1}^{(1)}(b)\,, \tag{4.5.9d}$$

$$\sum_{m=1}^{4} a_{mi} w_{m1}^{(2)}(b) - \underbrace{\frac{I_{ey_2}}{I_{ey_1}}}_{\alpha} \sum_{m=1}^{4} c_{mi} w_{m2}^{(2)}(b) = \sum_{m=1}^{4} b_{mi} w_{m1}^{(2)}(b)\,, \tag{4.5.9e}$$

$$\sum_{m=1}^{4} a_{mi} w_{m1}^{(3)}(b) - \underbrace{\frac{I_{ey_2}}{I_{ey_1}}}_{\alpha} \sum_{m=1}^{4} c_{mi} w_{m2}^{(3)}(b) = \sum_{m=1}^{4} b_{mi} w_{m1}^{(3)}(b)\,. \tag{4.5.9f}$$

Boundary conditions at $x = \ell$:

$$\sum_{m=1}^{4} c_{mi} w_{m2}(0) = 0\,, \tag{4.5.9g}$$

$$\sum_{m=1}^{4} c_{mi} w_{m2}^{(1)}(0) = 0\,. \tag{4.5.9h}$$

After substituting $w_{m1}$, $w_{m2}$ and $b_{m1}$ equation system (4.5.9) takes the form:

$$\begin{bmatrix} 1 & 0 & 0 & 0 & 0 & 0 & 0 & 0 \\ 0 & 1 & 0 & 0 & 0 & 0 & 0 & 0 \\ 0 & 0 & b^2 & b^3 & -1 & -b & -b^2 & -b^3 \\ 0 & 0 & 2b & 3b^2 & 0 & -1 & -2b & -3b^2 \\ 0 & 0 & 2 & 6b & 0 & 0 & -2\alpha & -6\alpha b \\ 0 & 0 & 0 & 6 & 0 & 0 & 0 & -6\alpha \\ 0 & 0 & 0 & 0 & 1 & \ell & \ell^2 & \ell^3 \\ 0 & 0 & 0 & 0 & 0 & 1 & 2\ell & 3\ell^2 \end{bmatrix} \begin{bmatrix} a_{11} \\ a_{21} \\ a_{31} \\ a_{41} \\ c_{11} \\ c_{21} \\ c_{31} \\ c_{41} \end{bmatrix} = \frac{1}{12 I_{ey_1}} \begin{bmatrix} -\xi^3 \\ 3\xi^2 \\ 2\xi^3 - 6\xi^2 b + 3\xi b^2 - b^3 \\ -6\xi^2 + 6\xi b - 3b^2 \\ 6\xi - 6b \\ -6 \\ 0 \\ 0 \end{bmatrix}. \tag{4.5.10}$$

Therefore, $G_{11}(x,\xi)$ and $G_{21}(x,\xi)$ are available as

$$\begin{aligned} G_{11}(x,\xi) = {} & \left(-\frac{\xi^3}{12 I_{ey_1}} \pm \frac{\xi^3}{12 I_{ey_1}}\right) + \left(\frac{3}{12 I_{ey_1}}\xi^2 \pm -\frac{3}{12 I_{ey_1}}\xi^2\right)x + \\ & + \left\{ \frac{3\xi}{12 \mathcal{D} I_{ey_1}} \left[ (\ell - b)^4 + \alpha \left( -4b^3\alpha\xi + 2\alpha b^2\xi^2 + 4b^3\xi - 2b^2\xi^2 + 2\ell^2\xi^2 - \right.\right.\right. \\ & \left.\left.\left. - 4\ell^3\xi + 4b\ell^3 - 6b^2\ell^2 + 4\ell b^3 + \alpha b^4 - 2b^4 \right) \right] \pm \frac{3\xi}{12} \right\} x^2 + \\ & + \left\{ -\frac{1}{12 \mathcal{D} I_{ey_1}} \left[ (\ell - b)^4 + \alpha \left( 4b\ell^3 - 6b^2\ell^2 + 4\ell b^3 + \alpha b^4 - 2b^4 - 6\ell^2\xi^2 + \right.\right.\right. \end{aligned}$$

$$+4\alpha b\xi^3 - 6\alpha b^2\xi^2 + 4\ell\xi^3 - 4b\xi^3 + 6b^2\xi^2)\big] \pm -\frac{1}{12}\Big\} x^3, \quad (4.5.11)$$

$$G_{21}(x,\xi) = \frac{1}{6\mathcal{D}I_{ey1}}\xi^2\left(\ell - x\right)^2\left[3\ell^2 x - 6\ell b^2 + 6b^3 - 3b^2 x - 3b^2\xi + 6b^2\alpha\ell - 6b^3\alpha + \right.$$
$$\left. +3b^2\alpha x - \xi\ell^2 + 4\xi\ell b - 2\xi\ell x + 2bx\xi - 4\xi\alpha b\ell + 3\xi\alpha b^2 - 2\xi b\alpha x\right], \quad (4.5.12)$$

where

$$\mathcal{D} = (\ell - b)^4 + \alpha b\left(\alpha b^3 - 2b^3 + 4\ell b^2 - 6\ell^2 b + 4\ell^3\right). \quad (4.5.13)$$

4.5.2.3. *Calculations when* $\xi \in (b,\ell)$*:* According to equations (2.2.22) and (2.2.23), while using Property 4, the equality $w_{m1}(x) = w_{m2}$ and equation (4.5.8), it follows that

$$\begin{bmatrix} b_{12} \\ b_{22} \\ b_{32} \\ b_{42} \end{bmatrix} = \frac{1}{12I_{ey_2}} \begin{bmatrix} \xi^3 \\ -3\xi^2 \\ 3\xi \\ -1 \end{bmatrix}. \quad (4.5.14)$$

The boundary and continuity conditions lead to

$$\begin{bmatrix} 1 & b & b^2 & b^3 & 0 & 0 & -b^2 & -b^3 \\ 0 & 1 & 2b & 3b^2 & 0 & 0 & -2b & -3b^2 \\ 0 & 0 & 2\alpha & 6\alpha b & 0 & 0 & -2 & -6b \\ 0 & 0 & 0 & \alpha & 0 & 0 & 0 & -1 \\ 0 & 0 & 0 & 0 & 1 & 0 & 0 & 0 \\ 0 & 0 & 0 & 0 & 0 & 1 & 0 & 0 \\ 1 & \ell & \ell^2 & \ell^3 & 0 & 0 & 0 & 0 \\ 0 & 1 & 2\ell & 3\ell^2 & 0 & 0 & 0 & 0 \end{bmatrix} \begin{bmatrix} a_{12} \\ a_{22} \\ a_{32} \\ a_{42} \\ c_{12} \\ c_{22} \\ c_{32} \\ c_{42} \end{bmatrix} = \frac{-1}{12I_{ey_2}} \begin{bmatrix} \xi^3 - 3b\xi^2 + 3b^2\xi - b^3 \\ -3\xi^2 + 6b\xi - 3b^2 \\ \alpha\left(6\xi - 6b\right) \\ -\alpha \\ 0 \\ 0 \\ -\xi^3 + 3\xi^2\ell - 3\xi\ell^2 + \ell^3 \\ 3\xi^2 - 6\ell\xi + 3\ell^2 \end{bmatrix}. \quad (4.5.15)$$

As a consequence, the Green functions are

$$G_{12}(x,\xi) = \frac{1}{6\mathcal{D}I_{ey_1}}x^2\left(\ell - \xi\right)^2\left[3\ell^2\xi - 6b^2\ell + 6b^3 - 3b^2\xi + 6b^2\alpha\ell - 6b^3\alpha + 3b^2\alpha\xi \right.$$
$$\left. -x\ell^2 + 4x\ell b - 2x\ell\xi - 3xb^2 + 2xb\xi - 4x\alpha b\ell + 3x\alpha b^2 - 2xb\alpha\xi\right], \quad (4.5.16)$$

$$G_{22}(x,\xi) =$$
$$= \frac{1}{12\mathcal{D}I_{ey_2}}\left[-\left(\ell - b\right)\left(-2b\ell + \xi\ell + b\xi\right)\left(-2\ell^2b^2 + 2b\ell^2\xi + \ell^2\xi^2 + 2b^2\ell\xi - 4b\ell\xi^2 + b^2\xi^2\right) - \right.$$
$$- b\alpha\left(6b\xi\ell^4 - 12\ell^2\xi b^3 + 6b^3\xi\ell^2\alpha + 12\ell^2b^2\xi^2 + 4\ell^3\xi^3 - 12b\ell^3\xi^2 - 4\ell^4b^2 + 8\ell^3b^3 - \right.$$
$$\left. \left. -4b^3\ell^3\alpha + 2\xi^3b^3 - b^3\xi^3\alpha - 4b^2\xi^3\ell\right)\right] \pm \frac{\xi^3}{12I_{ey_2}} +$$
$$+ \left\{-\frac{3}{12\mathcal{D}I_{ey_2}}\left[\left(\ell - b\right)\left(4\ell^3b\xi - 2\ell^3b^2 - \ell^3\xi^2 - 5\ell^2\xi^2b + 4\ell^2b^2\xi - 2\ell^2b^3 + 4\ell b\xi^3 - 5\ell\xi^2b^2 + 4\ell b^3\xi - \xi^2b^3\right) - \right.\right.$$
$$- b\alpha\left(-b^3\alpha\xi^2 - 2\ell^4b - 8\ell b^3\xi + 4b^3\alpha\ell\xi - 4\ell b\xi^3 + 4\ell^4\xi + 4\ell^2\xi^3 - 4\ell^3\xi^2 + \right.$$
$$\left. \left. \left. +4\ell\xi^2b^2 + 2\xi^2b^3 + 4\ell^2b^3 - 2b^3\ell^2\alpha\right)\right] \pm \frac{-3\xi^2}{12I_{ey_2}}\right\} x +$$
$$+ \left\{\frac{3}{12\mathcal{D}I_{ey_2}}\left[\left(\ell - b\right)\left(-4b^2\xi^2 - 4b^2\ell^2 - 4\xi^2\ell^2 + 2b\xi^3 + b^3\xi + \xi\ell^3 + 2\xi^3\ell + 5b\xi\ell^2 - 4b\xi^2\ell + 5b^2\xi\ell\right) - \right.\right.$$
$$\left. \left. -b\alpha\left(4b^2\xi^2 + 4b^2\ell^2 - 2b\xi^3 - 2b^3\xi - 4b\ell^3 + 4\xi\ell^3 + b^3\alpha\xi - 4b^2\xi\ell\right)\right] \pm \frac{3\xi}{12I_{ey_2}}\right\} x^2 +$$
$$+ \left\{-\frac{1}{12\mathcal{D}I_{ey_2}}\left[\left(\ell - b\right)\left(b - 2\xi + \ell\right)\left(2b\xi - 4b\ell - 2\xi^2 + \ell^2 + 2\xi\ell + b^2\right) + \right.\right.$$

$$+b\alpha\left(4\xi^3+4\ell^3-b^3\alpha-6b\xi^2-4b^2\ell-12\xi\ell^2+2b^3+12b\xi\ell\right)\Big]\pm\frac{-1}{12I_{ey_2}}\Big\}x^3 \quad (4.5.17)$$

The unit of the Green function is $1/\mathrm{N\,mm}^2$.

If we introduce the dimensionless distributed load

$$\mathfrak{f}_{zi}=\frac{f_{zi}}{I_{ey_i}}=\frac{L^3\hat{f}_{zi}}{I_{ey_i}} \quad (4.5.18)$$

and multiply equations $(4.5.2)_1$ by $1/I_{ey_i}$, then

$$w_i^{(4)}=\mathfrak{f}_{zi}(x)\,. \quad (4.5.19)$$

What is found now is a three-point boundary value problem. The dimensionless Green function for this three-point boundary value problem is

$$\mathcal{G}(x,\xi)=\begin{cases}\mathcal{G}_{11}(x,\xi)=I_{ey_1}G_{11}(x,\xi) & \text{if } x,\xi\in[0,b],\\ \mathcal{G}_{21}(x,\xi)=I_{ey_1}G_{21}(x,\xi) & \text{if } x\in[b,\ell] \text{ and } \xi\in[0,b],\\ \mathcal{G}_{12}(x,\xi)=I_{ey_2}G_{12}(x,\xi) & \text{if } x\in[0,b] \text{ and } \xi\in[b,\ell],\\ \mathcal{G}_{22}(x,\xi)=I_{ey_2}G_{22}(x,\xi) & \text{if } x,\xi\in[b,\ell],\end{cases} \quad (4.5.20)$$

$\mathcal{G}(x,\xi)$ depends on $I_{ey_1}$ and $I_{ey_2}$ via $\alpha$, as the beam is stepped. The solution for equilibrium problem is therefore

$$w(x)=\int_0^\ell \mathcal{G}(x,\xi)\mathfrak{f}(\xi)\mathrm{d}\xi,\qquad \mathfrak{f}(\xi)=\begin{cases}\mathfrak{f}_{z1}(\xi) & \text{if } \xi\in[0,b],\\ \mathfrak{f}_{z2}(\xi) & \text{if } \xi\in[b,\ell].\end{cases}$$

Although the three-point boundary value problem is not self-adjoint, the symmetry conditions

$$\begin{cases}\mathcal{G}_{11}(x,\xi)=\mathcal{G}_{11}(\xi,x) & \text{if } x,\xi\in[0,b],\\ \frac{\mathcal{G}_{21}(x,\xi)}{I_{ey1}}=\frac{\mathcal{G}_{12}(\xi,x)}{I_{ey2}} & \text{if } x\in[b,\ell] \text{ and } \xi\in[0,b],\\ \mathcal{G}_{22}(x,\xi)=\mathcal{G}_{22}(\xi,x) & \text{if } x,\xi\in[b,\ell]\end{cases} \quad (4.5.21)$$

are fulfilled.

If we write $\hat{b}$, $L$ ,$\hat{x}$ and $\hat{\xi}$ for $b$, $\ell$, $x$ and $\xi$ in Eqs. (4.5.20), the Green function is available for the cube of the length unit. Figure 4.2 shows this Green function for a FFStep beam with $L=100$ mm, $\hat{b}=50$ mm, $\hat{\xi}=75$ mm and $\alpha$= 0.512.

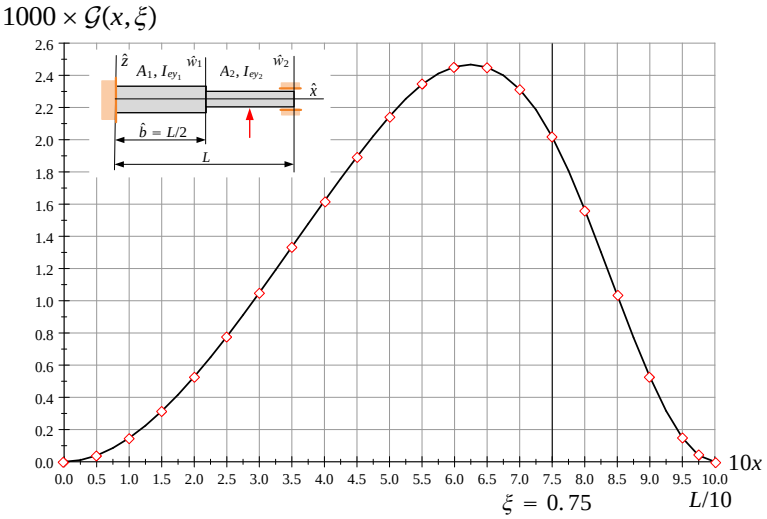


FIGURE 4.2. The Green function of an FFStp beam

**4.5.3. Green function – PPStep.** Repeating the calculation steps detailed in Subsection 4.5.2 for PPStep beams yields [**81**]:

$$G_{11}(x,\xi) = \frac{1}{12I_{ey_1}}\left\{(-\xi^3 \pm \xi^3) + \right.$$
$$+\left[\frac{\xi}{\alpha\ell^2}\left(4\left(\ell-b\right)^3+\alpha\left(12\ell b\left(\ell-b\right)+2\xi^2\ell+4b^3-3\xi\ell^2\right)\right)\pm\left(-3\xi^2\right)\right]x+$$
$$\left.+\left(-3\xi\pm 3\xi\right)x^2+\left(-\frac{1}{\ell}\left(\ell-2\xi\right)\pm(-1)\right)x^3\right\}, \quad (4.5.22a)$$

$$G_{21}(x,\xi) = \frac{2\xi\left(\ell-x\right)}{12I_{ey_1}\alpha\ell^2}\left(2x\ell^2-3\ell b^2-x^2\ell+2b^3+\alpha\left(3\ell b^2-\xi^2\ell-2b^3\right)\right). \quad (4.5.22b)$$

and

$$G_{12}(x,\xi) = \frac{2x\left(\ell-\xi\right)}{12I_{ey_2}\ell^2}\left(2\xi\ell^2-3\ell b^2-\xi^2\ell+2b^3+\alpha\left(3\ell b^2-2b^3-x^2\ell\right)\right), \quad (4.5.23a)$$

$$G_{2I}(x,\xi) = \frac{2\xi\left(\ell-x\right)}{12I_{ey_1}\alpha\ell^2}\left(2x\ell^2-3\ell b^2-x^2\ell+2b^3+\alpha\left(3\ell b^2-\xi^2\ell-2b^3\right)\right) =$$
$$= \frac{2\xi\left(\ell-x\right)}{12I_{ey_2}\ell^2}\left(2x\ell^2-3\ell b^2-x^2\ell+2b^3+\alpha\left(3\ell b^2-\xi^2\ell-2b^3\right)\right). \quad (4.5.23b)$$

With (4.5.20), the eigenvalue problem can be rewritten into

$$w(x) = \lambda_d\int_0^\ell \mathcal{G}(x,\xi)w(\xi)\left\{\begin{array}{ll} 1 & \text{if } \xi\in[0,b],\\ \kappa & \text{if } \xi\in[b,\ell].\end{array}\right\}\mathrm{d}\xi\,, \quad (4.5.24)$$

where

$$\lambda = \frac{\lambda}{I_{ey_1}} = \frac{\rho_{a1}A_1L^4}{I_{ey_1}}\omega^2, \qquad \text{and} \qquad \kappa = \frac{\rho_{a2}A_2I_{ey_1}}{\rho_{a1}A_1I_{ey_2}} \quad (4.5.25)$$

is the new eigenvalue.

**4.5.4. Example 1.** Consider the FFStep beam as shown in Figure 4.3. It is assumed that $[\nu = 1 \text{ if } \hat{x}\in[0,\hat{b})]$ $(\nu = 0.95, 0.90, 0.85, 0.80, 0.75 \text{ if } \hat{x}\in(\hat{b},L])$. The cross-sectional parameters and material distribution are the same as those mentioned in the example of the previous chapter, except that the height $c = \nu a$ is now a parameter.

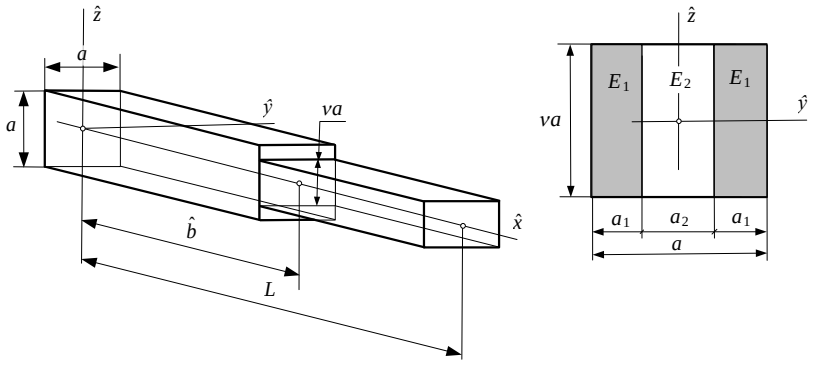


FIGURE 4.3. A stepped beam with rectangular cross section

TABLE 42. Data for the cross sections

| $\nu$ | $\rho_{a1}=\rho_{a2}=\rho_a$ kg/mm$^3$ | $I_{ey1}$ kg mm$^3$/$s^2$ | $I_{ey2}$ kg mm$^3$/$s^2$ | $\alpha=\frac{I_{ey2}}{I_{ey1}}$ | $\kappa$ |
|---|---|---|---|---|---|
| 0.95 | $4.423333\times10^{-6}$ | $9.5\times10^{14}$ | $8.145\,1\times10^{14}$ | 0.857375 | 1.1080332 |
| 0.90 | | | $6.925\,5\times10^{14}$ | 0.729000 | 1.2345679 |
| 0.85 | | | $5.834\,2\times10^{14}$ | 0.614125 | 1.3840835 |
| 0.80 | | | $4.8640\times10^{14}$ | 0.512000 | 1.5625000 |
| 0.75 | | | $4.007\,8\times10^{14}$ | 0.421875 | 1.7777778 |

The related eigenvalue problem is solved numerically using a solution algorithm that is based on the boundary element method [**78**]. Figure 4.4 shows the numerical results for $\sqrt{\lambda_1}/4.73004^2$ as function of parameter $b$. Each curve in Figure 4.4 represents a different value of the parameter $\alpha$. With $\lambda_1$ it follows form Eq. (4.5.25) that

$$\omega_1=\frac{1}{L^2}\sqrt{\frac{I_{ey_1}}{\rho_{a1}A_1}\lambda_1}\,. \tag{4.5.26}$$

Assume that $\nu=0.8$ and $b=0.5$, thus

$$\sqrt{\lambda_1}=4.73004^2\times0.88372654=19.771\,859$$

and

$$\omega_1=181.098\,36\ \text{ r/s}.$$

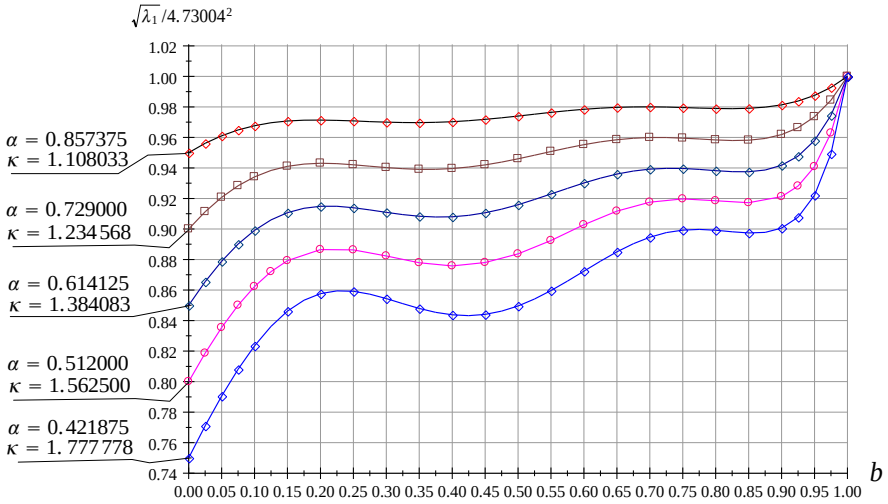


FIGURE 4.4. The first eigenvalue as a function of $b$; $\alpha$ and $\kappa$ are parmeters [**82**].

If there is no step in the beam cross-section, the eigenvalues coincide with that presented in Figure 3.4 for $b=0$ and $c=1$.

## 4.6. Axially loaded stepped beams

**4.6.1. Governing equations.** Equilibrium problems of axially loaded beams are governed by

$$\begin{aligned}K_{1a}(w_1(x))&=I_{ey_1}w_1^{(4)}\pm N_1L^2w_1^{(2)}=f_{z1}(x),\ \ x\in[0,b];\\ K_{2a}(w_2(x))&=I_{ey_2}w_2^{(4)}\pm N_2L^2w_2^{(2)}=f_{z2}(\hat{x}),\ \ x\in[b,l]\end{aligned} \tag{4.6.1}$$

where $N_1 > 0$ and $N_2 > 0$ are axial compressive forces. These equations are associated with boundary and continuity conditions in Table 41. If $f_{z1}(x) = f_{z2}(x) = 0$, $N_1 = N_2 = N$ and $N > 0$, we get an problem for the critical load $N_{crit}$.

Given that we know the Green functions $G_c(x,\xi)$ ($N$ is compressive) and $G_t(x,\xi)$ ($N$ is tensile) solution for the dimensionless deflection $w(x)$ ($w(x) = w_1(x)$ if $x \in [0,b]$; $w(x) = w_2(x)$ if $x \in [b,\ell]$) is given by integral (4.5.3).

When the axially loaded beam does transverse vibrations, there is a homogeneous integral equation (4.5.6) with ($G = G_c(x,\xi)$) [$G = G_t(x,\xi)$] as the kernel function.

**4.6.2. Green function for compressive force case.** With

$$\mathcal{N}_1 = \frac{NL^2}{I_{ey_1}} \quad \text{and} \quad \mathcal{N}_2 = \frac{NL^2}{I_{ey_2}} \tag{4.6.2}$$

the particular solutions to the dimensionless displacements in equations (4.6.1) are given by

$$w_{11} = 1,\ \ w_{12} = x,\ \ w_{13} = \cos p_1 x,\ \ w_{14} = \sin p_1 x\,, \quad x \in [0,b)\,, \quad p_1 = \sqrt{\mathcal{N}_1}; \tag{4.6.3a}$$

$$w_{21} = 1,\ \ w_{22} = x,\ \ w_{23} = \cos p_2 x,\ \ w_{24} = \sin p_2 x\,, \quad x \in (b, \ell = 1]\,, \quad p_2 = \sqrt{\mathcal{N}_2}. \tag{4.6.3b}$$

If $\xi \in (0,b)$, we repeat the calculation steps detailed in Subsection 4.5.2.2. Therefore, we get the following systems for FFStep beams:

$$\begin{bmatrix} 1 & \xi & \cos p_1\xi & \sin p_1\xi \\ 0 & 1 & -p_1 \sin p_1\xi & p_1 \cos p_1\xi \\ 0 & 0 & -p_1^2 \cos p_1\xi & -p_1^2 \sin p_1\xi \\ 0 & 0 & p_1^3 \sin p_1\xi & -p_1^3 \cos p_1\xi \end{bmatrix} \begin{bmatrix} b_{11} \\ b_{21} \\ b_{31} \\ b_{41} \end{bmatrix} = \begin{bmatrix} 0 \\ 0 \\ 0 \\ -\frac{1}{2I_{ey_1}} \end{bmatrix}, \quad \begin{bmatrix} b_{11} \\ b_{21} \\ b_{31} \\ b_{41} \end{bmatrix} = \frac{1}{2I_{ey_1}} \begin{bmatrix} \frac{\xi}{p_1^2} \\ -\frac{1}{p_1^2} \\ -\frac{\sin p_1\xi}{p_1^3} \\ \frac{\cos p_1\xi}{p_1^3} \end{bmatrix} \tag{4.6.4}$$

and

$$\begin{bmatrix} 1 & 0 & 1 & 0 & 0 & 0 & 0 & 0 \\ 0 & 1 & 0 & p_1 & 0 & 0 & 0 & 0 \\ 1 & b & \cos p_1 b & \sin p_1 b & -1 & -b & -\cos p_2 b & -\sin p_2 b \\ 0 & 1 & -p_1 \sin p_1 b & p_1 \cos p_1 b & 0 & -1 & p_2 \sin p_2 b & -p_2 \cos p_2 b \\ 0 & 0 & -p_1^2 \cos p_1 b & -p_1^2 \sin p_1 b & 0 & 0 & \alpha p_2^2 \cos p_2 b & \alpha p_2^2 \sin p_2 b \\ 0 & 0 & p_1^3 \sin p_1 b & -p_1^3 \cos p_1 b & 0 & 0 & -\alpha p_2^3 \sin p_2 b & \alpha p_2^3 \cos p_2 b \\ 0 & 0 & 0 & 0 & 1 & \ell & \cos p_2 \ell & \sin p_2 \ell \\ 0 & 0 & 0 & 0 & 0 & 1 & -p_2 \sin p_2 \ell & p_2 \cos p_2 \ell \end{bmatrix} \begin{bmatrix} a_{11} \\ a_{21} \\ a_{31} \\ a_{41} \\ c_{11} \\ c_{21} \\ c_{31} \\ c_{41} \end{bmatrix} =$$

$$= \frac{1}{2I_{ey_1} p_1^3} \begin{bmatrix} -p_1\xi + \sin p_1\xi \\ p_1 - p_1 \cos p_1\xi. \\ p_1\xi - p_1 b + \sin p_1 (b-\xi) \\ -p_1 + p_1 \cos p_1 (b-\xi) \\ -p_1^2 \sin p_1 (b-\xi) \\ -p_1^3 \cos p_1 (b-\xi) \\ 0 \\ 0 \end{bmatrix} \tag{4.6.5}$$

When considering PPStep beams, note that the functions $b_i$ are the same as those for FFStep beams. The second equation system is of the form:

$$\begin{bmatrix} 1 & 0 & 1 & 0 & 0 & 0 & 0 & 0 \\ 0 & 0 & 1 & 0 & 0 & 0 & 0 & 0 \\ 1 & b & \cos p_1 b & \sin p_1 b & -1 & -b & -\cos p_2 b & -\sin p_2 b \\ 0 & 1 & -p_1 \sin p_1 b & p_1 \cos p_1 b & 0 & -1 & p_2 \sin p_2 b & -p_2 \cos p_2 b \\ 0 & 0 & -p_1^2 \cos p_1 b & -p_1^2 \sin p_1 b & 0 & 0 & \alpha p_2^2 \cos p_2 b & \alpha p_2^2 \sin p_2 b \\ 0 & 0 & p_1^3 \sin p_1 b & -p_1^3 \cos p_1 b & 0 & 0 & -\alpha p_2^3 \sin p_2 b & \alpha p_2^3 \cos p_2 b \\ 0 & 0 & 0 & 0 & 1 & \ell & \cos p_2 \ell & \sin p_2 \ell \\ 0 & 0 & 0 & 0 & 0 & 0 & \cos p_2 \ell & \sin p_2 \ell \end{bmatrix} \begin{bmatrix} a_{11} \\ a_{21} \\ a_{31} \\ a_{41} \\ c_{11} \\ c_{21} \\ c_{31} \\ c_{41} \end{bmatrix} =$$

$$= \frac{1}{2I_{ey_1} p_1^3} \begin{bmatrix} -p_1\xi + \sin p_1 \xi \\ \sin p_1 \xi \\ p_1 \xi - p_1 b + \sin p_1 (b - \xi) \\ -p_1 + p_1 \cos p_1 (b - \xi) \\ -p_1^2 \sin p_1 (b - \xi) \\ -p_1^3 \cos p_1 (\xi - b) \\ 0 \\ 0 \end{bmatrix} \tag{4.6.6}$$

Note that the notations for the unknowns are the same as before.
If $\xi \in (b, \ell)$ – repeating the steps of Subsection 4.5.2.3 – yields for FFStep beams:

$$\begin{bmatrix} 1 & \xi & \cos p_2 \xi & \sin p_2 \xi \\ 0 & 1 & -p_2 \sin p_2 \xi & p_2 \cos p_2 \xi \\ 0 & 0 & -p_2^2 \cos p_2 \xi & -p_2^2 \sin p_2 \xi \\ 0 & 0 & p_2^3 \sin p_2 \xi & -p_2^3 \cos p_2 \xi \end{bmatrix} \begin{bmatrix} b_1 \\ b_2 \\ b_3 \\ b_4 \end{bmatrix} = \begin{bmatrix} 0 \\ 0 \\ 0 \\ -\frac{1}{2I_{ey_1}} \end{bmatrix}, \quad \begin{bmatrix} b_{12} \\ b_{22} \\ b_{32} \\ b_{42} \end{bmatrix} = \frac{1}{2I_{ey_1}} \begin{bmatrix} \frac{\xi}{p_2^2} \\ -\frac{1}{p_2^2} \\ -\frac{\sin p_2 \xi}{p_2^3} \\ \frac{\cos p_2 \xi}{p_2^3} \end{bmatrix} \tag{4.6.7}$$

and

$$\begin{bmatrix} 1 & b & \cos p_2 b & \sin p_2 b & -1 & -b & -\cos p_1 b & -\sin p_1 b \\ 0 & 1 & -p_2 \sin p_2 b & p_2 \cos p_2 b & 0 & -1 & p_1 \sin p_1 b & -p_1 \cos p_1 b \\ 0 & 0 & -\alpha p_2^2 \cos p_2 b & -\alpha p_2^2 \sin p_2 b & 0 & 0 & p_1^2 \cos p_1 b & p_1^2 \sin p_1 b \\ 0 & 0 & \alpha p_2^3 \sin p_2 b & -\alpha p_2^3 \cos p_2 b & 0 & 0 & -p_1^3 \sin p_1 b & p_1^3 \cos p_1 b \\ 0 & 0 & 0 & 0 & 1 & 0 & 1 & 0 \\ 0 & 0 & 0 & 0 & 0 & 1 & 0 & p_1 \\ 1 & \ell & \cos p_2 \ell & \sin p_2 \ell & 0 & 0 & 0 & 0 \\ 0 & 1 & -p_2 \sin p_2 \ell & p_2 \cos p_2 \ell & 0 & 0 & 0 & 0 \end{bmatrix} \begin{bmatrix} a_{12} \\ a_{22} \\ a_{32} \\ a_{42} \\ c_{12} \\ c_{22} \\ c_{32} \\ c_{42} \end{bmatrix} =$$

$$= -\frac{1}{2I_{ey_2} p_2^3} \begin{bmatrix} p_2 \xi - p_2 b + \sin p_2 (b - \xi) \\ p_2 \cos p_2 (b - \xi) - p_2 \\ -\alpha p_2^2 \sin p_2 (b - \xi) \\ -\alpha p_2^3 \cos p_2 (b - \xi) \\ 0 \\ 0 \\ -p_2 \xi + p_2 \ell - \sin p_2 (\ell - \xi) \\ p_2 - p_2 \cos p_2 (\ell - \xi) \end{bmatrix} \tag{4.6.8}$$

Moving on now to PPStep beams, the functions $b_{i2}$ are unchanged. The second equation system is

$$\begin{bmatrix} 1 & b & \cos p_2 b & \sin p_2 b & 0 & -b & 0 & -\sin p_1 b \\ 0 & 1 & -p_2 \sin p_2 b & p_2 \cos p_2 b & 0 & -1 & 0 & -p_1 \cos p_1 b \\ 0 & 0 & -\alpha p_2^2 \cos p_2 b & -\alpha p_2^2 \sin p_2 b & 0 & 0 & 0 & p_1^2 \sin p_1 b \\ 0 & 0 & \alpha p_2^3 \sin p_2 b & -\alpha p_2^3 \cos p_2 b & 0 & 0 & 0 & p_1^3 \cos p_1 b \\ 0 & 0 & 0 & 0 & 1 & 0 & 0 & 0 \\ 0 & 0 & 0 & 0 & 0 & 0 & 1 & 0 \\ 1 & \ell & \cos p_2 \ell & \sin p_2 \ell & 0 & 0 & 0 & 0 \\ 0 & 0 & -\cos p_2 \ell & -\sin p_2 \ell & 0 & 0 & 0 & 0 \end{bmatrix} \begin{bmatrix} a_{12} \\ a_{22} \\ a_{32} \\ a_{42} \\ c_{12} \\ c_{22} \\ c_{32} \\ c_{42} \end{bmatrix} =$$

$$= -\frac{1}{2I_{ey_2} p_2^3} \begin{bmatrix} p_2\xi - p_2 b + \sin p_2 (b - \xi) \\ p_2 \cos p_2 (b - \xi) - p_2 \\ -\alpha p_2^2 \sin p_2 (b - \xi) \\ -\alpha p_2^3 \cos p_2 (b - \xi) \\ 0 \\ 0 \\ -p_2\xi + p_2\ell - \sin p_2 (\ell - \xi) \\ \sin p_2 (\ell - \xi) \end{bmatrix} \tag{4.6.9}$$

The closed form solution for $a_{11}(\xi), \ldots, c_{42}(\xi)$ are very long formulae and thus, are omitted.

The dimensionless Green functions $\mathcal{G}_c(x, \xi)$ can be found using Eq. (4.5.20).

Figure 4.5 shows the dimensionless Green function $\mathcal{G}_c(x, \xi)$ for FFStep case if $\xi = 0.75$.

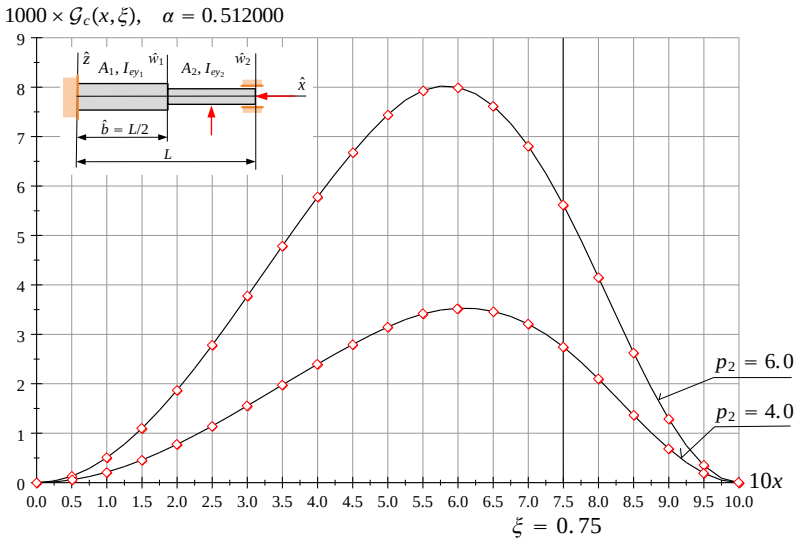


FIGURE 4.5. The Green function of an FFStp beam subjected to a compressive force.

**4.6.3. Green function for tensile force.** Recalling equations (4.6.2) the particular solutions to the dimensionless displacements are given by

$$w_{11} = 1, \quad w_{12} = x, \quad w_{13} = \cosh p_1 x, \quad w_{14} = \sinh p_1 x\,, \quad x \in [0, b); \tag{4.6.10a}$$

$$w_{21} = 1, \quad w_{22} = x, \quad w_{23} = \cosh p_2 x, \quad w_{24} = \sinh p_2 x\,, \quad x \in (b, \ell = 1]. \tag{4.6.10b}$$

The structure of the Green function is the same as before. Assume that $\xi \in (0, b)$. For FFStep beams, the computation steps are given in Subsection 4.5.2.2. This line of thought yields:

$$\begin{bmatrix} 1 & \xi & \cosh p_1\xi & \sinh p_1\xi \\ 0 & 1 & p_1 \sinh p_1\xi & p_1 \cosh p_1\xi \\ 0 & 0 & p_1^2 \cosh p_1\xi & p_1^2 \sinh p_1\xi \\ 0 & 0 & p_1^3 \sinh p_1\xi & p_1^3 \cosh p_1\xi \end{bmatrix} \begin{bmatrix} b_1 \\ b_2 \\ b_3 \\ b_4 \end{bmatrix} = \begin{bmatrix} 0 \\ 0 \\ 0 \\ -\frac{1}{2} \end{bmatrix}, \quad \begin{bmatrix} b_{1I} \\ b_{2I} \\ b_{3I} \\ b_{4I} \end{bmatrix} = \frac{1}{2I_{ey_1}} \begin{bmatrix} -\frac{\xi}{p_1^2} \\ \frac{1}{p_1^2} \\ \frac{\sinh p_1\xi}{p_1^3} \\ -\frac{\cosh p_1\xi}{p_1^3} \end{bmatrix} \tag{4.6.11}$$

Utilizing the boundary conditions, the equation system for $a_{iI}$ and $c_{iI}$ becomes

$$\begin{bmatrix} 1 & 0 & 1 & 0 & 0 & 0 & 0 & 0 \\ 0 & 1 & 0 & p_1 & 0 & 0 & 0 & 0 \\ 1 & b & \cosh p_1 b & \sinh p_1 b & -1 & -b & -\cosh p_2 b & -\sinh p_2 b \\ 0 & 1 & p_1 \sinh p_1 b & p_1 \cosh p_1 b & 0 & -1 & -p_2 \sinh p_2 b & -p_2 \cosh p_2 b \\ 0 & 0 & p_1^2 \cosh p_1 b & p_1^2 \cosh p_1 b & 0 & 0 & -\alpha p_2^2 \cosh p_2 b & -\alpha p_2^2 \sinh p_2 b \\ 0 & 0 & p_1^3 \sinh p_1 b & p_1^3 \cosh p_1 b & 0 & 0 & -\alpha p_2^3 \sinh p_2 b & -\alpha p_2^3 \cosh p_2 b \\ 0 & 0 & 0 & 0 & 1 & \ell & \cosh p_2 \ell & \sinh p_2 \ell \\ 0 & 0 & 0 & 0 & 0 & 1 & p_2 \sinh p_2 \ell & p_2 \cosh p_2 \ell \end{bmatrix} \begin{bmatrix} a_{1I} \\ a_{2I} \\ a_{3I} \\ a_{4I} \\ c_{1I} \\ c_{2I} \\ c_{3I} \\ c_{4I} \end{bmatrix} =$$

$$= \frac{1}{2I_{ey_1} p_1^3} \begin{bmatrix} p_1\xi - \sinh p_1 \xi \\ -p_1 + p_1 \cosh p_1 \xi. \\ -p_1\xi + p_1 b - \sinh p_1 (b - \xi) \\ p_1 - p_1 \cosh p_1 (b - \xi) \\ -p_1^2 \sinh p_1 (b - \xi) \\ -p_1^3 \cosh p_1 (b - \xi) \\ 0 \\ 0 \end{bmatrix} \tag{4.6.12}$$

The functions $b_{iI}$ will not change for the current boundary conditions. As for the second equation system, we have from the boundary conditions that:

$$\begin{bmatrix} 1 & 0 & 1 & 0 & 0 & 0 & 0 & 0 \\ 0 & 0 & 1 & 0 & 0 & 0 & 0 & 0 \\ 1 & b & \cosh p_1 b & \sinh p_1 b & -1 & -b & -\cosh p_2 b & -\sinh p_2 b \\ 0 & 1 & p_1 \sinh p_1 b & p_1 \cosh p_1 b & 0 & -1 & -p_2 \sinh p_2 b & -p_2 \cosh p_2 b \\ 0 & 0 & p_1^2 \cosh p_1 b & p_1^2 \cosh p_1 b & 0 & 0 & -\alpha p_2^2 \cosh p_2 b & -\alpha p_2^2 \sinh p_2 b \\ 0 & 0 & p_1^3 \sinh p_1 b & p_1^3 \cosh p_1 b & 0 & 0 & -\alpha p_2^3 \sinh p_2 b & -\alpha p_2^3 \cosh p_2 b \\ 0 & 0 & 0 & 0 & 1 & \ell & \cosh p_2 \ell & \sinh p_2 \ell \\ 0 & 0 & 0 & 0 & 0 & 0 & \cosh p_2 \ell & \sinh p_2 \ell \end{bmatrix} \begin{bmatrix} a_{1I} \\ a_{2I} \\ a_{3I} \\ a_{4I} \\ c_{1I} \\ c_{2I} \\ c_{3I} \\ c_{4I} \end{bmatrix} =$$

$$= \frac{1}{2I_{ey_1} p_1^3} \begin{bmatrix} p_1\xi - \sinh p_1 \xi \\ -\sinh p_1 \xi \\ -p_1\xi + p_1 b - \sinh p_1 (b - \xi) \\ p_1 - p_1 \cosh p_1 (b - \xi) \\ -p_1^2 \sinh p_1 (b - \xi) \\ -p_1^3 \cosh p_1 (b - \xi) \\ 0 \\ 0 \end{bmatrix} \tag{4.6.13}$$

Next, $\xi \in (b, \ell)$. Recalling the calculation steps from Subsection 4.5.2.3, we obtain the following equation systems for $b_{iII}$, $a_{iII}$ and $c_{iII}$:

$$\begin{bmatrix} 1 & \xi & \cosh p_2 \xi & \sinh p_2 \xi \\ 0 & 1 & p_2 \sinh p_2 \xi & p_2 \cosh p_2 \xi \\ 0 & 0 & p_2^2 \cosh p_2 \xi & p_2^2 \sinh p_2 \xi \\ 0 & 0 & p_2^3 \sinh p_2 \xi & p_2^3 \cosh p_2 \xi \end{bmatrix} \begin{bmatrix} b_1 \\ b_2 \\ b_3 \\ b_4 \end{bmatrix} = \begin{bmatrix} 0 \\ 0 \\ 0 \\ -\frac{1}{2I_{ey_2}} \end{bmatrix}, \quad \begin{bmatrix} b_{1II} \\ b_{2II} \\ b_{3II} \\ b_{4II} \end{bmatrix} = \frac{1}{2I_{ey_2}} \begin{bmatrix} -\frac{\xi}{p_2^2} \\ \frac{1}{p_2^2} \\ \frac{\sinh p_2 \xi}{p_2^3} \\ -\frac{\cosh p_2 \xi}{p_2^3} \end{bmatrix}, \tag{4.6.14}$$

$$\begin{bmatrix} 1 & b & \cosh p_2 b & \sinh p_2 b & -1 & -b & -\cosh p_1 b & -\sinh p_1 b \\ 0 & 1 & p_2 \sinh p_2 b & p_2 \cosh p_2 b & 0 & -1 & -p_1 \sinh p_1 b & -p_1 \cosh p_1 b \\ 0 & 0 & \alpha p_2^2 \cosh p_2 b & \alpha p_2^2 \sinh p_2 b & 0 & 0 & -p_1^2 \cosh p_1 b & -p_1^2 \sinh p_1 b \\ 0 & 0 & \alpha p_2^3 \sinh p_2 b & -\alpha p_2^3 \cosh p_2 b & 0 & 0 & -p_1^3 \sinh p_1 b & -p_1^3 \cosh p_1 b \\ 0 & 0 & 0 & 0 & 1 & 0 & 1 & 0 \\ 0 & 0 & 0 & 0 & 0 & 1 & 0 & p_1 \\ 1 & \ell & \cosh p_2 \ell & \sinh p_2 \ell & 0 & 0 & 0 & 0 \\ 0 & 1 & p_2 \cosh p_2 \ell & p_2 \sinh p_2 \ell & 0 & 0 & 0 & 0 \end{bmatrix} \begin{bmatrix} a_{1II} \\ a_{2II} \\ a_{3II} \\ a_{4II} \\ c_{1II} \\ c_{2II} \\ c_{3II} \\ c_{4II} \end{bmatrix} =$$

$$= \frac{1}{2I_{ey_2} p_2^3} \begin{bmatrix} p_2\xi - p_2 b + \sinh p_2 (b-\xi) \\ p_2 \cosh p_2 (b-\xi) - p_2 \\ \alpha p_2^2 \sinh p_2 (b-\xi) \\ \alpha p_2^3 \cosh p_2 (b-\xi) \\ 0 \\ 0 \\ -p_2\xi + p_2\ell - \sinh p_2 (\ell-\xi) \\ p_2 - p_2 \cosh p_2 (\ell-\xi) \end{bmatrix}. \quad (4.6.15)$$

Again, for PPStep beams $b_{iII}$ will not change; while the notations for the functions $a_{iII}$ and $b_{iII}$ are the same as before. The boundary conditions yield

$$\begin{bmatrix} 1 & b & \cosh p_2 b & \sinh p_2 b & 0 & -b & 0 & -\sinh p_1 b \\ 0 & 1 & p_2 \sinh p_2 b & p_2 \cosh p_2 b & 0 & -1 & 0 & -p_1 \cosh p_1 b \\ 0 & 0 & \alpha p_2^2 \cosh p_2 b & \alpha p_2^2 \sinh p_2 b & 0 & 0 & 0 & -p_1^2 \sinh p_1 b \\ 0 & 0 & \alpha p_2^3 \sinh p_2 b & -\alpha p_2^3 \cosh p_2 b & 0 & 0 & 0 & -p_1^3 \cosh p_1 b \\ 0 & 0 & 0 & 0 & 1 & 0 & 0 & 0 \\ 0 & 0 & 0 & 0 & 0 & 0 & 1 & 0 \\ 1 & \ell & \cosh p_2 \ell & \sinh p_2 \ell & 0 & 0 & 0 & 0 \\ 0 & 0 & \cosh p_2 \ell & \sinh p_2 \ell & 0 & 0 & 0 & 0 \end{bmatrix} \begin{bmatrix} a_{1II} \\ a_{2II} \\ a_{3II} \\ a_{4II} \\ c_{1II} \\ c_{2II} \\ c_{3II} \\ c_{4II} \end{bmatrix} =$$

$$= \frac{1}{2p_2^3} \begin{bmatrix} p_2\xi - p_2 b + \sinh p_2 (b-\xi) \\ p_2 \cosh p_2 (b-\xi) - p_2 \\ \alpha p_2^2 \sinh p_2 (b-\xi) \\ \alpha p_2^3 \cosh p_2 (b-\xi) \\ 0 \\ 0 \\ -p_2\xi + p_2\ell - \sinh p_2 (\ell-\xi) \\ -\sinh p_2 (\ell-\xi) \end{bmatrix} \quad (4.6.16)$$

The closed-form solution for the unknowns $a_{1II}(\xi), \ldots, c_{4II}(\xi)$ are again very long formulae and so are neglected.

## 4.7. Effect of the axial load on the frequencies

**4.7.1. Governing equations.** Here we seek the effect of the axial load on the transverse vibrational frequencies. With the Green functions in hand, the eigenvalue problems can be transformed into eigenvalue problems governed by homogeneous Fredholm integral equations:

$$w(x) = \lambda \int_0^\ell \mathcal{G}_c(x,\xi) w(\xi) \left\{ \begin{array}{l} 1 \text{ if } \xi \in [0,b], \\ \kappa \text{ if } \xi \in [b,\ell]. \end{array} \right\} \mathrm{d}\xi \,, \quad (4.7.1)$$

for the case of a compressive force and

$$w(x) = \lambda \int_0^\ell \mathcal{G}_t(x,\xi) w(\xi) \left\{ \begin{array}{l} 1 \text{ if } \xi \in [0,b], \\ \kappa \text{ if } \xi \in [b,\ell]. \end{array} \right\} \mathrm{d}\xi \,, \quad (4.7.2)$$

for the case of a tensile force. Here $\lambda$ and $\kappa$ are given by equation (4.5.25). We focus on the lowest value of the critical force. The solution to the corresponding eigenvalue problem is given in Appendix A.2.1.

**4.7.2. Example 2.** Two problems are solved numerically here. For the first problem, it is assumed that $\nu = 0.90$; then $\alpha = 0.7290$ and $\kappa = 1.2345679$ for a FFStep beam. As for the second problem, $\alpha = 0.65610000$ and $\kappa = 1.234586718$ for a PPStep beam. These data are taken from Table 42. The first eigenfrequency and the critical forces of the FFStep/PPStep beams are calculated and the computational results are given in Tables 43 and 44.

TABLE 43. Values of $\lambda_1$

| | $\sqrt{\lambda_1(b)}/4.73004^2$ | | | | |
|---|---|---|---|---|---|
| *beam* | $b = 0.2$ | $b = 0.4$ | $b = 0.5$ | $b = 0.6$ | $b = 0.8$ |
| *FFStep* | 0.94306087 | 0.93958134 | 0.94601385 | 0.95527766 | 0.95835369 |
| *PPStep* | 0.90273411 | 0.92130879 | 0.93858272 | 0.95892739 | 0.99240078 |

TABLE 44. Critical force

| | $\sqrt{N_{2\,\mathrm{crit}}(b)}$ | | | | |
|---|---|---|---|---|---|
| *beam* | $b = 0.2$ | $b = 0.4$ | $b = 0.5$ | $b = 0.6$ | $b = 0.8$ |
| *FFStep* | 6.53688650 | 6.58893781 | 6.73840194 | 6.94801747 | 7.08637924 |
| *PPStep* | 3.16728280 | 3.30994880 | 3.43419178 | 3.58174237 | 3.82743853 |

Let us note the first eigenfrequency for [compression] {tension} by $[\omega_{1c}]$ $\{\omega_{1t}\}$. The first eigenfrequency of the unloaded beam is $\omega_1$.

4.7.2.1. *Solutions to Problem 1.*
(i) *Results if* $b = 0.2$*:*
Table 45 contains the computational results.

TABLE 45. Eigenfrequency as a function of the axial load

| $b = 0.2$ | | |
|---|---|---|
| $N/N_{crit} = \mathcal{N}_2/\mathcal{N}_{2crit}$ | $\omega_{1c}^2/\omega_{1\text{ no load}}^2$ | $\omega_{1t}^2/\omega_{1\text{ no load}}^2$ |
| 0.000 | 0.99996606 | 1.00003393 |
| 0.100 | 0.90306768 | 1.09641322 |
| 0.200 | 0.80558100 | 1.19233938 |
| 0.300 | 0.70750101 | 1.28780763 |
| 0.400 | 0.60878458 | 1.38284459 |
| 0.500 | 0.50938378 | 1.47747462 |
| 0.600 | 0.40924518 | 1.57172007 |
| 0.700 | 0.30830903 | 1.66560145 |
| 0.800 | 0.20650822 | 1.75913769 |
| 0.900 | 0.10376710 | 1.85234623 |
| 1.000 | 0.00000000 | 1.94524322 |

Graphical representation of these results is presented in Figure 4.6.

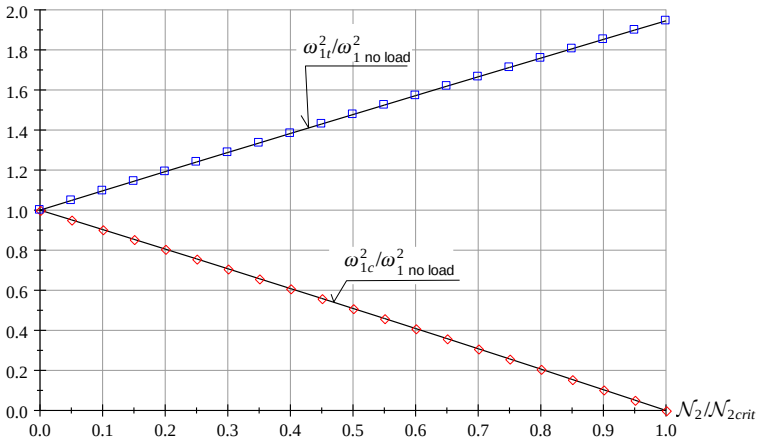


FIGURE 4.6. Graphical representation of the results presented in Table 45

It is noted that the quotients $\omega_{1c}^2/\omega_{1\text{ no load}}^2$ and $\omega_{1t}^2/\omega_{1\text{ no load}}^2$ are almost linear functions in $\mathcal{N}_2/\mathcal{N}_{2crit}$. The quadratic polynomials

$$\begin{aligned}\frac{\omega_{1c}^2}{\omega_{1\text{ no load}}^2} &= -3.752\,898\,481\times 10^{-2}\frac{\mathcal{N}_2^2}{\mathcal{N}_{2crit}^2} - 0.961\,635\,336\frac{\mathcal{N}_2}{\mathcal{N}_{2crit}} + 0.999\,602\,766\,,\\ \frac{\omega_{1t}^2}{\omega_{1\text{ no load}}^2} &= -1.936\,132\,658\times 10^{-2}\frac{\mathcal{N}_2^2}{\mathcal{N}_{2crit}^2} + 0.964\,285\,910\frac{\mathcal{N}_2}{\mathcal{N}_{2crit}} + 1.000\,174\,954\end{aligned} \tag{4.7.3a}$$

fit onto the computed results with at least a four digit accuracy.
(ii) *Results if* $b = 0.5$*:*

$$\begin{aligned}\frac{\omega_{1c}^2}{\omega_{1\text{ no load}}^2} &= -3.843\,202\,128\times 10^{-2}\frac{\mathcal{N}_2^2}{\mathcal{N}_{2crit}^2} - 0.960\,668\,935\frac{\mathcal{N}_2}{\mathcal{N}_{2crit}} + 0.999\,576\,294\,,\\ \frac{\omega_{1t}^2}{\omega_{1\text{ no load}}^2} &= -1.938\,551\,945\times 10^{-2}\frac{\mathcal{N}_2^2}{\mathcal{N}_{2crit}^2} + 0.963\,587\,738\frac{\mathcal{N}_2}{\mathcal{N}_{2crit}} + 1.000\,178\,405\,.\end{aligned} \tag{4.7.3b}$$

(iii) *Results if* $b = 0.8$*:*

$$\begin{aligned}\frac{\omega_{1c}^2}{\omega_{1\text{ no load}}^2} &= -3.098\,719\,962\times 10^{-2}\frac{\mathcal{N}_2^2}{\mathcal{N}_{2crit}^2} - 0.968\,372\,084\frac{\mathcal{N}_2}{\mathcal{N}_{2crit}} + 0.999\,693\,086\,,\\ \frac{\omega_{1t}^2}{\omega_{1\text{ no load}}^2} &= -1.664\,490\,344\times 10^{-2}\frac{\mathcal{N}_2^2}{\mathcal{N}_{2crit}^2} + 0.970\,329\,880\frac{\mathcal{N}_2}{\mathcal{N}_{2crit}} + 1.000\,142\,979\,.\end{aligned} \tag{4.7.3c}$$

4.7.2.2. *Solutions to Problem 2.*
(i) *Results if* $b = 0.2$. The numerical results are collected in Table 46.
Figure 4.7 is the graphical representation of the findings.

TABLE 46. Eigenfrequency as a function of the axial load

| $b = 0.2$ | | |
|---|---|---|
| $N/N_{crit} = \mathcal{N}_2/\mathcal{N}_{2crit}$ | $\omega_{1c}^2/\omega_{1\text{ no load}}^2$ | $\omega_{1t}^2/\omega_{1\text{ no load}}^2$ |
| 0.000 | 0.99985049 | 1.00014949 |
| 0.100 | 0.90001388 | 1.09998352 |
| 0.200 | 0.80002506 | 1.19996457 |
| 0.300 | 0.70003341 | 1.29994325 |
| 0.400 | 0.60003881 | 1.39991964 |
| 0.500 | 0.50004109 | 1.49989385 |
| 0.600 | 0.40004012 | 1.59986595 |
| 0.700 | 0.30003571 | 1.69983602 |
| 0.800 | 0.20002769 | 1.79980415 |
| 0.900 | 0.10001586 | 1.89977039 |
| 1.000 | 0.00000000 | 1.99973481 |

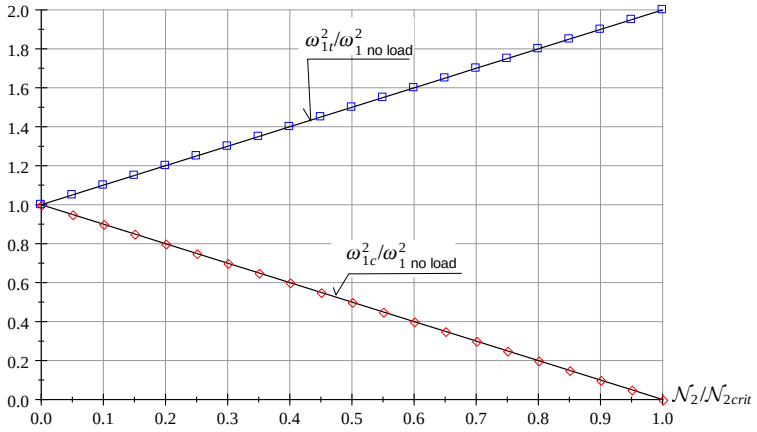


FIGURE 4.7. Graphical representation of the results presented in Table 46

The quadratic approximations

$$\begin{aligned}\frac{\omega_{1c}^2}{\omega_{1\text{ no load}}^2} &= -3.331\,337\,633\times10^{-4}\frac{\mathcal{N}_2^2}{\mathcal{N}_{2crit}^2} - 0.999\,625\,6857\frac{\mathcal{N}_2}{\mathcal{N}_{2crit}} + 0.999\,945\,6098,\\ \frac{\omega_{1t}^2}{\omega_{1\text{ no load}}^2} &= 6.307\,884\,335\times10^{-5}\frac{\mathcal{N}_2^2}{\mathcal{N}_{2crit}^2} + 0.999\,631\,7373\frac{\mathcal{N}_2}{\mathcal{N}_{2crit}} + 1.000\,053\,866.\end{aligned} \tag{4.7.4a}$$

fit onto the numerical results with a four to five digit accuracy.

(ii) *Results if* $b = 0.5$*:*

$$\begin{aligned}\frac{\omega_{1c}^2}{\omega_{1\text{ no load}}^2} &= -4.104\,840\,441\times10^{-3}\frac{\mathcal{N}_2^2}{\mathcal{N}_{2crit}^2} - 0.995\,790\,1871\frac{\mathcal{N}_2}{\mathcal{N}_{2crit}} + 0.999\,920\,6831,\\ \frac{\omega_{1t}^2}{\omega_{1\text{ no load}}^2} &= -2.080\,081\,369\times10^{-3}\frac{\mathcal{N}_2^2}{\mathcal{N}_{2crit}^2} + 0.9959923923\frac{\mathcal{N}_2}{\mathcal{N}_{2crit}} + 1.000\,062431.\end{aligned} \tag{4.7.4b}$$

(iii) *Results if* $b = 0.8$*:*

$$\begin{aligned}\frac{\omega_{1c}^2}{\omega_{1\text{ no load}}^2} &= -5.252\,032\,453\times10^{-4}\frac{\mathcal{N}_2^2}{\mathcal{N}_{2crit}^2} - 0.999\,440\,542\,7\frac{\mathcal{N}_2}{\mathcal{N}_{2crit}} + 0.999\,959\,9196,\\ \frac{\omega_{1t}^2}{\omega_{1\text{ no load}}^2} &= -1.137\,211\,210\times10^{-4}\frac{\mathcal{N}_2^2}{\mathcal{N}_{2crit}^2} + 0.999\,462\,7271\frac{\mathcal{N}_2}{\mathcal{N}_{2crit}} + 1.000\,038\,224.\end{aligned} \tag{4.7.4c}$$

If $b = 0$ or $b = 1$, the beams behave as if they were fixed-fixed beam/pinned-pinned, without a step. Then the quadratic approximation for $\omega_{1c}^2/\omega_{1\text{ no load}}^2$ coincides with that published in [**78**].

CHAPTER 5

# Stability of imperfect curved beams

## 5.1. Governing equations

Let us consider a fixed-fixed arch as it is shown in Figure 5.1. The cross-sectional coordinates are denoted as $\eta$ and $\zeta$, while the axis $\xi$ aligns with the circumferential direction. Notably, axis $\eta$ serves as a major principal axis of the arch. The arch has a length of $S$, with an included angle of $2\theta$, and an initial constant radius of curvature $R$. Additionally, $\varphi$ and $s = R\varphi$ represent the angle and arc coordinates, respectively. The mechanical load is applied at the crown point, where $\varphi = 0$. This configuration represents a scenario where the load is positioned at the symmetry axis of the perfect arch.

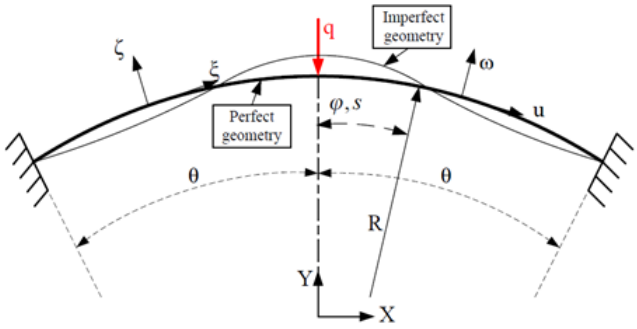


FIGURE 5.1. Arch geometry configuration.

It is assumed also that the arch has a small scale arbitrary geometrical imperfection through initial radial displacements $h(\varphi)$. It causes strain but the initial state is considered to be stress free. The total longitudinal normal strain at any material point, according to the Euler-Bernoulli hypothesis, is

$$\varepsilon_\xi = \frac{R}{R+\zeta}\left[\frac{\mathrm{d}u}{\mathrm{d}s} + \frac{w+h}{R} + \zeta\left(\frac{\mathrm{d}u}{R\mathrm{d}s} - \frac{\mathrm{d}^2w}{\mathrm{d}s^2} + \frac{\mathrm{d}^2h}{\mathrm{d}s^2}\right)\right] + \frac{1}{2}\left(\frac{u}{R} - \frac{\mathrm{d}w}{\mathrm{d}s} + \frac{\mathrm{d}h}{\mathrm{d}s}\right)^2, \tag{5.1.1}$$

where (in this Chapter) $u$ and $w$ are the axial and radial displacements on the centroidal axis, respectively. Here, it can be assumed that $w >> u$ due to the shallowness of the arch, which is generally accepted in the literature – see **[64]**. Thus, the effective strain that induces stress is

$$\varepsilon_{eff} = \frac{R}{R+\zeta}\left[\frac{\mathrm{d}u}{\mathrm{d}s} + \frac{w}{R} + \zeta\frac{\mathrm{d}^2w}{\mathrm{d}s^2}\right] + \frac{1}{2}\frac{\mathrm{d}^2w}{\mathrm{d}s^2} + \frac{\mathrm{d}w}{\mathrm{d}s}\frac{\mathrm{d}h}{\mathrm{d}s}. \tag{5.1.2}$$

The membrane strain at an arbitrary point on the centroidal axis ($\zeta = 0$) is

$$\varepsilon_{m,eff} = \frac{\mathrm{d}u}{\mathrm{d}s} + \frac{w}{R} + \frac{1}{2}\psi^2 + \psi\frac{\mathrm{d}h}{\mathrm{d}s} = \varepsilon_m + \frac{\mathrm{d}w}{\mathrm{d}s}\frac{\mathrm{d}h}{\mathrm{d}s} \quad , \quad \psi = \frac{\mathrm{d}w}{\mathrm{d}s} \tag{5.1.3}$$

where $\psi$ is the rotation. There is an extra term in equation (5.1.3) in comparison to the perfect arch **[83]** on account of the initial displacements. In the above theoretical formulation, the nonlinear term is $\frac{1}{2}\psi^2$ in the rotation field of the arch, which is not negligible compared

to the other terms, and it contributes as the cause of non-linearity. The axial force $N$ and the bending moment $M$ can be represented as follows using the Hooke law [**84**]:

$$N = \int_A \sigma_\xi \mathrm{d}A = \int_A E\varepsilon_{eff}\mathrm{d}A \simeq A_e\varepsilon_{m,eff} + \frac{I_e}{R}\frac{\mathrm{d}^2 w}{\mathrm{d}s^2}, \tag{5.1.4}$$

$$M = \int_A \sigma_\xi \mathrm{d}A = \int_A E\varepsilon_{eff}\zeta\mathrm{d}A \simeq -I_e\left(\frac{\mathrm{d}^2 w}{\mathrm{d}s^2} + \frac{w}{R^2}\right), \tag{5.1.5}$$

Here, $I_e$ is the $E$-weighted moment of inertia about the major principal axis $\eta$ and $A_e$ the E- weighted area of the cross section:

$$I_e = E\int_A \zeta^2\,\mathrm{d}A; \qquad A_e = \int_A E\mathrm{d}A. \tag{5.1.6}$$

The cross-sectional radius of gyration is, thereby, defined by $r = \sqrt{I_e/A_e}$. The bending moment and axial force have a mutual effect on the membrane strain:

$$N + \frac{M}{R} = A_e\varepsilon_{m,eff}. \tag{5.1.7}$$

Using the principle of virtual work, the nonlinear pre-buckling equilibrium configuration is established from

$$\int_V \sigma_\xi \delta\varepsilon_{eff}\,\mathrm{d}V - q\;\delta w|_{\varphi=0} = 0. \tag{5.1.8}$$

As detailed in Appendix A.3.1, the principle yields the following coupled differential equations of equilibrium

$$\frac{\mathrm{d}N}{\mathrm{d}s} + \frac{1}{R}\left[\frac{\mathrm{d}M}{\mathrm{d}s} - \left(N + \frac{M}{R}\right)\left(\frac{u}{R} - \frac{\mathrm{d}w}{\mathrm{d}s}\right)\right] = 0, \tag{5.1.9}$$

$$\frac{\mathrm{d}}{\mathrm{d}s}\left[\frac{\mathrm{d}M}{\mathrm{d}s} - \left(N + \frac{M}{R}\right)\left(\frac{u}{R} - \frac{\mathrm{d}w}{\mathrm{d}s}\right)\right] - \frac{N}{R} = 0. \tag{5.1.10}$$

The fundamental equations with kinematical quantities can be found by recalling Eqs. (5.1.3)- (5.1.10). Details are provided in Appendix A.3.1 and A.3.2 that lead to

$$\varepsilon'_{m,eff} = 0 \tag{5.1.11}$$

and

$$W'''' + (\mu^2 + 1)W'' + \mu^2 W = (\mu^2 - 1)(1 + H'') \tag{5.1.12}$$

given that

$$\{W; H\} = \{\frac{w}{R}; \frac{h}{R}\}\ ,\ \mu^2 = 1 - \kappa\varepsilon_{m,eff};\ \kappa = \frac{A_e R^2}{I_e} = \frac{R^2}{r^2}; \qquad \lambda = \sqrt{\kappa}\theta^2 = \frac{S\theta}{2r} \tag{5.1.13}$$

are dimensionless parameters.
In which $\lambda$ is the slenderness of the arch [**61**]. The initial imperfection can be arbitrary continuous function, e.g., having the form

$$H(\varphi) = A_0 + A_i\sum_i \sin(i\frac{\pi\varphi}{\theta}) + \sum_j A_j \sin(j\frac{\pi\varphi}{2\theta}) \tag{5.1.14}$$

with $A_0, A_i$ and $A_j$ being the amplitude coefficients and $i\ ,\ j \in \mathbb{R}$. These parameters control the error shape and magnitude.

Once $H$ is given, the general solution to (5.1.12) can be found. After that, the above equations are extended with boundary conditions. The displacement and rotation are zero at the supports whereas all the fields are continuous, with the exception of the shear force,

which displays a discontinuity of value $Q$ at the crown point. These conditions is terms of dimensionless displacements are

$$W|_{\varphi=-\theta} = W''\Big|_{\varphi=-\theta} = W|_{\varphi=\theta} = W''\Big|_{\varphi=\theta} = 0, \tag{5.1.15}$$

$$W|_{\varphi=-\alpha} = W|_{\varphi=+\alpha} \qquad W'\Big|_{\varphi=-\alpha} = W'|_{\varphi=+\alpha}\,, \tag{5.1.16}$$

$$W''\Big|_{\varphi=-\alpha} = W''\Big|_{\varphi=+\alpha} \qquad -W'''\Big|_{\varphi=-\alpha} + W'''\Big|_{\varphi=+\alpha} = -\frac{2Q}{\theta}, \tag{5.1.17}$$

where $Q$ is the dimensionless load defined by $Q = \frac{qR^2\theta}{2I_e}$.

Since the membrane strain is constant, it thus means

$$\varepsilon_{m,eff} = \frac{1}{2\theta}[U' + W + \frac{1}{2}\left(W'\right)^2 + W'H'] = const. \tag{5.1.18}$$

This finding links the external load and the strain for the imperfect shallow arch as

$$\varepsilon_{m,\mathrm{eff}} = \frac{1}{2\theta}\int_{-\vartheta}^{\vartheta}\left[-U' + W + 0.5\,(W')^2 + W'H'\right]\mathrm{d}\varphi = \mathrm{const.} \tag{5.1.19}$$

that is

$$\sum_{k=0}^{2} B_k Q^k = 0 \tag{5.1.20}$$

in short. With $B_k = B_k(A_0, A_i, A_j, \kappa, i, j, I_e, A_e, R, S, \theta)$ being coefficients. The coefficients $B_0, B_1, B_2$ can be found once the initial displacements are selected. Eq. (5.1.21) serves the base for stability investigations since it expresses the nonlinear relationship between the load and strain, it can be used to find the equilibrium path for arches. The local maxima of this path is found by the mathematical condition

$$\frac{d}{d\mu}(\sum_{k=0}^{2} B_k P^k) = 0 \tag{5.1.21}$$

for a given geometry and imperfection. These limit points hold the typical buckling loads.

## 5.2. Symmetric imperfection

In this section, we present computational results that consider the a small, symmetric, cosine-shaped initial imperfection of the form:

$$H = a\cos(n\frac{\pi\varphi}{2\theta}), \tag{5.2.1}$$

where $a$ a represents the dimensionless amplitude of the imperfection, and $n$ is an odd integer, representing the mode number. Examples of some imperfection profiles are shown in Figure 5.2. When $a = 0$, the structure corresponds to a perfect, unperturbed, circular arch. I investigated this case in detail separately in [**83**]. In the forthcoming, if there is no further indication, results are given for arches with $S/r = 200$, $S = 10875$ mm and $E = 210$ GPa.

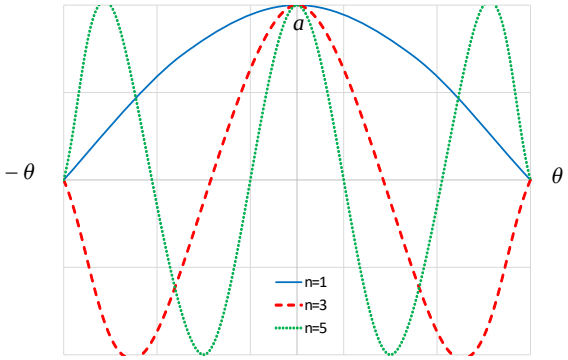


FIGURE 5.2. Some examples of symmetric initial imperfection shapes.

Figure 5.3.a illustrates the significant influence of the first mode imperfection ($n = 1$) on the buckling loads of arches with small included angles. In contrast, for arches with larger included angles, the critical loads vary only by a few percent. The choice of $a = -0.01$ results in the highest allowable buckling loads, as well as the greatest geometric lower limit at which buckling occurs. In this case, the buckling loads are highly uniform, making them almost independent of the arch angle. In contrast, the curve representing $a = +0.01$ approaches to the buckling load of a perfect arch from below, with progressively diminishing relative differences.

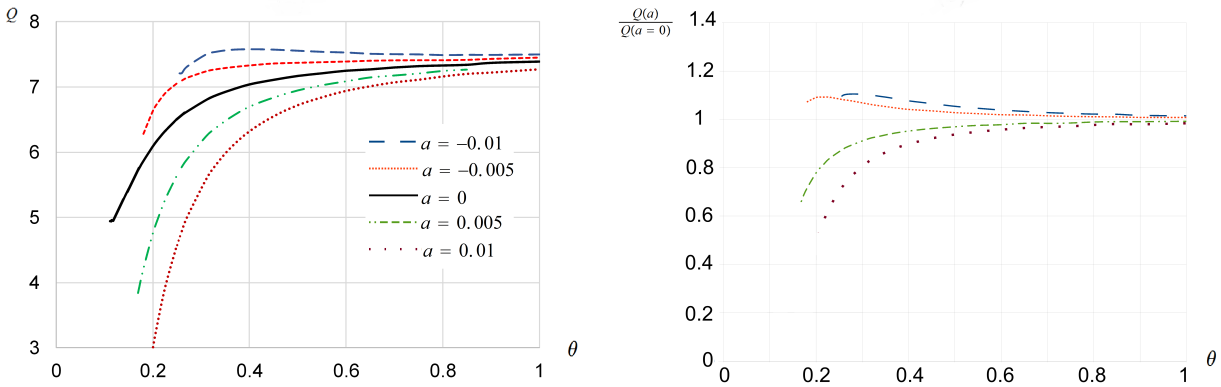


FIGURE 5.3. (a) buckling load, (b) relative buckling load as function of $\theta$,$n = 1$ .

The relative load values in Figure 5.3.b provide insight into the impact of geometric imperfections on load-bearing capacity. As visible, the critical load increases continuously with the a value. The reason behind this finding is that when the magnitude is positive, it effectively 'flattens' the arch, whereas negative $a$ makes it a slightly bit 'more curved' overall. As a result, the load-bearing capabilities of arches can become even better when a small imperfection is included.

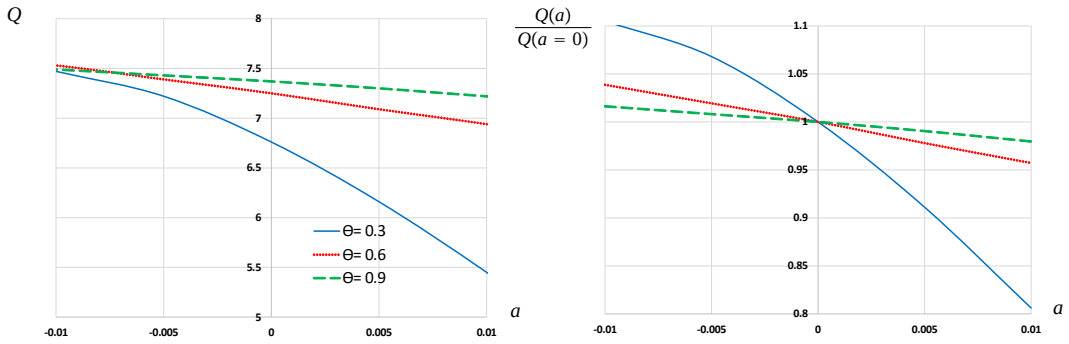


FIGURE 5.4. (a) buckling load,(b) relative buckling load dependence on $a$, $n = 1$.

To assess how a continuously varying imperfection affects the critical loads for $n = 1$, Figure 5.4.a is referenced. In all cases presented, the loads decrease monotonically, with the steepest decline occurring at $\theta = 0.3$. The angles $\theta = 0.3$ and $\theta = 0.6$ exhibit nonlinear behavior, while $\theta = 0.9$ follows a linear trend. The smallest angle consistently shows the lowest buckling loads. As depicted in Figure 5.4.b, the relative load values indicate that the allowable load, compared to a perfect arch, can increase by up to 10%, but may also decrease significantly by almost 19%.

In terms of the dimensionless load-relative strain relationships, Figure 5.5 compares five samples of a magnitude with $\theta = 0.4$. Notably, all curves begin from the origin ($Q = 0$, $\varepsilon_{m,eff}(a) = 0$), indicating $\mu = 0$. The curves exhibit a local maximum point as $\varepsilon_{m,eff}$ increases from 0. Subsequently, the load decreases. There is one higher and one lower limit point, regardless of the imperfection magnitude. It is noteworthy that the parameter $a$ exerts a significant influence on determining the curve endpoints, which manifest different values on the vertical axis. In contrast to $a = 0$, as long as $a < 0$ , the strain decreases and the critical load increases. Greater strain and smaller limit points values (upper & lower) are indicated by greater $a > 0$. The position of the branch intersection point is not constant in $\varepsilon_{m,eff}$ or $Q$, but rather a quasi-linear function of $a$.

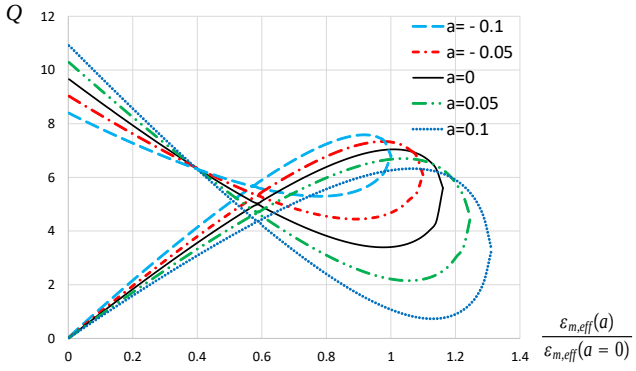


FIGURE 5.5. Load - dimensionless strain variations when $\theta = 0.4$ and $n = 1$.

The dimensionless load-crown point displacement $W_0 = W(\varphi = 0))$ when $n = 1$ and $\theta = 0.4$, is shown in Figure 5.6. The position of the upper limit point is in indirect proportion to $a$: bigger magnitude indicates less displacement and a lower buckling load the upper limit point is moved backward. On the other hand, the lower limit point possesses the exact opposite properties.

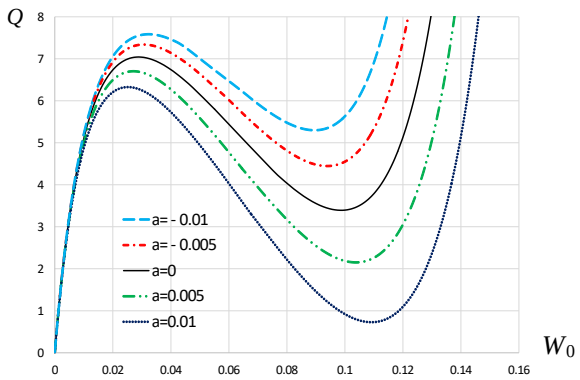


FIGURE 5.6. Load - dimensionless crown displacements when $\theta = 0.4$ and $n = 1$.

Concentrating on the third imperfection mode ($n = 3$), Figure 5.7. illustrates the findings related to the variation of critical load with respect to $\theta$. The results indicate that for negative amplitudes, there is an inverse relationship between the critical load and the included angle. Furthermore, a greater difference in the critical load is observed for any given parameter $a$ as $\theta$ approaches to 1, compared to the previous analysis with $n = 1$ for the same geometry.

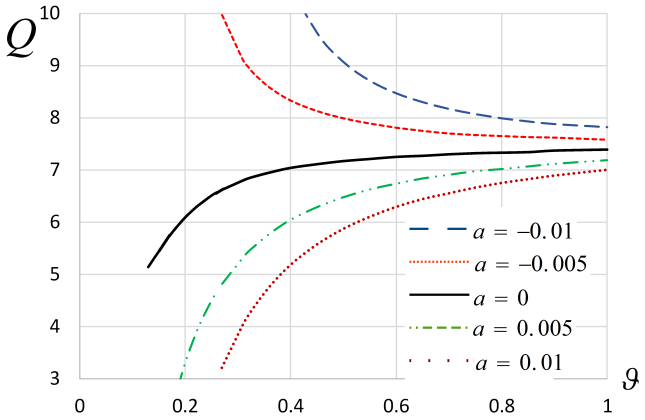


FIGURE 5.7. Buckling - load against arch semi-vertex angle $\theta$, $n = 1$.

Figure 5.8a. illustrates the continuous decrease in buckling load as $a$ increases if $n = 3$. Similar to previous observations in Figure 5.4, the steepest decline is noted for $\vartheta = 0.3$. Two of the curves exhibit nonlinear behavior, and this time, the effect of the imperfection is significantly more pronounced compared to the first mode. The relative load falls within approximately $\pm 50\%$ of the perfect arch.

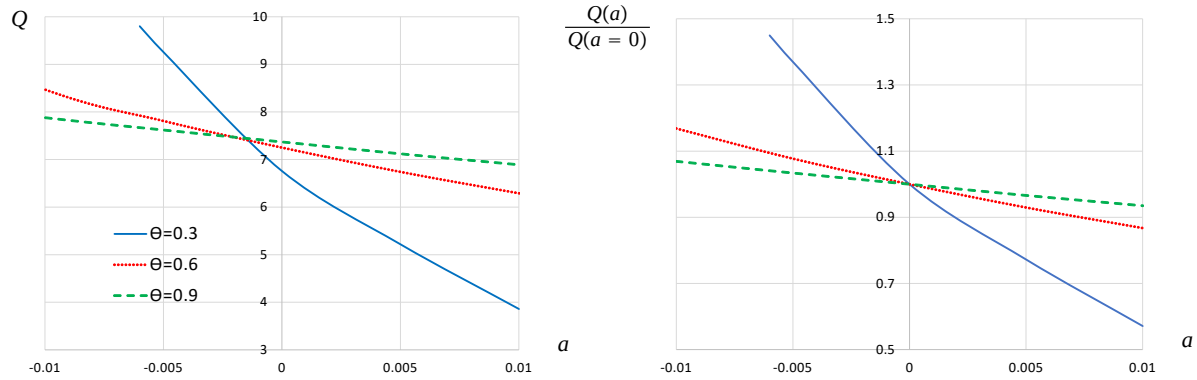


FIGURE 5.8. (a)Buckling load, (b) relative buckling load changes–dependence on $a$, $n = 1$

The impact of $S/r$ on the buckling load, as shown in Figure 5.9 for four different values, is now examined. It is observed that the critical load increases as the $S/r$ quotient increases, indicating that arches with higher $S/r$ ratios can sustain greater loads. As $a$ increases, the buckling load decreases in a non-linear and monotonous way. Within the chosen range, the variation between the lowest and highest loads is substantial, influenced solely by a small imperfection.

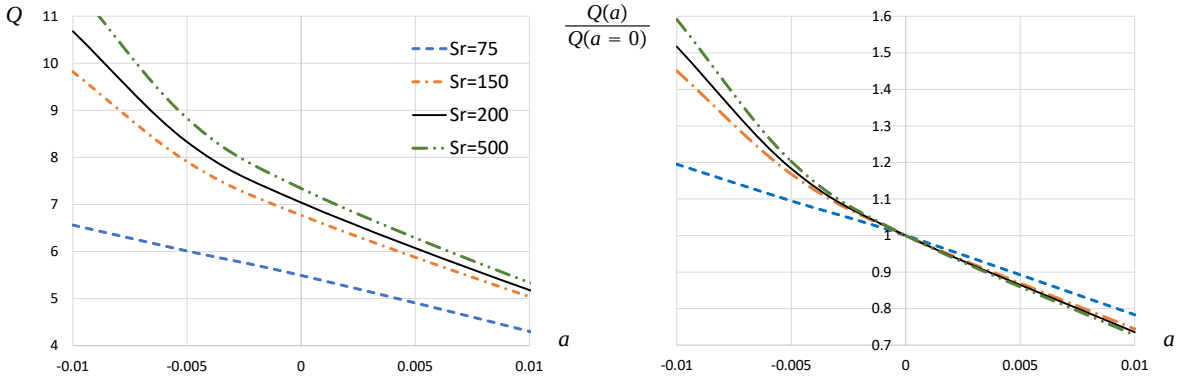


FIGURE 5.9. Variation of the (a) buckling load, (b) relative buckling load when $\vartheta = 0.4$, $n = 3$ dependence on $S/r$.

As illustrated in Figure 5.10 for $Q$-$\varepsilon_{m,eff}$, the intersections of the branches are now in close proximity, significantly nearer to each other compared to the lower mode, as seen in Figure 5.5. When the parameter $a$ is positive, the lower limit point is only marginally affected. However, the upper limit is considerably influenced by $a$.

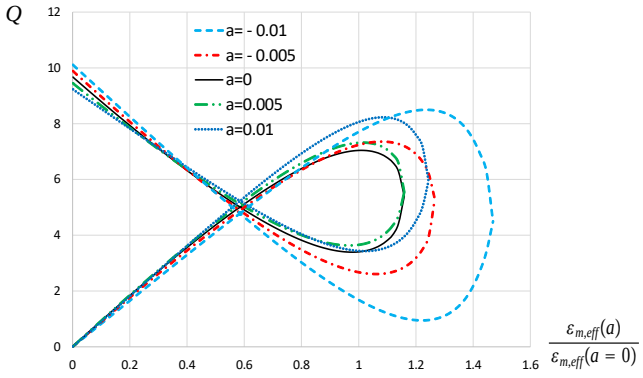


FIGURE 5.10. Load-relative strain relationships when $n = 9$, $\vartheta = 0.4$ .

### 5.3. Asymmetric imperfection

In this section, we present computational results that consider a small asymmetric sine-shaped initial imperfection of the form

$$H = a \sin(n\frac{\pi\varphi}{\theta}) \tag{5.3.1}$$

which is shown in Figure 5.11 for some shape examples.

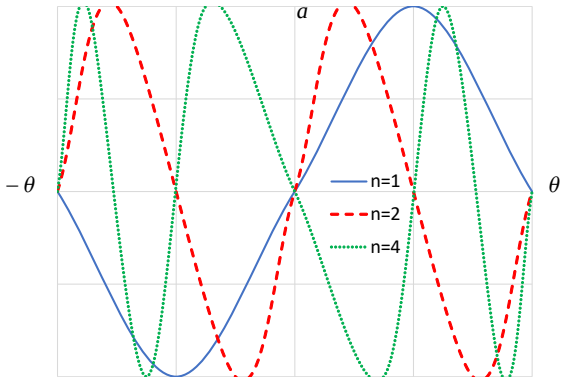


FIGURE 5.11. Some asymmetric initial imperfection shapes.

The critical load-angle curve for the perfect arch ($a = 0$), as depicted in Figure. 5.12, exhibits a monotonic behavior, starting with a steep gradient and gradually flatten near $\theta = 0.5$. When small imperfections are introduced, they generally lead to a reduction in the buckling load. However, an exception is observed for small angles below $\theta = 0.2$, where the imperfection enhances the stiffness of the structure, effectively improving its resistance to buckling. Notably, at $\theta = 0.11$, the critical load shows the largest discrepancy, with a deviation of approximately 33% compared to the perfect arch. In contrast, at $\theta = 1$, the difference is significantly smaller, around 2.5%. This trend highlights the sensitivity of the critical load to imperfections, which becomes more pronounced at certain angles. Across most of the range, a larger magnitude of the imperfection consistently results in a greater deviation from the perfect case, regardless of the sign of $a$.

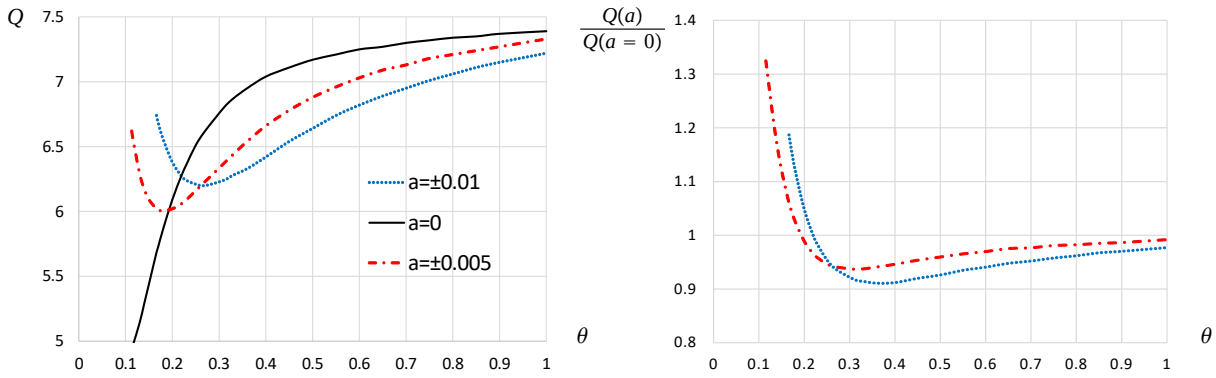


FIGURE 5.12. (a) Critical load, (b) relative critical load dependence on $\theta$ when $n = 1$.

Comparing this behavior to the first-mode cosine shape imperfection discussed earlier reveals several key differences. The sine-shaped imperfection converges more slowly to the critical load of the perfect arch. Furthermore, the sine imperfection more consistently reduces the buckling load, whereas the cosine imperfection results in more significant reductions, particularly at lower angles. These differences underscore how the type of imperfection function influences the buckling response.

The dimensionless load-strain relationships for $\theta = 0.4$ are presented in Figure. 5.13. Up to the intersection of the upper and lower branches, the results remain effectively independent of the parameter $a$. Beyond this intersection, the independence persists over a short range; however, differences eventually arise in both the buckling strain and the buckling load. As the imperfection magnitude increases, both of these values exhibit a gradual decrease, reflecting the influence of imperfections on the structure's stability. This behavior contrasts significantly with the case of symmetric imperfections discussed in the previous subsection. For symmetric imperfections, the intersection point was dependent on $a$, with changes in $a$ causing the intersection to shift both horizontally and vertically. Moreover, in the symmetric case, the starting point of the upper branch was also affected by the imperfection amplitude.

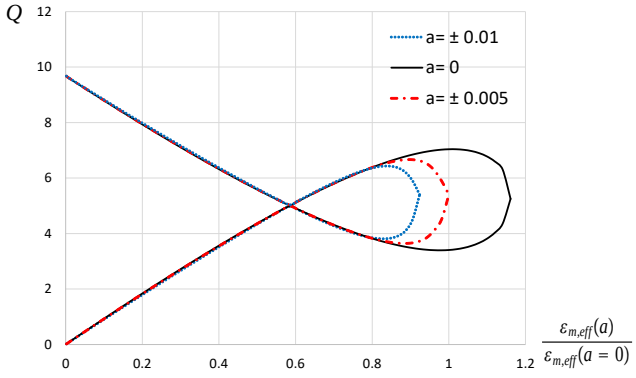


FIGURE 5.13. Load-relative strain relations when $\theta = 0.4$ and $n = 1$.

Figure 5.14 illustrates the relationship between the dimensionless crown displacement and the dimensionless load. As the load increases, the primary stable branch is initially steep, leading up to the upper limit point. This upper limit point, representing the lowest load and displacement at which instability occurs, is first reached when $a = 0.01$. Beyond this point, the curve transitions into an unstable branch, which is steepest for the perfect geometry ($a = 0$), and continues until it reaches the lower limit point. Following this, a

remote stable branch emerges, where further increases in load once again corresponds to increases in displacement.

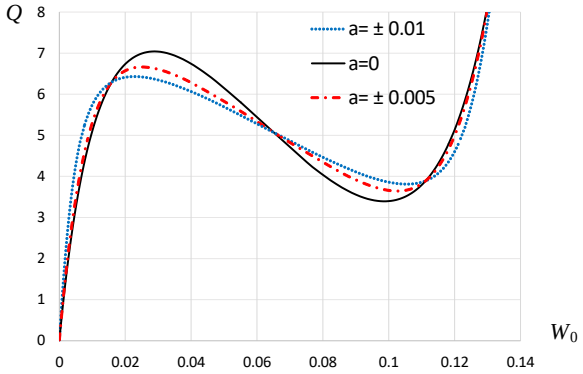


FIGURE 5.14. Load-displacement relations when $\theta = 0.4$ and $n = 1$ .

These results can be directly compared to Figure. 5.6, which examines the case of asymmetric initial imperfection; in the earlier analysis, the primary branch was observed to remain nearly independent of imperfections up to a load of approximately $Q \approx 5$. In contrast, for the current sine-shaped imperfection with $a = 0.01$, a noticeable divergence occurs much earlier, around $Q \approx 2$. Another key difference lies in the behavior of the remote stable branches; for the sine imperfection, these branches are significantly closer to each other, indicating less sensitivity to the imperfection amplitude in this region. Furthermore, the unstable branches intersect with the perfect case for the sine imperfection, a phenomenon not observed for the cosine error. These distinctions highlight the influence of the initial imperfection on the load-displacement response, particularly in the transitions between stable, unstable, and remote branches.

Figure 5.15 explores the impact of increasing imperfection magnitude on the critical dimensionless load for three selected angles. All curves start from the load corresponding to the perfect arch ($a = 0$). As the imperfection magnitude grows, the critical load decreases across all cases. The most significant drop occurs at $\vartheta = 0.3$, where the load demonstrates a steep decline. In contrast, the change for $\theta = 0.9$ is relatively minor, following an almost linear trend. Within the range considered, the maximum load reduction does not exceed 7.7%, indicating a relatively low sensitivity to imperfections. These findings bear some resemblance to those observed for the cosine-shaped imperfection. In both cases, the smallest angle experiences the greatest reduction in critical load. However, the relative buckling load in the cosine error scenario spans a range nearly three times larger, highlighting more pronounced sensitivity to imperfection in that case.

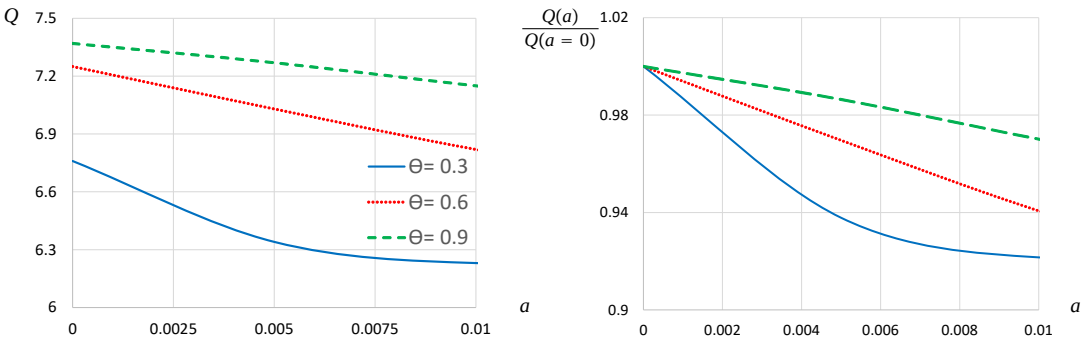


FIGURE 5.15. (a) Critical load, (b) relative load dependence on imperfection magnitude if $n = 1$.

This paragraph examines the behavior associated with second-mode imperfections. The typical load-angle curves are shown in Figure 5.16. It shows a similar shape with those for $n = 1$, although the specific values differ. It is consistent with the first mode – at lower angles, the presence of imperfections can enhance structural stiffness.

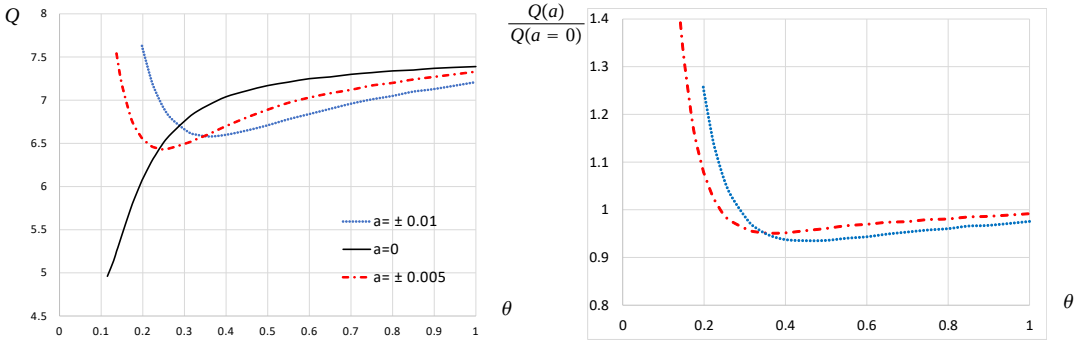


FIGURE 5.16. (a) Critical load, (b) critical relative load distribution for arches when $n = 2$.

Comparing this behavior to the $n = 1$ case, a similar relative change in load is observed, but it occurs at slightly higher angles. Overall, the relative differences between the $n = 1$ and $n = 2$ modes are minimal, particularly when compared to the more significant variations seen in the lowest cosine patterns. This indicates that the impact of the mode shape on load response diminishes as the mode number increases.

Figure 5.17 examines the continuous variation of the imperfection parameter $a$ and its effect on the lowest buckling load. The analysis reveals that imperfections consistently reduce the buckling load across all cases. However, only at $\theta = 0.3$ does the initial decline eventually transitions into a rise, though it never fully reaches the value of the perfect case. In contrast, for other angles, such as $\theta = 0.9$, the buckling load decreases steadily without any recovery. The magnitude of the impact varies with the angle. At $\theta = 0.3$, the maximum reduction in the buckling load is approximately $-4\%$, while at $\theta = 0.9$, it is around $-3\%$. These reductions are notably smaller than those observed for cosine-shaped imperfections but are comparable in scale to the effects seen in the first sine mode.

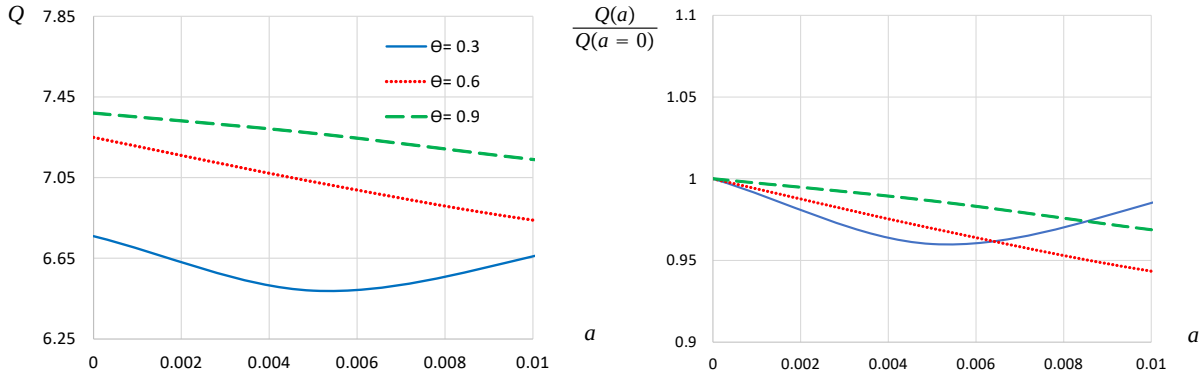


FIGURE 5.17. (a) Critical load, (b) relative load dependence on imperfection magnitude if $n = 2$ .

Next, the analysis focuses on the impact of $S/r$ on the lowest buckling load of arches at $\theta = 0.4$, as shown in Figure 5.18. The results show that the highest selected $S/r$ values correspond to the greatest buckling loads, while $S/r = 75$ is associated with the lowest loads.

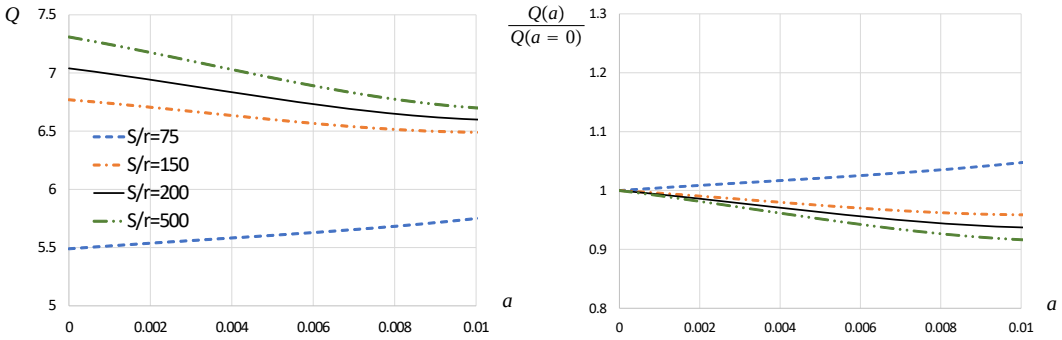


FIGURE 5.18. (a) Critical load, (b) relative critical load changes in terms of $a$ for $n = 2$,as function of $S/r$.

Notably, the behavior of the $S/r = 75$ curve is distinct, as it exhibits an increase in the buckling load with respect to $a$, whereas all other $S/r$ relationships show a decreasing trend. The maximum relative increase for $S/r = 75$ is approximately 5.1%, while the largest observed decrease across the other cases is nearly 9%. These changes are significantly smaller in magnitude compared to those observed in the cosine imperfection case, highlighting a reduced sensitivity of the buckling load to imperfections under these conditions.

As shown in Figure. 5.19 for $\theta = 0.4$, the buckling load increases, along with the critical strain, as a small imperfection is introduced. In this respect, the behavior of the curves and their characteristics are the exact opposite of those presented in Figure 5.13.

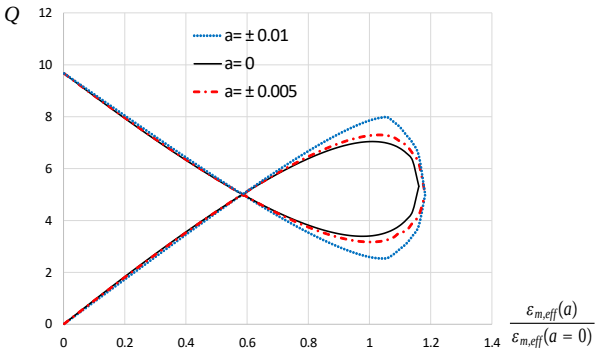


FIGURE 5.19. Load - relative strain relations when $\vartheta = 0.4$ and $n = 10$ .

Figure 5.20 depicts the effect of varying the imperfection mode at a fixed angle of $\theta = 0.4$. Both the critical strain and buckling load show an upward trend, with the curves remaining closely aligned for a significant range. Even after their intersection, the curves continue to exhibit a high degree of similarity, highlighting the consistent influence of imperfection mode on the structural response within this range.

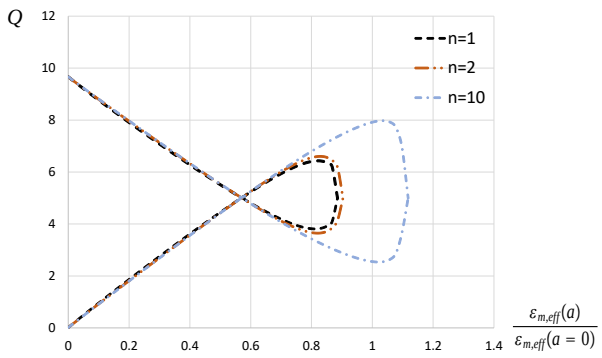


FIGURE 5.20. Load-strain relations when $\theta = 0.4$, $a = 0.01$ - the effect of imperfection mode $n$.

Furthermore, Figure 5.21 reveals two stable equilibrium branches separated by an unstable equilibrium branch.

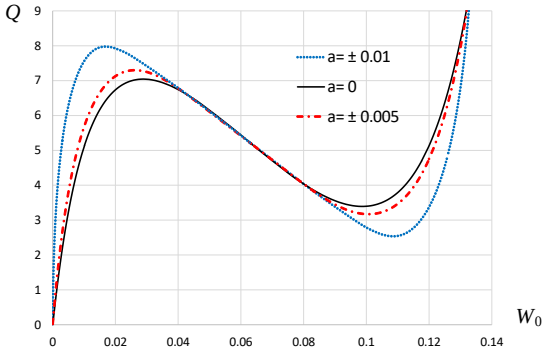


FIGURE 5.21. Load-displacement plots for $\vartheta = 0.4$, $n = 10$.

These findings are consistent with the patterns observed in the previous figures, with the additional insight that the presence of imperfections reduces the dimensionless displacement. At the same time, the displacements increase due to the influence of the initial shape error. It is noted that this Chapter was based on Author publication {1}.

CHAPTER 6

# Summary of the theses

**Thesis 1.**

I have investigated the stability problem of straight compressed beams with three supports. The intermediate support is a linear spring, restraining transverse motion, its position is arbitrary. Three end-support arrangements were considered: fixed-fixed, fixed-pinned, pinned-pinned. The beam has cross-sectional inhomogeneity and the cross-sections are uniform.

For these three-point boundary value problems, the definition of the Green function was discussed. The related Green functions were given in closed-form for the selected problems. The eigenvalue problems for the critical load were replaced by eigenvalue problems governed by homogeneous Fredholm integral equations with kernels derived from these Green functions. Then the latter eigenvalue problems were converted to algebraic form using the boundary element method. In limiting cases regarding the position of the intermediate support and the spring stiffness, the classical results for fixed-fixed, fixed-pinned, pinned-pinned beams were found.

**Thesis 2.**

I have investigated the free vibrations of straight uniform beams with four supports. The free vibration problems I attacked were considered as four-point boundary value problems. To find solutions, I generalized the concept of the Green function for four-point boundary value problems, extending the definition that was introduced for three-point boundary value problems. All the properties and construction steps concerning these Green functions have been clarified.

The Green functions were provided in closed-form for straight beams with cross-sectional inhomogeneity that have two intermediate roller supports at arbitrary positions, while the ends are either fixed-fixed or pinned-roller supported. With the related Green functions as kernels, the assigned four-point eigenvalue problems were transformed to homogeneous Fredholm integral equations. These were replaced by algebraic eigenvalue problems, which were then solved numerically. In limiting cases regarding the position of the intermediate supports, the classical results for fixed-fixed, fixed-pinned, pinned-pinned beams are found.

**Thesis 3.**

The Green function definition was extended to coupled boundary value problems, when the differential operators have the same order but are different in the two domains. The properties and construction steps were clarified in details. With the introduced method, I investigated the free and loaded vibrations together with the stability of stepped straight beams with cross-sectional heterogeneity. As regards the end supports, the beams are fixed-fixed or pinned-pinned. The location of the step is arbitrary. The concentrated axial load is exerted at one end of the beam.

The Green functions were determined in closed-form for compressive and tensile axial load as well. The stability problem was investigated for compressive load, while the loaded vibration frequencies for both loading cases. The ratio of the natural circular frequency square for the axially loaded beam and of the free vibrations (no axial load on the beam)

increases for tensile load, and decreases for compressive load. This relationship, as a function of the load magnitude, is almost linear.

**Thesis 4.**

I have investigated the in-plane limit-point stability of shallow arches. The perfect arches are circular but contain initial geometrical imperfections. I incorporated the effect of arbitrary initial displacements to the mechanical model which is geometrically non-linear. The imperfections cause initial strains but the initial stresses were neglected. The static equilibrium equations were found with the principle of virtual work. I developed analytical solutions for some symmetric and anti-symmetric imperfection shapes.

I evaluated the results for the buckling loads and in-plane behaviour. The lowest mode shape errors have greatest effects on the lowest buckling load for smaller opening angles. This effect can be positive or negative too, depending on the actual imperfection parameters. The equilibrium path can show two kinds of behaviour. When snap-through buckling is not possible, there is one stable equilibrium branch. When there exists a buckling load, the number of equilibrium branches is three: one primary and remote stable, with an unstable between.

## Related publications by the author in the topics of the Thesis


{1} L. P. Kiss and A. Messaoudi: *Assessments of the non-linear instability of arches with imperfect geometry.* Structures, 71, 108031 (2025), (Q1, IF:3.9). doi.org/10.1016/j.istruc.2024.108031

{2} A. Messaoudi and L. Kiss: *Vibration and stability of curved beams using the finite element method.* Annals of Faculty of Engineering Hunedoara. International Journal of Engineering, 21(2) pp 119-124(2023).

{3} A. Messaoudi, L. Kiss and G. Szeild: *Green functions for four-point boundary value problems with applications to heterogeneous beams.* Applications in Engineering Science, 17 Paper 100165. 16 p.(2024), (Q2, IF: 2.2). https://doi.org/10.1016/j.apples.2023.100165

{4} A. Messaoudi and L. Kiss: *Investigations on the limit-point buckling of curved beams.* Multidiszciplináris Tudományok: A Miskolci Egyetem Közleménye, 13(2), pp 78-86 (2023). https://doi.org/10.35925/j.multi.2023.2.7

{5} A. Messaoudi and L. Kiss: *Stability studies of straight beams using finite element method.* Annals of Faculty of Engineering Hunedoara. International Journal of Engineering, 20(3), pp 135-138(2022)

{6} L. P. Kiss, G. Szeidl, A. Messaoudi: *Stability of heterogeneous beams with three supports through Green functions.* Meccanica. 57(6), pp 1369-1390 (2022), (Q2, IF: 1.9). https://doi.org/10.1007/s11012-022-01490-z

{7} L. P. Kiss, G. Szeidl, A. Messaoudi: *Vibration of an axially loaded heterogeneous fixed–fixed beam with an intermediate roller support.* Journal of the Brazilian Society of Mechanical Sciences and Engineering. 44(10), paper 461 (2022), (Q2, IF: 1.8). https://doi.org/10.1007/s40430-022-03732-3

{8} A. Messaoudi and L. Kiss: *A short review on the buckling of compressed columns.* Multidiszciplináris Tudományok. A Miskolci Egyetem Közleménye, 12(1), pp 103-111(2022).

{9} A. Messaoudi and L. Kiss: *Buckling of beams with a boundary element technique.* Journal of Engineering Studies and Research,28(2), pp 25-32(2022). https://doi.org/10.29081/jesr.v28i2.003

{10} A. Messaoudi and G. Szedil: *A novel approach to the vibration problem of some stepped beams.* Doktoranduszok Fóruma , Miskolc, 2022. november 17. Miskolci Egyetem, pp 1-6(2023). ISBN: 9789633583289

{11} A. Messaoudi and L. Kiss: *Buckling of beams by means of a Green function technique.* 2nd Baskent International Conference on Multidisciplinary Studies, Ankara, Turkey,24 - 25 Feb, pp 197-203(2022). ISBN: 9786257464772

{12} A. Messaoudi and G. Szedil: *Stability investigation using Green's functions.* Doktoranduszok Fóruma, Miskolc, 11.18.2021, pp 1-7(2022). ISBN: 9789633582602

{13} A. Messaoudi And L. Kiss: *Numerical buckling analysis of straight beams*, 8th International Mardin Aruklu Scientific Researches Conference, Turkey 04 - 06 June. pp 1090-1095(2022),ISBN: 9786258323337

APPENDIX A

# Some related calculations and transformations

## A.1. Characteristic equations used in Chapter 2

In this section, we present the characteristic equations that were solved for benchmark purposes.

If the axial force is compressive ($N > 0$) then, as per Eqs. (2.1.9), the stability of straight beams are governed by

$$\frac{\mathrm{d}^4 w}{\mathrm{d}x^4} + p^2 \frac{\mathrm{d}^2 w}{\mathrm{d}x^2} = 0 \qquad p^2 = \mathcal{N} = L^2 \frac{N}{I_{ey}} \tag{A.1.1}$$

The general solutions on the left and right beam parts are

$$w_r = a_1 + a_2 x + a_3 \cos px + a_4 \sin px, \qquad x \in [0, b] \tag{A.1.2a}$$

and

$$w_\ell = c_1 + c_2 x + c_3 \cos px + c_4 \sin px, \quad x \in [b, \ell = 1] \tag{A.1.2b}$$

where $a_k$ and $c_k$ $(k = 1, \ldots, 4)$ are coefficients.

For FssF beams, the related boundary and continuity conditions are

$$w_r(0) = 0\,, \quad w_r^{(1)}(0) = 0\,; \qquad w_\ell(1) = 0\,, \quad w_\ell^{(1)}(1) = 0\,, \tag{A.1.3a}$$

$$\begin{aligned} w_r(b-0) &= w_\ell(b+0)\,, \\ w_r^{(1)}(b-0) &= w_\ell^{(1)}(b+0)\,, \\ w_r^{(2)}(b-0) &= w_\ell^{(2)}(b+0)\,, \\ w^{(3)}(b-0) - \chi w(b) &= w^{(3)}(b+0). \end{aligned} \tag{A.1.3b}$$

The above set self-adjoint eigenvalue problem determines the following equation system:

Boundary conditions if $x = 0$:

$$\begin{aligned} a_1 + a_3 &= 0\,, \\ a_2 + p a_4 &= 0\,. \end{aligned}$$

Continuity conditions at $x = b$:

$$\begin{aligned} c_1 + c_2 b + c_3 \cos pb + c_4 \sin pb - (c_1 + c_2 b + c_3 \cos pb + c_4 \sin pb) &= 0, \\ a_2 - p a_3 + p a_4 \cos pb - (c_2 - p c_3 \sin pb + p c_4 \cos pb) &= 0, \\ -a_3 \cos pb - a_4 \sin pb - (-c_3 \cos pb - c_4 \sin pb) &= 0, \end{aligned}$$

$$p^3 a_3 \sin pb - p^3 a_4 \cos pb - \chi(a_1 + a_2 b + a_3 \cos pb + a_4 \sin pb) - \\ - (p^3 c_3 \sin pb - p^3 c_4 \cos pb) = 0$$

Boundary conditions at $x = 1$:

$$\begin{aligned} c_1 + c_2 + c_3 \cos p + c_4 \sin p &= 0\,, \\ c_2 - p c_3 \sin p + p c_4 \cos p &= 0\,. \end{aligned}$$

As the system is homogeneous, non-trivial solutions exist if the determinant of the coefficient matrix vanishes, so

$$-\begin{vmatrix} 1 & 0 & 1 & 0 & 0 & 0 & 0 & 0 \\ 0 & 1 & 0 & p & 0 & 0 & 0 & 0 \\ 1 & b & \cos pb & \sin pb & -1 & -b & -\cos pb & -\sin pb \\ 0 & 1 & -p\sin pb & p\cos pb & 0 & -1 & p\sin pb & -p\cos pb \\ 0 & 0 & -\cos pb & -\sin pb & 0 & 0 & \cos pb & \sin pb \\ \chi & \chi b & \chi\cos pb - p^3\sin pb & \chi\sin pb + p^3\cos pb & 0 & 0 & p^3\sin pb & -p^3\cos pb \\ 0 & 0 & 0 & 0 & 1 & 1 & \cos p & \sin p \\ 0 & 0 & 0 & 0 & 0 & 1 & -p\sin p & p\cos p \end{vmatrix} =$$

$$= 2p^4\cos p + p^5\sin p - 2p^4 + \chi p\big(2\left(\sin p(b-1) + \sin p - \sin bp\right) -$$

$$-\frac{1}{2}p\left(\cos\left(p-2bp\right) - 2p\cos\left(p-bp\right) + \frac{3}{2}p\cos p\right) - 2p^2b\left(\cos p(b-1) - \cos bp\right) +$$

$$+ p^2b\left(b-1\right)\sin p\big) = 0\,. \quad \text{(A.1.4)}$$

In special case, if $\chi \to \infty$ or $\chi = 0$ we find

$$2(\sin p(b-1) + \sin p - \sin bp) - \frac{1}{2}p\left(\cos\left(p-2bp\right) - 2p\cos\left(p-bp\right) + \frac{3}{2}p\cos p\right) -$$

$$- 2p^2b\left(\cos p(b-1) - \cos bp\right) + p^2b(b-1)\sin p = 0 \quad \text{(A.1.5a)}$$

and

$$2\cos p + p\sin p - 2 = 0\,. \quad \text{(A.1.5b)}$$

The critical value of $p$ is $2\pi$ for fixed-fixed beams.

For FssP beams, the characteristic equation is

$$\begin{vmatrix} 1 & 0 & 1 & 0 & 0 & 0 & 0 & 0 \\ 0 & 1 & 0 & p & 0 & 0 & 0 & 0 \\ 1 & b & \cos pb & \sin pb & -1 & -b & -\cos pb & -\sin pb \\ 0 & 1 & -p\sin pb & p\cos pb & 0 & -1 & p\sin pb & -p\cos pb \\ 0 & 0 & -\cos pb & -\sin pb & 0 & 0 & \cos pb & \sin pb \\ \chi & \chi b & \chi\cos pb - p^3\sin pb & \chi\sin pb + p^3\cos pb & 0 & 0 & p^3\sin pb & -p^3\cos pb \\ 0 & 0 & 0 & 0 & 1 & 1 & \cos p & \sin p \\ 0 & 0 & 0 & 0 & 0 & 0 & cosp & sinp \end{vmatrix}$$

$$= \chi(bp^2(1-b)\cos p - p(1-b)\sin p + 2p(1-b)\sin p(1-b) - p\cos pb\sin p(1-b)$$

$$- \cos p + \cos pb\cos p(1-b)) + p^3\sin p - p^4\cos p \quad \text{(A.1.6)}$$

If $\chi \to \infty$ or $\chi = 0$ we find

$$bp^2(1-b)\cos p - p(1-b)\sin p + 2p(1-b)\sin p(1-b) - p\cos pb\sin p(1-b)$$

$$- \cos p + \cos pb\cos p(1-b) = 0 \quad \text{(A.1.7a)}$$

and

$$\sin p - p\cos p = 0\,. \quad \text{(A.1.7b)}$$

The critical value of $p$ is $1.43029\pi$ for fixed-pinned beams.

For PssP beams, since $a_1 = a_3 = 0$, we have

$$\begin{vmatrix} b & \sin pb & -1 & -b & -\cos pb & -\sin pb \\ 1 & p\cos pb & 0 & -1 & p\sin pb & -p\cos pb \\ 0 & -\sin pb & 0 & 0 & \cos pb & \sin pb \\ -\chi b & -p^3\cos pb - \chi\sin pb & 0 & 0 & -p^3\sin pb & p^3\cos pb \\ 0 & 0 & 1 & 1 & \cos p & \sin p \\ 0 & 0 & 0 & 0 & \cos p & \sin p \end{vmatrix} =$$

$$= p^3\sin p - \chi\left(pb\left(1-b\right)\sin p - (\cos pb)\cos p(1-b) + \cos p\right) = 0. \quad \text{(A.1.8)}$$

In case $\chi \to \infty$ or $\chi = 0$ we have

$$pb\left(1-b\right)\sin p - (\cos pb)\cos p(1-b) + \cos p = 0 \quad \text{(A.1.9a)}$$

and

$$\sin p = 0\,. \tag{A.1.9b}$$

The critical value of $p$ is $\pi$ for pinned-pinned beams.

## A.2. Stability issue of beam under a compressive force of Chapter 4

**A.2.1. FFStep case .** Based on (4.6.1), the stability of stepped beams is governed by equation

$$K_{1a}(w_1(x)) = 0, \qquad K_{2a}(w_2(x)) = 0 \tag{A.2.1}$$

which is paired with the boundary and continuity conditions of Table 41. Using the solutions of (4.6.3) and $p_2 = \sqrt{\mathcal{N}_2}$, the equation system for the unknowns is

$$\begin{bmatrix}
1 & 0 & 1 & 0 & 0 & 0 & 0 & 0 \\
0 & 1 & 0 & p_2\gamma & 0 & 0 & 0 & 0 \\
1 & b & \cos bp_2\gamma & \sin bp_2\gamma & -1 & -b & -\cos p_2 b & -\sin p_2 b \\
0 & 1 & -p_2\gamma\sin bp_2\gamma & p_2\gamma\cos bp_2\gamma & 0 & -1 & p_2\sin p_2 b & -p_2\cos p_2 b \\
0 & 0 & -\cos bp_2\gamma & -\sin bp_2\gamma & 0 & 0 & \cos p_2 b & \sin p_2 b \\
0 & 0 & \gamma\sin bp_2\gamma & -\gamma\cos bp_2\gamma & 0 & 0 & -\sin p_2 b & \cos p_2 b \\
0 & 0 & 0 & 0 & 1 & \ell & \cos p_2\ell & \sin p_2\ell \\
0 & 0 & 0 & 0 & 0 & 1 & -p_2\sin p_2\ell & p_2\cos p_2\ell
\end{bmatrix}
\begin{bmatrix} a_{11} \\ a_{21} \\ a_{31} \\ a_{41} \\ a_{12} \\ a_{22} \\ a_{32} \\ a_{42} \end{bmatrix}
= \begin{bmatrix} 0 \\ 0 \\ 0 \\ 0 \\ 0 \\ 0 \\ 0 \\ 0 \end{bmatrix} \tag{A.2.2}$$

$$\gamma = \sqrt{\alpha}$$

The characteristic equation therefore, is

$$\begin{aligned}
\mathcal{D} = {} & \frac{1}{2}p_2\cos\left(p_2\left(b-\ell\right)+b\gamma p_2\right) - \frac{1}{2}p_2\cos\left(p_2\left(b-\ell\right)-b\gamma p_2\right) + 2\gamma p_2 + \\
& + \frac{1}{2}\gamma^2 p_2\cos\left(p_2\left(b-\ell\right)+b\gamma p_2\right) - \frac{1}{2}\gamma^2 p_2\cos\left(p_2\left(b-\ell\right)-b\gamma p_2\right) - \\
& - \gamma p_2\cos\left(p_2\left(b-\ell\right)+b\gamma p_2\right) - \gamma p_2\cos\left(p_2\left(b-\ell\right)-b\gamma p_2\right) + \\
& + \frac{1}{2}\gamma\ell p_2^2\sin\left(p_2\left(b-\ell\right)+b\gamma p_2\right) + \frac{1}{2}\gamma\ell p_2^2\sin\left(p_2\left(b-\ell\right)-b\gamma p_2\right) - \\
& - \frac{1}{2}\gamma^2\ell p_2^2\sin\left(p_2\left(b-\ell\right)+b\gamma p_2\right) + \frac{1}{2}\gamma^2\ell p_2^2\sin\left(p_2\left(b-\ell\right)-b\gamma p_2\right) = 0
\end{aligned} \tag{A.2.3}$$

In special case $\alpha = b = \ell = 1$ and $p_2 = p$. Then the characteristic equation for a uniform fixed-fixed beam is

$$\mathcal{D} = 2 - 2\cos p - p\sin p = 0 \tag{A.2.4}$$

yielding $p = 2\pi$.

Equation (A.2.3) can be solved numerically. Figure 1.1 illustrates the critical force $\sqrt{N_{2\,\mathrm{crit}}(b)}$ against $b$.

**A.2.2. PPStep beams .** Under such support conditions, the equation system is

$$\begin{bmatrix}
1 & 0 & 1 & 0 & 0 & 0 & 0 & 0 \\
0 & 0 & 1 & 0 & 0 & 0 & 0 & 0 \\
1 & b & \cos bp_2\gamma & \sin bp_2\gamma & -1 & -b & -\cos p_2 b & -\sin p_2 b \\
0 & 1 & -p_2\gamma\sin bp_2\gamma & p_2\gamma\cos bp_2\gamma & 0 & -1 & p_2\sin p_2 b & -p_2\cos p_2 b \\
0 & 0 & -\cos bp_2\gamma & -\sin bp_2\gamma & 0 & 0 & \cos p_2 b & \sin p_2 b \\
0 & 0 & \gamma\sin bp_2\gamma & -\gamma\cos bp_2\gamma & 0 & 0 & -\sin p_2 b & \cos p_2 b \\
0 & 0 & 0 & 0 & 1 & \ell & \cos p_2\ell & \sin p_2\ell \\
0 & 0 & 0 & 0 & 0 & 0 & \cos p_2\ell & \sin p_2\ell
\end{bmatrix}
\begin{bmatrix} a_{11} \\ a_{21} \\ a_{31} \\ a_{41} \\ a_{12} \\ a_{22} \\ a_{32} \\ a_{42} \end{bmatrix}
= \begin{bmatrix} 0 \\ 0 \\ 0 \\ 0 \\ 0 \\ 0 \\ 0 \\ 0 \end{bmatrix} \tag{A.2.5}$$

$$\gamma = \sqrt{\alpha}$$

So the characteristic equation is

$$\mathcal{D} = -\gamma\ell\cos b\gamma p_2\sin p_2\left(\ell - b\right) - \ell\sin b\gamma p_2\cos p_2\left(\ell - b\right) = 0 \tag{A.2.6}$$

In special case, when $\alpha = b = \ell = 1$ and $p_2 = p$, then it is a uniform pinned-pinned beam with

$$\mathcal{D} = \sin p = 0 \tag{A.2.7}$$

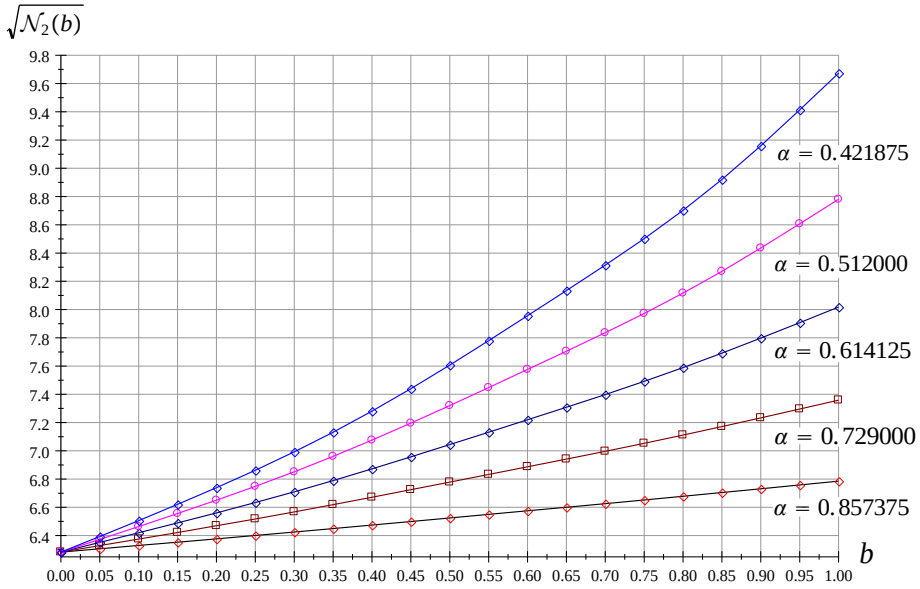


FIGURE 1.1. Critical force against $b$, $\alpha$ is a parameter

from where $p = \pi$ is the smallest root for $p$.

Equation (A.2.6) was solved numerically. Figure 1.2 depicts the critical force $\sqrt{N_{2\,\mathrm{crit}}(b)}$ variation against $b$.

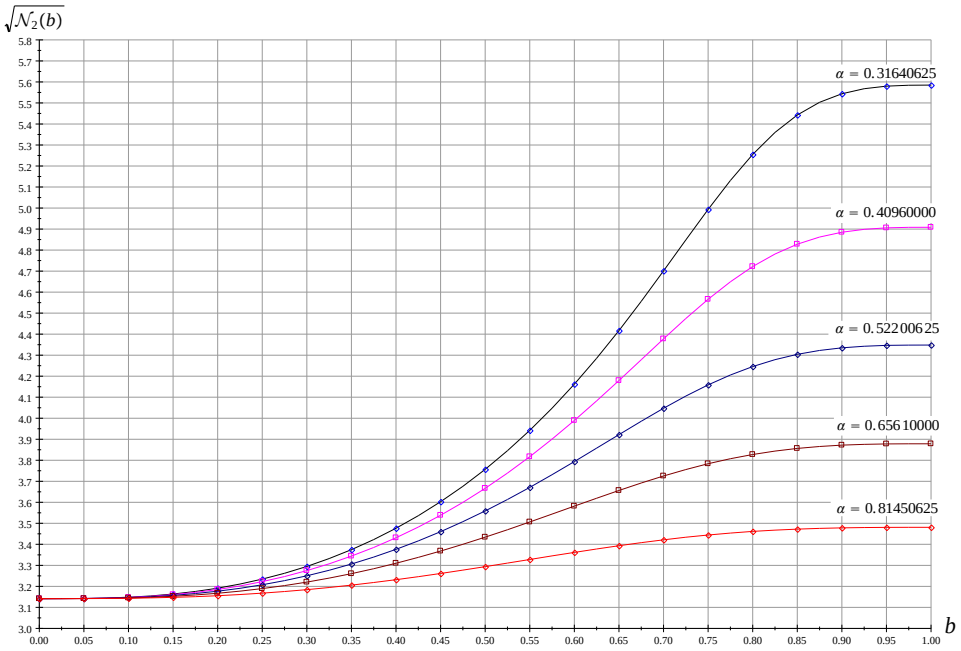


FIGURE 1.2. Critical force against $b$, $\alpha$ is a parameter

### A.3. Some detailed transformations of Chapter 5

**A.3.1. The principle of virtual work .** The internal virtual work in the arch is transformed using Eqs. 5.1.1-5.1.9, hence

$$\int_L \int_A (1+\frac{\zeta}{R})\sigma_\xi [\frac{R}{R+\zeta}(\frac{d\delta u}{ds}+\frac{\delta w}{R}+\zeta\frac{d\delta\psi}{ds})+\psi\delta\psi+\frac{d\delta w}{ds}\frac{\mathrm{d}h}{\mathrm{d}s}]dAds =$$

$$\int_L \{\int_A \sigma_\xi dA(\frac{d\delta u}{ds}+\frac{\delta w}{R})+\int_A \zeta\sigma_\xi dA\frac{d\delta\psi}{ds}+\int_A (1+\frac{\zeta}{R})\sigma_\xi dA\psi(\frac{\delta u}{ds}-\frac{d\delta w}{ds})+\int_A (1+\frac{\zeta}{R})\sigma_\xi dA\frac{d\delta w}{ds}\frac{\mathrm{d}h}{\mathrm{d}s}\}ds =$$
$$\int_L [N(\frac{d\delta u}{ds}+\frac{\delta w}{R})+M\frac{d\delta\psi}{ds}+\left(N+\frac{M}{R}\right)\psi(\frac{\delta u}{R}-\frac{d\delta\psi}{ds})+\left(N+\frac{M}{R}\right)\frac{d\delta w}{ds}\frac{\mathrm{d}h}{\mathrm{d}s}]ds. \quad (A.3.1)$$

Further using Here, applying the integration by parts theorem returns

$$-\int_L \left(\frac{dN}{ds}+\frac{1}{R}\frac{dM}{ds}-\frac{1}{R}(N+\frac{M}{R})\psi\right)\delta u ds -$$
$$\int_L \left(\frac{d^2M}{ds^2}-\frac{N}{R}-\frac{d}{ds}\left(N+\frac{M}{R}\right)\psi-\left(N+\frac{M}{R}\right)\frac{\mathrm{d}^2h}{\mathrm{d}s^2}\right)\delta w ds = 0 \quad (A.3.2)$$

These integrands express the equilibrium equations.

The first term shows that the membrane strain is constant over the centroidal axis

$$\varepsilon_{m,eff}^{'} = 0 \quad (A.3.3)$$

**A.3.2. The equilibrium expressed with the displacements.** Here, we transform the second integrand in A.3.2, with the aid of Eqs. 5.1.1-5.1.7, thus

$$\frac{N}{R}=\frac{A_e\varepsilon_{m,eff}}{R}-\frac{M}{R^2}=\frac{I_e}{R^3}\frac{A_e}{I_e}\varepsilon_{m,eff}-\frac{M}{R^2}=\frac{I_e}{R^3}\kappa\varepsilon_{m,eff}+\frac{I_e}{R^4}(w^{''}+w), \quad (A.3.4)$$
$$-\frac{I_e}{R^4}(w^{''}+w)-\frac{I_e}{R^4}\frac{A_eR^2}{I_e}R\varepsilon_{m,eff}\psi^{'}-\frac{I_e}{R^3}\kappa\varepsilon_{m,eff}-\frac{I_e}{R^4}(w^{''}+w)=0 \quad (A.3.5)$$

Overall, it yields

$$(w^{''''}+w^{''})+R\kappa\varepsilon_{m,eff}(\psi^{'}+1+H^{''})+(w^{''}+w)=0, \quad (A.3.6)$$

where

$$R\varepsilon_{m,eff}(1+\psi^{'})=R\varepsilon_{m,eff}\left[1+\frac{1}{R}(R\varepsilon_{m,eff}-w-\frac{1}{2}\psi^{2}R-w^{''})\right]\approx$$
$$R\varepsilon_{m,eff}(1+\varepsilon_{m,eff})-\varepsilon_{m,eff}(w^{''}+w)\approx R\varepsilon_{m,eff}-\varepsilon_{m,eff}(w^{''}+w). \quad (A.3.7)$$

Finally, the radial equilibrium of the imperfect arch is determined by

$$w^{''''}+2w^{''}+w-\kappa\varepsilon_{m,eff}(w^{''}+w+h^{''})=-\kappa R\varepsilon_{m,eff} \quad (A.3.8)$$

or briefly, with dimensionless displacements, it is

$$W^{''''}+(\mu^2+1)W^{''}+\mu^2W=(\mu^2-1)(1+H^{''}). \quad (A.3.9)$$

# Bibliography


1. D. Gönczi. Finite element investigation in the forming process of aluminium aerosol cans. *Acta Technica Corviniensis - Bulletin of Engineering*, 13(4):19–22, 2020.
2. A. Baksa, D. Gönczi, L. P. Kiss, P. Z. Kovács, and Zs. Lukács. Experimental and numerical investigations on the stability of cylindrical shells. *Journal of Engineering Studies and Research*, 26(4):34–39, 2020.
3. C. M. Wang, C. Y. Wang, and J. N. Reddy. *Exact solutions for buckling of structural members*. CRC Press, 2004.
4. S. Jerath. *Structural stability theory and practice: buckling of columns, beams, plates and shells*. Wiley, 2020.
5. K. Murawski. *Technical Stability of Continuously Loaded Thin-walled Slender Columns*. Lulu Press, 2017.
6. K. Murawski. Technical stability of very slender rectangular columns compressed by ball-and-socket joints without friction. *International Journal of Structural Glass and Advanced Materials Research*, 4(1):186–208, 2020.
7. K. Murawski. Comparison of the known hypotheses of lateral buckling in the elastic-plastic states of thin-walled semi-slender columns. *International Journal of Structural Glass and Advanced Materials Research*, 4(1):233–253, 2020.
8. A. M. Wahrhaftig, K. M. M Magalhães, R. M. L. R. F. Brasil, and K. Murawski. Evaluation of mathematical solutions for the determination of buckling of columns under self-weight. *Journal of Vibration Engineering & Technologies*, 4(1):233–253, 2020.
9. P.S. Harvey and T.M.N. Cain. Buckling of elastic columns with initial imperfections and load eccentricity. *Structures*, 23:660–664, 2020.
10. R. Adman and M. Saidani. Elastic buckling of columns with end restraint effects. *Journal of Constructional Steel Research*, 87:1–5, 2013.
11. S. B. Coşkun and M. T. Atay. Determination of critical buckling load for elastic columns of constant and variable cross-sections using variational iteration method. *Computers & Mathematics with Applications*, 58(11):2260–2266, 2009. New Analytical Methods and Applications.
12. K. V. Singh and G. Li. Buckling of functionally graded and elastically restrained non-uniform columns. *Composites Part B: Engineering*, 40(5):393–403, 2009.
13. P. S. Harvey, L. N. Virgin, and M. H. Tehrani. Buckling of elastic columns with second-mode imperfections. *Meccanica*, 54:1245–1255, 2019.
14. Lawrence Virgin. Tailored buckling constrained by adjacent members. *Structures*, 16:20–26, 2018.
15. H. Madah and O. Amir. Concurrent structural optimization of buckling-resistant trusses and their initial imperfections. *International Journal of Solids and Structures*, 162:244–258, 2019.
16. G. Green. *An Essey on the Application of Mathematical Analysis to the Theories of Electricity and Magnetism*. Notthingam: Printed for the author by T. Wheelhouse, 1828.
17. M. Bocher. Boundary problems and Green's functions for linear differential and difference equations. *Annals of Mathematics*, 13(1/4):71–88, 1911-1912.
18. E. L. Ince. *Ordinary Differential Equations*. Longmans, Green and Co., London, 1926.
19. L. Collatz. *Eigenwertaufgaben mit Technischen Anwendungen*. Akademische Verlagsgesellschaft Geest & Portig K.G., 1963. Russian Edition in 1968.
20. L. Collatz. *The Numerical Treatment of Differential Equations*. Springer-Verlag, Berlin-Heidelberg GMBH, 3rd edition edition, 1966.
21. G. Szeidl. *Effect of the change in length on the natural frequencies and stability of circular beams*. PhD thesis, Department of Mechanics, University of Miskolc, Hungary, 1975. (in Hungarian).
22. Zengqin Zhao. Solutions and Green's functions for some linear second-order three-point boundary value problems. *Computers & Mathematics*, 56:104–113, 2008.
23. I. Y. Karaca. Fourth-order four-point boundary value problem on time scales. *Appl. Math. Letters*, 21:1057–1063, 2008.
24. B. Liu. Positive solutions of a nonlinear four-point boundary value problems in Banach spaces. *J. Math. Anal. Appl.*, 305:253–276, 2005.

25. X. Zhang and L. Liu. Positive solutions of fourth-order four-point boundary value problems with p-Laplacian operator. *J. Math. Anal. Appl.*, 336:1414–1423, 2007.
26. Y. Lin and J. Lin. Numerical method for solving the nonlinear four-point boundary value problems. *Commun. Nonlinear Sci. Numer. Simulat.*, 15:3855–3864, 2010.
27. P. Wolfe. Buckling of a nonlinearly elastic column: variational principles, bifurcation and asymptotics. *Rocky Mt J Math*, 25(2):789–813, 1995.
28. Y.Khan and W.Al-Hayani. A nonlinear model arising in the buckling analysis and its new analytic approximate solution. *Z Naturforsch*, 68:355–361, 2013.
29. Li .XF. Huang .Y. Buckling analysis of nonuniform and axially graded columns with varying flexural rigidity. *J Eng Mech*, 68:355–361, 2011.
30. A. Barari, H. D. Kaliji, M. Ghadimi, and G. Domiarry. Non-linear vibration of Euler-Bernoulli beams. *Lat. Am. J. Sol. Struc.*, 8:139–148, 2011.
31. J.A. Loya, J. Aranda-Ruiz, and R. Zaera. Natural frequencies of vibration in cracked timoshenko beams within an elastic medium. *Theo. Appl. Fract. Mech.*, 118:103257, 2022.
32. K. Saurabh. Vibration analysis of non-uniform axially functionally graded beam resting on pasternak foundation. *Mat. Today: Proc.*, 2022.
33. G.S. Pavan, H. Muppidi, and J. Dixit. Static, free vibrational and buckling analysis of laminated composite beams using isogeometric collocation method. *Eur. J. Mech. - A/Solids*, 96:104758, 2022.
34. V. Stojanovic, P. Kozic, R. Pavlovic, and G. Janevski. Effect of rotary inertia and shear on vibration and buckling of a double beam system under compressive axial loading. *Arch. Appl. Mech.*, 81:1993–2005, 2011.
35. A. Mirzabeigy and R. Madoliat. Large amplitude free vibration of axially loaded beams resting on variable elastic foundation. *Alexandria Eng. J.*, **55**(2):1107–1114, 2016.
36. M.A. De Rosa, P.M. Bellés, and M.J. Maurizi. Free vibrations of stepped beams with intermediate elastic supports. *Journal of Sound and Vibration*, 181(5):905–910, 1995.
37. W Jong-Shyong and C. Bo-Hau. Free vibration of axial-loaded multi-step timoshenko beam carrying arbitrary concentrated elements using continuous-mass transfer matrix method. *Eur. J. Mech. - A/Sol.*, **38**:20–37, 2013.
38. M.A. Mahmoud. Free vibrations of tapered and stepped, axially functionally graded beams with any number of attached masses. *Engineering Structures*, 267:114696, 2022.
39. Q. Mao. Free vibration analysis of multiple-stepped beams by using adomian decomposition method. *Mathematical and Computer Modelling*, 54(1):756–764, 2011.
40. B. Bozyigit, Y. Yesilce, and S. Catal. Free vibrations of axial-loaded beams resting on viscoelastic foundation using Adomian decomposition method and differential transformation. *Eng. Sci. Tech., Int. J.*, 21(2):1181–1193, 2018.
41. Y.X. Li and J. Gong. Free and forced vibration analysis of general multiple beam systems. *Int.J. Mech. Sci.*, 235:107716, 2022.
42. K. Xie, Y. Wang, and T. Fu. Nonlinear vibration analysis of third-order shear deformable functionally graded beams by a new method based on direct numerical integration technique. *Int. J. Mech. Mater. Des.*, 16:839–855, 2020.
43. S. Talik, M. Claeys, J.-J. Sinou, and J.-P. Lambelin. An efficient approach for predicting the nonlinear vibrations of a beam system subjected to multipoint correlated random excitation. *Eur. J. Mech. - A/Solids*, 96:104769, 2022.
44. K. Meera Saheb, G. Kanneti, and P. Sathujoda. Large amplitude forced vibrations of timoshenko beams using coupled displacement field method. *Forces Mech.*, 7:100079, 2022.
45. A. Bizzi, E. L. Fortaleza, and T. S. N. Guenka. Dynamics of heavy beams: Closed-form vibrations of gravity-loaded rayleigh–timoshenko columns. *J. Sound Vib.,*, **510**,:116259, 2021.
46. E. Manoach, J Warminski, L. Kloda, A. Warminska, and S. Doneva. Nonlinear vibrations of a bi-material beam under thermal and mechanical loadings. *Mech. Sys. Signal Proc.*, 177:109127, 2022.
47. Li. X.Y, X. Zhao, and Y.H. Li. Green's functions of the forced vibration of Timoshenko beams with damping effect. *J. Sound Vib.*, 333(6):1781–1795, 2014.
48. S. H. Mojtaba, A. Aftabi Sani, B. Mehri, and M. Mofid. Green's function for uniform euler–bernoulli beams at resonant condition: Introduction of fredholm alternative theorem. *Applied Mathematical Modelling*, 39(12):3366–3379, 2015.
49. X. Zhao, W.D. Zhu, and Y.H. Li. Analytical solutions of nonlocal coupled thermoelastic forced vibrations of micro-/nano-beams by means of green's functions. *Journal of Sound and Vibration*, 481:115407, 2020.
50. H. Hesheng, C. Dengqing, and L Lun. Green's functions for forced vibration analysis of bending-torsion coupled timoshenko beam. *Applied Mathematical Modelling*, 45:621–635, 2017.

51. L. Euler. Sûr la force des colonnes. *Memoires de l'Academie de Barlin*, 1759.
52. A.R. Liu, Z.C. Yang, M.A. Bradford, and Y.–L. Pi. Nonlinear dynamic buckling of fixed shallow arches under an arbitrary step radial point load. *Journal of Engineering Mechanics*, 144(4):04018012, 2018.
53. A.R. Liu, Y.H. Huang, J.Y. Fu, Q.C. Yu, and R. Rao. Experimental research on stable ultimate bearing capacity of leaning–type arch rib systems. *Journal of Constructional Steel Research*, 114:281–292, 2015.
54. G. J. Simitses. *An Introduction to the Elastic Stability of Structures*. Prentice-Hall, 1976.
55. S. P. Timoshenko and J. M. Gere. Theory of elastic stability. *McGraw Hill*, 1961.
56. P. R. Calboun and D. A. DaDeppo. Nonlinear finite element analysis of clamped arches. *Journal of Structural Engineering, ASCE*, 109(3):599–612, 1983.
57. Z. M. Elias and K. L. Chen. Nonlinear shallow curved beam finite element. *Journal of Engineering Mechanics, ASCE*, 114(6):1076–1087, 1988.
58. Y.–L. Pi and M. A. Bradford. In-plane strength and design of fixed steel i-section arches. *Engineering Structures*, 26(3):291–301, 2004.
59. B. Moghaddasie and I. Stanciulescu. Equilibria and stability boundaries of shallow arches under static loading in a thermal environment. *Latin American Journal of Solids and Structures*, 51:132–144, 2013.
60. M. A. Bradford, T. Wang, Y-L. Pi, and R. I. Gilbert. In-plane stability of parabolic arches with horizontal spring supports. *Journal of Structure and Engineering I: Theory*, 133(8):1130–1137, 2007.
61. M. A. Bradford, B. Uy, and Y.-L. Pi. In-plane elastic stability of arches under a central concentrated load. *Journal of Engineering Mechanics*, 128(7):710–719, 2002.
62. A. Gjelsvik and S. R. Bodner. Energy criterion and snap-through buckling of arches. *Journal of Engineering Mechanics ASCE*, 88(5):87–134, 1962.
63. Y. L. Pi, M. A. Bradford, and F. Tin-Loi. Non-linear in-plane buckling of rotationally restrained shallow arches under a central concentrated load. *International Journal of Non-Linear Mechanics*, 43(1):1–17, 2008.
64. Y.-L. Pi, M. A. Bradford, and A. Liu. Nonlinear equilibrium and buckling of fixed shallow arches subjected to an arbitrary radial concentrated load. *International Journal of Structural Stability and Dynamics*, 17(8):1–17, 2017.
65. Y. B. Yang and M. A. Shieh. Solution method for nonlinear problems with multiple critical points. *AIAA Journal*, 28(12):2110–2116, 1995.
66. S. R. Kuo and Y. B. Yang. Tracing postbuckling paths of structures containing multi loops. *International Journal of Numerical Methods in Engineering*, 38(23):4053–4075, 1995.
67. L. P. Kiss. Vibrations and stability of heterogeneous curved beams. *PHD Thesis. Institute of Applied Mechanics, University of Miskolc, Hungary*, 2015.
68. L. P. Kiss. Nonlinear stability analysis of fgm shallow arches under an arbitrary concentrated radial force. *Mechanics and Materials in Design*, 16(1):91–108, 2020.
69. J. Cai, Y. Xu, J. Feng, and J. Zhang. In-plane elastic buckling of shallow parabolic arches under an external load and temperature changes. *Journal of Structure Engineering*, 138(11):1300–1309, 2012.
70. H.L. Schreyer. The effect of initial imperfections on the buckling load of shallow circular arches. *Journal of Applied Mechanics*, 39(2):445–450, 1972.
71. K. Der-Wang and C.K. Mak. Finite element analysis of buckling and post-buckling behaviors of arches with geometric imperfections. *Computers Structures*, 3(1):149–161, 1973.
72. T. Furtmüller, C. Adam, and X. Shen. Buckling and post-buckling analysis of three-layer shallow arches with geometric imperfections and interlayer slip. *Thin-Walled Structures*, 193, 2023.
73. Z. Jin, S-t Yan, and I. Paulmichl. Instability of imperfect non-uniform shallow arch under uniform radial pressure for pinned and fixed boundary conditions. *Thin-Walled Structures*, 132:56–67, 2018.
74. Chroscielewski.J and Eremeyev V. A . Can we really solve an arch stability problem? *International Journal of Engineering Science*, 2024.
75. A. Baksa and I. Ecsedi. A note on the pure bending of nonhomogeneous prismatic bars. *International Journal of Mechanical Engineering Education*, 37(2):1108–129, 2009.
76. G. Szeidl and L. Kiss. *Green Functions for Three Point Boundary Value Problems with Applications to Beams*, chapter 5, pages 121–161. Nova Science Publisher, Inc.
77. L. Kiss, G. Szeidl, and A. Messaoudi. Stability of heterogeneous beams with three supports through green functions. *Meccanica*, **57**:1369–1390, 2022.
78. G. Szeidl and L. P. Kiss. *Mechanical Vibrations, an Introduction*. Foundation of Engineering Mechanics. Springer Nature, Switzerland.
79. J. M. Hoene-Wroński. *Réfutation de la théorie des fonctions analytiques de Lagrange*. Blankenstein, Paris, 1812.

80. L. Kiss, G. Szeidl, and A. Messaoudi. Vibration of an axially loaded heterogeneous fixed–fixed beam with an intermediate roller support. *J. Brazilian Soc. Mech. Sci. Eng.*, **44**:461, 2022.
81. A. Messaoudi. Green functions for coupled boundary value problems – applications to pin-supported stepped heterogeneous beams. *Journal of Computational and Applied Mechanics; Accepted but not published yet*, 2024.
82. A. Messaoudi and G. Kiss, L.and Szeidl. Green functions for coupled boundary value problems with applications to stepped beams. *Submitted for review to the European Journal of Mechanics - A/Solids.*, 2024.
83. A.Messaoudi and L. P. Kiss. Investigations on the limit-point buckling of curved beams. *Multidiszciplináris tudományok, 13. kötet, 2. sz.,*, page 78–86, 2023.
84. L.P. Kiss. Sensitivity of FGM shallow arches to loading imperfection when loaded by a concentrated radial force around the crown. *Int. J. Non-Lin. Mech.*, 116:62–72, 2019.